Noise Suppression in OCDMA Networks using Nonlinear Optical Devices

A thesis submitted in partial fulfillment of the requirements
for the degree of Doctor of Philosophy
(Electronic Engineering)

by

Karl Dexter

B.Eng., MIEI, MIEEE

School of Electronic Engineering

Faculty of Engineering and Computing

Dublin City University

Research Supervisor

Prof. Liam P. Barry

2010

Declaration

I hereby certify that this material, which I now submit for assessment on the programme of study leading to the award of Doctor of Philosophy is entirely my own work, that I have exercised reasonable care to ensure that the work is original, and does not to the best of my knowledge breach any law of copyright, and has not been taken from the work of others save and to the extent that such work has been cited and acknowledged within the text of my work.

Signed
Student ID No:
Date

Acknowledgements

Firstly I would like to thank my supervisor Prof. Liam Barry for the opportunity to undertake this work. Without his continued motivation and support the completion of this work would have been impossible. I would also like to express my gratitude to both Dr. Paul Maguire and Dr. Douglas Reid whose guidance, knowledge and expertise where invaluable throughout the course of my studies in Dublin City University. I must also thank those whom I have collaborated with in Trinity College Dublin and the Optoelectronics Research Centre in the University of Southampton.

Thank you to all the members of the Radio and Optical Communications group past and present, and to Brendan in the VSG lab. Your friendship both in and outside of the lab have made these past four years infinitely more enjoyable and without which, the completion of this thesis would have been all the more difficult.

Finally, I would like to thank my friends and family, especially Niamh and my parents, Evans and Geraldine, for their commitment, support and encouragement throughout my time as an undergrad and postgrad in DCU. Thank you. This is for you.

<div align="right">
Karl Dexter,

June 2010.
</div>

Abstract

Optical code division multiple access (OCDMA) is a multiplexing technique that has a number of inherent advantages that make it suitable for use in passive optical networks, such as allowing subscribers to transmit information in an asynchronous fashion over a single optical fibre. This form of multiplexing can provide a higher degree of flexibility and simplicity in comparison to other techniques. However, due to the asynchronous nature of transmission, OCDMA networks suffer from multiple access interference (MAI) and optical beat noise which severely impairs system performance.

A number of solutions have been proposed to mitigate these noise sources. Increasing the optical code lengths used can reduce the level of optical beat noise, however this is generally at the expense of transmission speed and increased transmitter complexity. MAI suppression can be achieved through the use fibre-based nonlinear thresholders or optical time-gating. One problem with these solutions is the requirement of long lengths of nonlinear fibre that are susceptible to changes in environmental conditions. Therefore, this thesis focuses on the development and testing of a nonlinear optical receiver based on semiconductor devices for the suppression of noise in OCDMA systems.

The nonlinear optical process of two-photon absorption (TPA) in a commercially available 1.3 μm Fabry-Pérot laser is investigated as a method for optical thresholding in an OCDMA system. It is shown that the use of a saturable absorber (SA) directly before the TPA-based detector can provide additional suppression of MAI noise. However, the level of beat noise that is present on the optical signal can be increased due to the nonlinear responses of both devices. As a result, a gain-saturated semiconductor optical amplifier (SOA) is demonstrated as a method for the reduction of optical beat noise. It is shown that error-free performance can be achieved in an optical testbed designed to simulate an OCDMA system using an SA-SOA-TPA-based receiver. The performance improvement due to the suppression of MAI and beat noise using an SA-SOA receiver is examined in relation to a current fibre-based thresholding technique; a Mamyshev filter. It is shown that the SA-SOA receiver can offer a similar level of improvement when compared to the performance of a Mamyshev filter.

Table of Contents

List of Figures

List of Tables

List of Acronyms

ADSL	Asymmetric Digital Subscriber Loop
ASE	Amplified Spontaneous Emission
ATM	Asynchronous Transfer Mode
AWG	Arrayed Waveguide Grating
BER	Bit Error Rate
CCW	Counter-Clockwise
CD	Chromatic Dispersion
CDMA	Code Division Multiple Access
CHPC	Carrier-Hopping Prime Code
CRZ	Chirped Return-to-Zero
CS-RZ	Carrier-Suppressed Return-to-Zero
CW	Clockwise
CW	Continuous Wave
CWDM	Coarse Wavelength Division Multiplexing
DCA	Digital Communications Analyser
DCF	Dispersion Compensating Fibre
DFF	Dispersion-Flattened Fibre
DSLAM	Digital Subscriber Line-Access Multiplexer
DUT	Device Under Test
DWDM	Dense Wavelength Division Multiplexing
EAM	Electro-Absorption Modulator
ECL	External Cavity Laser
EDFA	Erbium Doped Fibre Amplifier
EPON	Ethernet Passive Optical Network
ETDM	Electrical Time Division Multiplexing
FBG	Fibre Bragg Grating
FEC	Forward-Error Correction
FP	Fabry-Pérot
FPA	Fabry-Pérot Amplifier
FTTH	Fibre-To-The-Home
FWM	Four-Wave Mixing
GPON	Gigabit Passive Optical Network
GPS	Global Positioning System

GS-SOA	Gain-Saturated Semiconductor Optical Amplifier
HBR	Holographic Bragg Reflector
HDTV	High Definition TV
HFC	Hybrid Fibre-Coax
HNLF	Highly Nonlinear Fibre
IP	Internet Protocol
ITU	International Telecommunications Union
LED	Light Emitting Diode
MAI	Multiple Access Interference
MAN	Metropolitan Area Network
MZM	Mach-Zhender Modulator
NOLM	Nonlinear Optical Loop Mirror
NRZ	Non-Return-to-Zero
NRZ-PSK	Non-Return-to-Zero Phase-Shift Keying
OADM	Optical Add/Drop Multiplexer
OBN	Optical Beat Noise
OBPF	Optical Bandpass Filter
OCDM	Optical Code Division Multiplexing
ODL	Optical Delay Line
OECD	Organisation for Economic Co-operation and Development
OEO	Optical-Electrical-Optical
OLT	Optical Line Terminal
ONU	Optical Network Unit
OOC	Optical Orthogonal Code
OSNR	Optical Signal-to-Noise Ratio
pA	Pico-Ammeter
PC	Polarisation Controller
PLC	Planar Lightwave Circuit
PLL	Phase-Locked Loop
PMD	Polarisation Mode Dispersion
PON	Passive Optical Network
POTS	Plain-Old-Telephone Service
PPG	Pulse Pattern Generator
PPLN	Periodically Poled Lithium-Niobate
PRBS	Pseudo-Random Bit Sequence
QAM	Quadrature Amplitude Modulation
RF	Radio Frequency

ROADM	Reconfigurable Optical Add/Drop Multiplexer
RSAM	Resonant Saturable Absorber Mirror
RZ	Return-to-Zero
RZ-DPSK	Return-to-Zero Differential-Phase-Shift Keying
SA	Saturable Absorber
SA-OCDMA	Spectral-Amplitude Optical Code Division Mutliple Access
SAE	Spectral Amplitude Encoding
SHG	Second Harmonic Generation
SMF	Single Mode Fibre
SNR	Signal-to-Noise Ratio
SOA	Semiconductor Optical Amplifier
SONET/SDH	Synchronous Optical Network/Synchronous Digital Hierarchy
SP-OCDMA	Spectral-Phase Optical Code Division Multiple Access
SPA	Single Photon Absorption
SPM	Self-Phase Modulation
SSFBG	Superstructured Fibre Bragg Grating
TDMA	Time Division Multiple Access
TFF	Thin-Film Filter
TMLL	Tuneable Mode-Locked Laser
TOAD	Terahertz Optical Asymmetric Demultiplexer
TP-OCDMA	Temporal-Phase Optical Code Division Multiple Access
TPA	Two-Photon Absorption
TS-OCDMA	Temporal-Spreading Optical Code Division Mulitple Access
TWA	Travelling Wave Amplifier
UDWDM	Ultra Dense Wavelength Division Multiplexing
VIPA	Virtually Imaged Phase Array
VOA	Variable Optical Attenuator
WDM	Wavelength Division Multiplexing
WDM/SCM	Wavelength Division Multiplexed/Subcarrier Multiplexed
WDMA	Wavelength Division Mutliple Access
WHTS	Wavelength-Hopping Time-Spreading
xDSL	xDigital Subscriber Loop

Introduction

The continued growth in demand for high-speed communications and media-rich content such as video streaming, VoIP and online gaming, has lead to a corresponding growth in demand for high-speed, symmetric internet connections for both business and residential consumers. To accommodate this increasing bandwidth demand, service providers have employed optical multiplexing techniques in both long-haul and metropolitan optical networks to take advantage of the enormous amounts of bandwidth provided by an optical fibre. However, as these backbone networks increase in capacity to meet growing demand, a bandwidth bottleneck develops in the access networks that provide the initial connection between the consumer and the network. This is due to the vast majority of the access networks employing electrical cables, which are severely limited in terms of possible speed and maximum transmission distance, to transmit information.

This last-mile bottleneck has resulted in increased interest from service providers to move optical fibre closer and closer to the consumer through deployments such as fibre-to-the-home (FTTH), creating an all-optical network. However, while wavelength division multiplexing (WDM) is the preferred multiplexing technique for the long-haul and metropolitan networks, it is not ideally suited to the access environment in terms of flexibility, scalability and cost effectiveness. Therefore there has been growing interest in alternative multiplexing techniques such as optical code division multiplexing (OCDM) for use in optical access networks. Code division multiplexed systems have a number of possible inherent advantages such as asynchronous transmission, reduced network management and improved network efficiency, leading to their successful deployment in mobile cellular networks worldwide.

While code division multiplexed systems have many advantages in comparison to alternate multiplexing techniques, the successful implementation of these types of systems in the optical domain is dependent on the ability of each receiver to recover the desired data stream while rejecting crosstalk noise introduced by other channels on the network. This crosstalk noise is a consequence of the multiplexing technique itself and can severely limit the overall performance and capacity of the system. Therefore, to realise an optical network implementing OCDM, some form of nonlinear optical thresholding is required at each receiver to remove unwanted noise while allowing the successful recovery of the desired data. This thesis investigates three different semiconductor-based optical devices that can be used for nonlinear optical thresholding in an OCDM receiver.

Main Contributions

The main contributions of this work are:

○ Investigation and characterisation of a 1.3 μm Fabry-Pérot laser diode as a nonlinear optical thresholder — A commercially available 1.3 μm FP laser was characterised as a nonlinear detector based on the nonlinear optical-to-electrical conversion process of two-photon absorption (TPA). The feasibility of using a TPA-based detector in an optical system was experimentally demonstrated with the measured data showing that an optical data pattern can be successfully recovered using a TPA-based detector. A four-channel optical code division multiple access (OCDMA) system was experimentally demonstrated using a standard linear detector and a TPA-based detector. It is shown that a significant performance improvement can be achieved in terms of the number of supported channels and the suppression of cross-channel noise when using a TPA-based detector compared to a standard linear detector.

○ Development of a nonlinear optical receiver using a saturable absorber, semiconductor optical amplifier and TPA-based detector — As the number of channels in an OCDMA system increases, the level of crosstalk and interferometric noise also increases severely limiting the capacity of the optical system. While a nonlinear device such as a TPA-based detector can suppress a large amount of crosstalk noise, its nonlinear response can increase the level of interferometric noise, reducing any improvement gained. It is demonstrated that a saturable absorber (SA) can be used to suppress the level of crosstalk noise before a gain-saturated semiconductor optical amplifier (SOA) is used to clamp the interferometric noise to a single level. A TPA-based detector is then used to suppress any remaining crosstalk noise. It is shown experimentally that this SA-SOA-TPA-based receiver can successfully support at least three optical channels in the presence of worst-case scenario crosstalk and interferometric noise.

○ Performance comparison of a SA-SOA receiver with alternative optical thresholding techniques — A number of different methods for the suppression of noise sources in OCDMA system have been demonstrated in the literature. The Mamyshev filtering technique is one method of optical thresholding in OCDMA systems that has been experimentally demonstrated. It is shown that an SA-SOA receiver can provide at least the same level of performance improvement as a Mamyshev filter when dealing with an optical signal in the presence of interference and interferometric noise. In addition, an SA-SOA receiver can be more easily implemented in comparison to a Mamyshev filter, with the performance of the latter being dependent on a number of

factors such as fibre nonlinearity, fibre dispersion and optical filter bandwidth.

Report Outline

This thesis is structured into six chapters as follows:

Chapter 1 outlines the motivation for the development of optical communication networks. Various multiplexing techniques that can be used to increase the capacity of an optical network are outlined. Network topologies are discussed with particular interest given to access networks. Within this section, current forms of electrical access networks are discussed with the problems facing these networks also highlighted. Various forms of optical access networks are then presented with attention given to an emerging network that gained significant interest in research; an optical code division multiple access network.

Chapter 2 focuses on the multiplexing technique of optical code division multiple access (OCDMA). The various methods proposed for optical encoding and decoding of a signal in an OCDMA network are presented. The advantages and disadvantages associated with each are also discussed. Since the performance of an OCDMA system relies on the optical codes used, the various forms of optical codes that have been presented in relation to this multiplexing technique are also discussed. OCDMA systems suffer from two major network impairments that can severely limit the capacity of the system. The source of these impairments is examined while experimentally demonstrated techniques for the removal of such noise sources are also explored.

Chapter 3 concerns itself with the development and characterisation of an nonlinear optical thresholder and detector based on the nonlinear optical-to-electrical conversion process of TPA. The principle behind TPA is discussed and a TPA-based detector is characterised in terms of its nonlinear output as a function of input optical power. The feasibility of using such a TPA-based device is demonstrated both experimentally and through simulation models. The performance improvement gained through the use of a TPA-based detector in comparison to standard detection techniques in an OCDMA system is investigated experimentally in a four-channel OCDMA system.

Chapter 4 explores the operation of two other optical devices whose nonlinear responses can be used for noise suppression in OCDMA systems; a saturable absorber and a semiconductor optical amplifier. The operating principle behind both of these devices as nonlinear

optical elements is presented. Experimental work shows that the addition of both an SA and an SOA to a receiver containing a TPA-based device can successfully suppress noise sources present on a decoded OCDMA signal.

Chapter 5 compares the performance of an OCDMA system using linear detection, an SA-SOA receiver and a Mamyshev filter-based receiver. A Mamyshev filter has been used in optical networks as an optical regenerator and has also been successfully demonstrated as an optical thresholder in OCDMA systems. A Mamyshev filter was constructed and characterised in terms of its nonlinear response. The performance of an optical system was experimentally demonstrated for all three receiver structures. These performance results are analysed and the improvement that can be gained by using the nonlinear receivers is ascertained.

Chapter 6 presents a brief summary and discusses the conclusions that can be drawn from the work presented in this thesis.

Chapter 1

High-Speed Optical Networks

1.1 Introduction

The demonstration of the first functional laser in 1960 [1] and the development of an optical waveguide in 1966 [2] marked the beginning of modern optical communication networks. From these demonstrations came the first generation of optical communication networks with the development of a GaAs semiconductor laser operating at 0.8 μm and a low-loss optical fibre in 1980 [3]. These networks operated at data rates of 45 Mb/s with repeater spacings of 10 km. It was quickly realised that the transmission distance between repeaters in these first generation optical networks could be increased by operating in the wavelength region near 1.3 μm. The reason for this was due to the low fibre loss and minimum dispersion experienced in an optical fibre at these wavelengths. Hence a worldwide effort was undertaken to develop InGaAsP semiconductor devices operating at 1.3 μm eventually resulting in second-generation lightwave systems operating at bit rates of up to 1.7 Gb/s with a repeater spacing of about 50 km in 1987.

The third generation networks shifted the operational wavelength once again, this time to 1.55 μm to take advantage of the low 0.2 dB/km loss in silica fibres at this wavelength. While dispersion is a problem at this wavelength, a solution could be found through the use of dispersion-shifted fibres or a single-mode laser transmitter. As a result, third generation optical networks operating at 2.5 Gb/s were available in 1990. The next major breakthrough occurred with the advent of optical amplification and optical multiplexing techniques. By 1990, comerically available optical amplifiers allowed for repeater spacings of 60–80 km with optical multiplexing techniques pushing data rates of fourth generation networks into the Tb/s range [3]. Current fifth generation networks focus on extending the wavelength range over which the data can be transmitted in addition to using optical multiplexing and

advanced modulation formats to increase the capacity of an optical link. An example of the enormous capacity of these networks was shown in 2010 with an experimental demonstration of a 240 km optical link with a capacity of 69.1 Tb/s [4].

The widescale adoption of optical communication networks and the proliferation of optical fibre through all layers of modern networks is clearly demonstrated in recent statistics presented by the organisation for economic co-operation and development (OECD) which show that fibre subscriptions now comprise 9% of all broadband connections in the OECD, with fibre accounting for 45% of all subscriptions in Japan and 39% in Korea. This movement of fibre-based subscriptions closer to the end user is due to the increase in high-bandwidth applications such as video-on-demand, mobile telephony, online gaming, high definition TV (HDTV) and internet-based services. To accommodate this increase in demand, network providers must employ some form of multiplexing to exploit the bandwidth capabilities of a single optical fibre in a cost-effective manner throughout the entire network and not just the backbone/core section of the network.

This chapter discusses a number of multiplexing techniques; electrical time division multiplexing (ETDM), wavelength division multiplexing (WDM), optical time division multiplexing (OTDM) and optical code division multiplexing (OCDM). Common network topologies will also be discussed with particular emphasis on access networks, both current and future all-optical alternatives.

1.2 Multiplexing Techniques

To increase the capacity of an optical link beyond the limit available for serial transmission, a service provider can either install an additional fibre or to use some form of multiplexing. Multiplexing allows multiple channels to be transmitted simultaneously over a single optical fibre, giving network providers access to the large bandwidth capabilities of a single fibre which can lead to increased throughput in the network without laying additional fibre. Optical multiplexing can be achieved through multiplexing either in the time domain, wavelength domain or some hybrid of both.

1.2.1 Electrical Time Division Multiplexing

Electrical time division multiplexing (ETDM) is a solution available to network providers for increasing channel bit rates while also aiming to reduce the footprint, management effort and complexity of the system [5]. Figure 1.1 shows a basic ETDM system. A number of incoming data signals are electrically multiplexed to form a single electrical signal. This

2

Fibre Transmission Line

DFB: Distributed Feedback Laser
EDFA: Erbium Doped Fibre Amplifier
MOD: Optical Modulator
MUX: Electrical Multiplexer
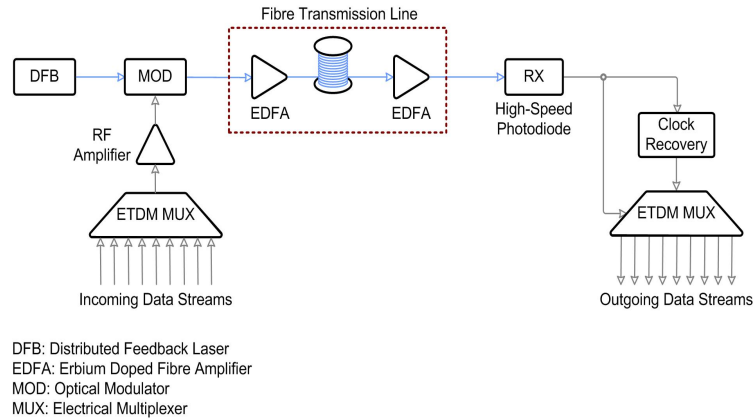
Figure 1.1: Basic Electrical Time Division Multiplexing system

aggregate electrical signal is then amplified using an electrical amplifier and is used to modulate an incoming optical carrier via a high-speed optical modulator. The optical signal then propagates over the fibre network where it is detected at the end by a high-speed photodiode. Clock recovery is applied to the resultant electrical signal in order to demultiplex the aggregate signal back into its constituent data signals using an electrical demultiplexer.

As 10 Gb/s systems are widely deployed, the next generation of systems are expected to move to higher data rates of 40 Gb/s, 100 Gb/s and higher. As the data rate continues rise, it becomes an increasing difficult task to implement ETDM due to a number of problems [6]. Firstly, high-speed lithium-niobate modulators require a large voltage swing of the applied modulation signal of several volts. This high voltage requirement is difficult to provide as the bandwidth increases. While 85.4 Gb/s ETDM transmission using a litium-niobate modulator driver has been experimentally demonstrated [7], when considering data rates of 100 Gb/s, packaging of electrical amplifier chips while maintaining sufficient bandwidth and gain remains difficult. One alternative would be to use an electroabsorption modulator (EAM) which has both a small footprint and steep modulation characteristic. An EAM operating at 40 Gb/s has been demonstrated in [8] using only a 1.1 V modulation swing.

ETDM also suffers from speed limitations at the receiver side. Experimental demonstrations of unitraveling carrier photodiodes operating at 100 Gb/s [9] have been shown, however the disadvantage of such a device is that the electrooptic bandwidth depends on the optical power. As a result, for best operation an optical power of more than + 14 dBm is required due to the low responsivity of the device. If the line rate of next-generation networks move to 40 Gb/s and and beyond through the use of advanced modulation formats, existing

3
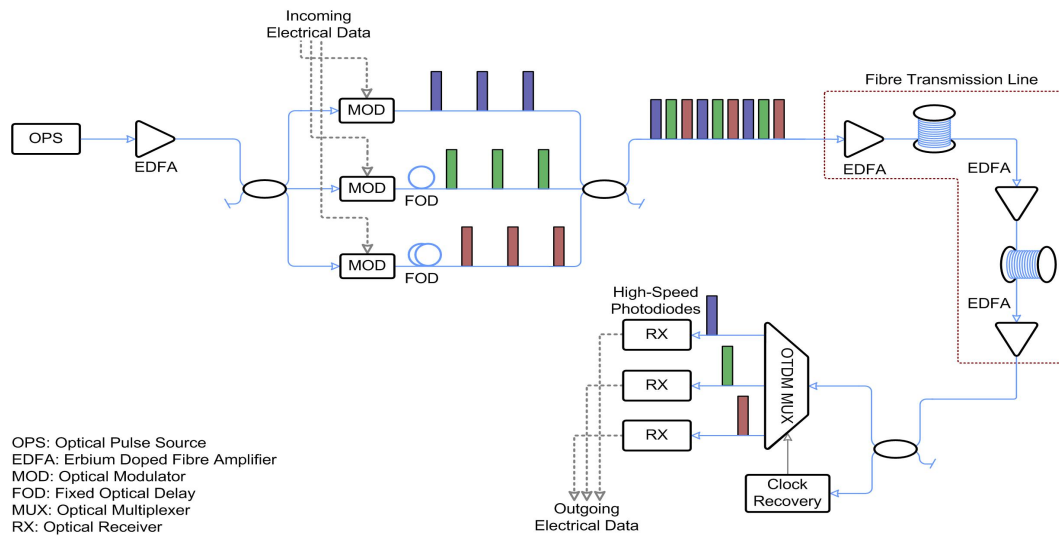
Figure 1.2: Basic Optical Time Division Multiplexing system.

electronic and optoelectronic technologies mean that an ETDM system operating at such a speed is currently difficult to achieve.

1.2.2 Optical Time Division Multiplexing

Optical time division multiplexing (OTDM) is an optical multiplexing technique that can be used to increase transmission rates up to and beyond 160 Gb/s, exceeding the current limit offered by ETDM. Recent demonstrations have shown that terabit-capacity OTDM with a single wavelength channel is possible [10, 11]. Figure 1.2 shows a basic OTDM system. An OTDM system operates by allocating each channel a specific bit slot in which to transmit its data. An optical pulse source generates a train of optical pulses at a repetition rate R. This pulse train is amplified to compensate for the losses experienced when the pulses are split into N copies using an optical splitter. Each pulse train is then modulated with an independent electrical data signal via an optical modulator resulting in a return to zero (RZ) data signal. Each optical signal is passed through a fixed fibre delay that delays each channel by $1/RN$ relative to each other, positioning each channel in its assigned bit slot. The optical signals are combined using an optical coupler, are amplified and transmitted over the optical link. At the receiver, optical clock recovery is performed to optically demultiplex the aggregate signal back into its constituent signals with are subsequently detected using a high-speed photodiode.

At the transmitter, one of the key components is the optical pulse source. The pulses

from this source must exhibit low temporal jitter, a high extinction ratio, low amplitude noise and have a pulse width that is significantly shorter that the bit period of the multiplexed signal [12]. Two examples of this would be through the use of a mode-locked laser diode [13] or by pulse carving using an EAM [14]. At the receiver side, optical clock recovery and demultiplexing is required to retrieve the constituent channels from the aggregate signal. A number of different demultiplexing techniques have been experimentally demonstrated to operate at 160 Gb/s, including electro-absorption modulators [15] four-wave mixing (FWM) in semiconductor optical amplifiers [16] and a terahertz optical asymmetric demultiplexer [17]. Optical clock recovery can be performed using an optoelectronic hybrid phase-locked loop (PLL) [18] or a self-pulsating laser diode [19]. However, as OTDM move towards 160 Gb/s transmission, the management and limits imposed regarding optical signal-to-noise ratio (OSNR), dispersion compensation, fibre nonlinearity and polarization mode dispersion (PMD) become more strict. While a number of techniques such as forward-error-correction [20], carrier-suppressed return-to-zero (CS-RZ) and RZ-differential-phase-shift-keying (RZ-DPSK) modulation formats [21, 22], have been introduced to limit the impact of dispersion and non-linearities on the system, 160 Gb/s OTDM is still in the development stage. An alternate multiplexing technique to OTDM is wavelength division multiplexing (WDM) where multiplexing is performed in the wavelength domain to increase the overall system capacity.

1.2.3 Wavelength Division Multiplexing

Wavelength division multiplexing (WDM) is a multiplexing technique that divides the available transmission spectrum up into specific wavelength bands over with each channel transmits its data. By assigning each channel a specific wavelength the overall data rate of the network can be vastly increased by more efficient use of the available fibre bandwidth [23]. Figure 1.3 shows a typical WDM system. Each optical source operates at a given wavelength with a narrow linewidth and is modulated either directly or externally with the electrical data to be transmitted. The multiple wavelengths from each source are multiplexed together and transmitted across the network. At the receiver side, each wavelength is demultiplexed from the aggregate signal using either optical filters tuned to each wavelength channel or using an arrayed waveguide grating (AWG) [24]. Each wavelength channel is then detected using a photodetector.

In WDM systems broadband optical amplification is one of the most important issues, with wide scale deployment of WDM systems resulting from the development of the erbium-doped fibre amplifier (EDFA) [25]. The transmission capacity of the network can be increased by increasing the bands over which an optical signal can be amplified. With the
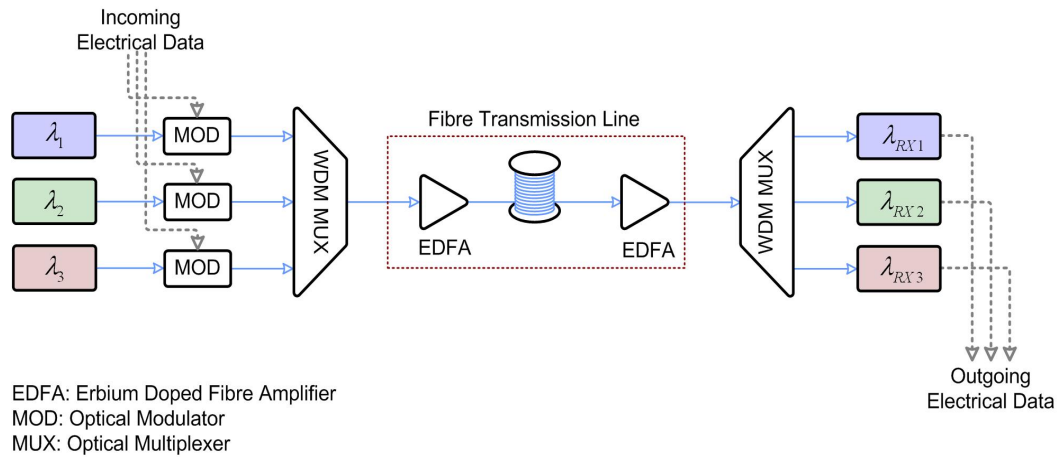
Figure 1.3: Basic Wavelength Division Multiplexing system.

development of optical amplifiers that can operate from 1480 nm to 1580 nm, the feasibility of transmission over 100 nm has been demonstrated [26]. This increase in operating bandwidth can be used in conjunction with narrower channel spacing to improve network capacity and efficiency. Channel spacing in current WDM systems can be as low as 50 GHz as given by the International Telecommunications Union (ITU) standardised grid [27]. Recently, dense WDM (DWDM) and ultra DWDM (UDWDM) employing channel spacings of 25 GHz and 12.5 GHz respectively have been demonstrated [28, 29]. However, as channel spacings become narrower care must be taken to ensure that the linewidth of each wavelength source is sufficiently small to avoid crosstalk with neighbouring channels. Some form of wavelength stabilisation is also required in UDWDM systems to prevent wavelength drift on each channel thus preventing channel interference. The bit rate of each WDM channel can be increased to 40 Gb/s or 80 Gb/s to increase the transmission capacity. However, as is the case for OTDM, as each wavelength channel transmits at higher bit-rates, techniques for the compensation of chromatic dispersion (CD) and PMD must be implemented [30, 31].

WDM system are popular with network operators because they allow them to expand the network without laying additional fibre or increasing the complexity of the system. Capacity of the network can be upgraded by simply upgrading the multiplexers and demultiplexers at each end. This ability to accommodate several generations of technology development without the need to overhaul the backbone network combined with the increased cost of scaling current synchronous optical network/synchronous digital hierarchy (SONET/SDH), has led to WDM becoming the primary network layer for current and future
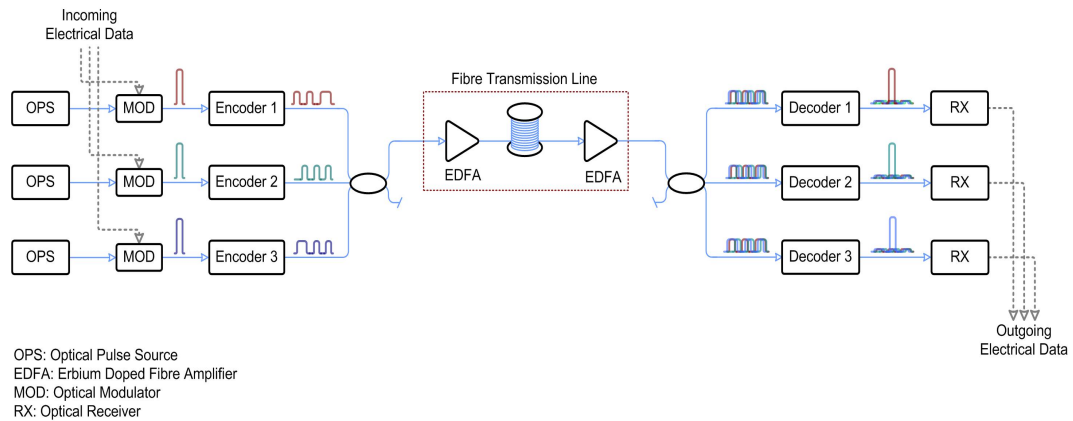
Figure 1.4: Basic Optical Code Division Multiplexing system.

service providers [32].

1.2.4 Optical Code Division Multiplexing

Optical code division multiplexing (OCDM) is an alternate multiplexing technique that has its origins in radio frequency (RF) communications [33, 34] but has been since applied to the optical domain due to a number of inherent advantages that the technique offers. Unlike WDM that provisions a dedicated wavelength per channel or OTDM that requires strict synchronisation between channels [35], OCDM provides channels with asynchronous access to the available bandwidth. As a result each channels transmission can overlap in both the time and wavelength domain. In such a system multiplexing is achieved through the use of optical codes. Each channel is assigned a unique optical code that is impressed upon the data before it is transmitted. Figure 1.4 shows a typical OCDM system. Each channel modulates an optical pulse train with the data for transmission. This data signal is then encoded using an optical encoder applying the optical code unique to that channel. The data signals from all channels are multiplexed asynchronously and transmitted over the network. At the receiver side, a copy of all transmitted data signals are passed to each decoder. The original signal is recovered by correlating the incoming aggregate signal with a stored version of the code used during the encoding process. The remaining data signals that do not match the decoding code remain improperly decoded.

As mentioned earlier OCDM offers several unique advantages such as asynchronous transmission, soft capacity on demand, the potential for secure transmission and quality of service control [36]. However OCDM does suffer from two main noise sources which can severely limit system performance. Multiple access interference (MAI) noise results from

7

the improperly decoded channels passing through the decoder and being incident on the photodetector. This MAI can limit system performance as it scales with the number of channels. The second noise source is optical beat noise (OBN) which is a result of square-law photodetection used in optical systems. Since the photodetector receives the signals from each channel these incident fields are mixed in the detector and can produce beating that occupies the same bandwidth of the desired signal. OBN can often exceed MAI in terms of limiting the performance of OCDM systems due to the fact that it scales with the number of detected fields, which is proportional to the number of channels [37]. A number of different techniques exist for the suppression/removal of MAI and OBN and will be discussed in greater detail in chapter two. OCDM technologies will also be discussed in greater detail in chapter two, with MAI and OBN suppression in OCDM system using nonlinear optical devices forming the main body of work completed for this thesis.

1.3   Network Topology

As high-bandwidth and on-demand applications continue to emerge, next-generation optical networks need to evolve from relatively static networks towards being more reconfigurable, having increased capacity, resiliency and the ability to carry a vast array of services. This insatiable desire for bandwidth is not only forcing metro and access networks to develop more flexible all-optical networks but its also forcing core or backbone networks to embrace new enabling technologies that increase the overall capacity that can keep up with demand.

1.3.1   Core Networks

Core networks are the backbone of any optical communications systems. Figure 1.5 shows a possible optical communication network showing the core, metro and access layers. The core network consists of a number of nodes interconnected by amplified fibre links using WDM. These networks are required to have terabit per second transmission capacity while also being capable of traveling over thousands of kilometers between transmitter and receiver. Legacy core networks typically operate at line rates of 2.5 Gb/s or sometimes 10 Gb/s with a total fibre capacity of 50-200 Gb/s [38]. The nodes in these legacy networks are generally optical-electrical-optical (OEO) based with all traffic routed through a node converted to the electrical domain irrespective of whether or not it was intended for that node. However, if fibre moves closer to the end consumer as envisaged through deployment such as fibre-to-the-home (FTTH) and provide the end user with data rates of up to 100 Mb/s, there will be a considerable strain on the core network. As a result, recent network deployments have introduced the optical bypass which allows data transiting the node
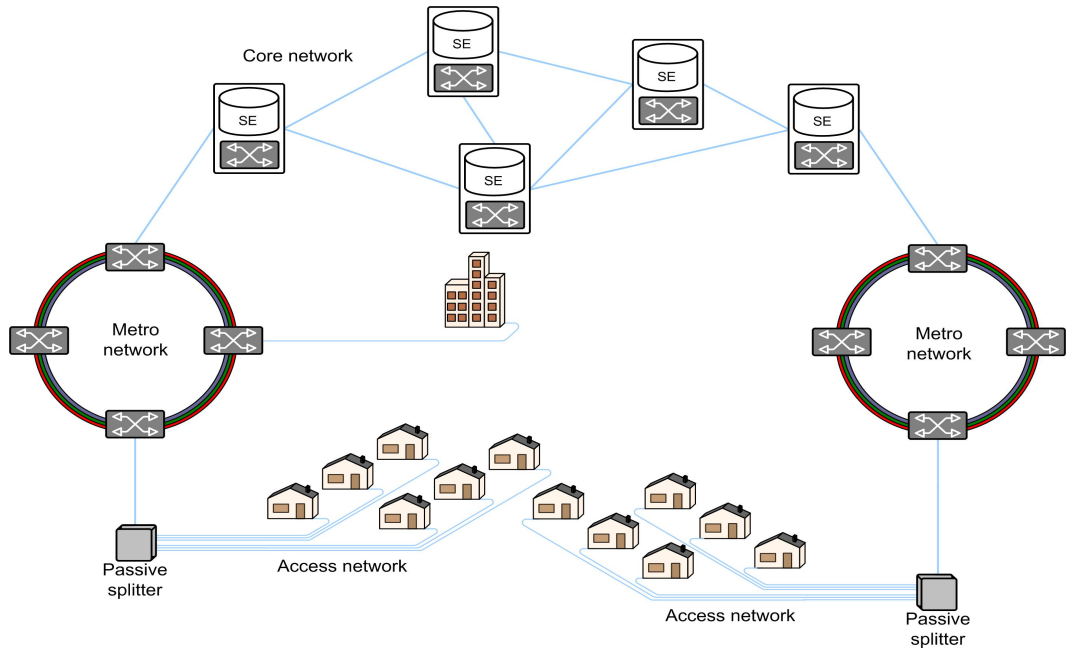
Figure 1.5: Optical telecommunications network.

to remain in the optical domain instead of undergoing the OEO conversion. These optical bypasses have resulted in up to 90 % of required OEO regenerations being eliminated when compared to legacy networks [39]. The line rate of the recently deployed networks is 10 Gb/s with support for future upgrades to 40 Gb/s. The number of wavelengths has been increased, covering both the C and L bands using Raman amplifiers in conjunction with EDFAs. As a result, the capacity of each fibre can now be over 3 Tb/s [40].

As previously mentioned, data sent over the core networks needs to travel over thousands of kilometers and still be detectable at the receiver. These large distances represent a significant challenge in core networks as a number of optical amplifiers are required to overcome attenuation losses in the fibre which results in the accumulation of amplified spontaneous emission (ASE) and a reduction of OSNR along the link [25, 41]. The OSNR at the receiver can be improved by increasing the transmit power, however, this increased optical power combined with the transmission distances in core networks can result in distortions of the signal due to nonlinear effects [42]. One method to overcome these effects is to use advance modulation formats in the network. Legacy networks originally used non-return-to-zero (NRZ) modulation however this moving towards RZ and chirped RZ (CRZ) [43, 44] which are both more tolerant to fibre nonlinearities. The RZ differential phase-shift keying (RZ-DPSK) modulation format has also been demonstrated in long-haul systems as it offers

a 3 dB sensitivity improvement over other formats while also having a significant tolerance to large amounts of accumulated dispersion [45].

1.3.2   Metro Networks

Metropolitan area networks (MANs) provide the link between the end consumers on the access network and long-haul core networks. With the increasing data rates being made available to users in the access networks, the metro networks, similar to the core networks, need to provide more reconfigurability and quick provisioning to meet demand. In Figure 1.5 the metro network is a ring network linking the consumers to the core network with a typical metro network spanning a maximum distance of ~ 280 km [46]. While a MAN is shared among fewer users than a core network, the network does need to interoperate with a range of traffic types such as internet protocol (IP), asynchronous transfer mode (ATM), Gigabit Ethernet etc [47]. As the distances covered in the network are much shorter than in the backbone networks, lower cost optical technologies can be used such as directly modulated lasers, less precise wavelength control, reduced need for regeneration etc. This is particularly important from the point of view of service providers as one of the main barriers to introducing new technology is cost. However, technology has matured to a point where the deployment of all-optical metro networks can be justified when serving large businesses, campuses etc.

Similar to core networks, metro networks suffer from a number of impairments that limit the size and performance of the network. These impairments include component insertion loss, noise accumulation, chromatic dispersion, laser frequency chirp and fibre nonlinearities [48]. Information can be added or dropped from the metro network to any of the access networks attached to the ring using an optical add/drop multiplexer (OADM) as shown in Figure 1.5. The OADM allows access to all wavelength channels in a WDM system and can be located at any point in the network to provide dynamic provisioning of services [49]. The OADM allows any incoming channel to be dropped; the information is passed to another fibre to continue to its destination. A replacement wavelength can be added and multiplexed with the remaining signal which then continues on through the network. These OADMs can also be reconfigurable (ROADM) with remote configuration of the add/drop multiplexer providing a more cost efficient method for the provisioning of services.

1.3.3   Access Networks

The access network, often referred to as the 'first/last mile', connects the consumer to the first node on the network and provides the gateway to the rest of the telecommunication net-
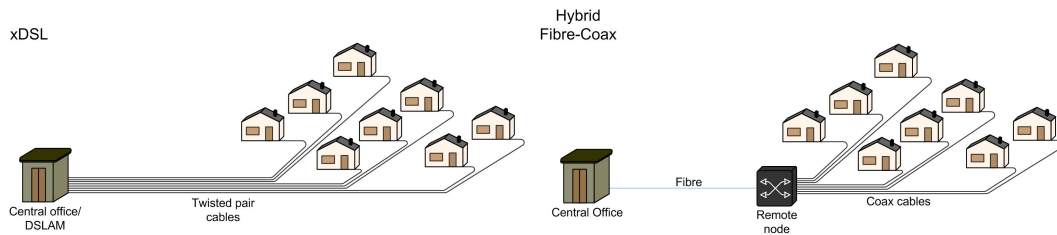
Figure 1.6: Typical access network layouts for ADSL and HFC.

work as shown in Figure 1.5. Although being the starting/ending point for large amounts of data through on-demand streaming, HDTV etc., access networks have yet to fully adopt fibre as the main transmission medium between the consumer and the service providers. One of the main impediments for optical access networks has been the high costs associated with directly replacing the copper network with fibre. This is due to the fact that this part of the network is provided to each customer on a unique basis i.e. a direct line from the premises to the network node, resulting in high deployment costs especially in rural networks where customers tend to be more geographically spread out than in urban networks. However, recently fibre-to-the-home (FTTH) has experienced double-digit growth in Europe, several Asian countries and the United States [50]. As a result, this "last-mile bottleneck" has received a lot of attention in the research community in how to best implement an all-optical access network and is discussed in more detail in the next section.

1.4 Optical Access Networks

Fibre has been envisioned as a provider of broadband services to residential customers for 30 years. Although the first installed FTTH was trialled in Japan in 1977 [51], it has only recently become a viable alternative to current electrical connections. Most broadband connections today rely on networks comprised of ordinary telephone wire or some form of hybrid fibre-coax (HFC) connection. While these electrical solutions form the vast majority of connections at the present time, their bandwidth capabilities and short transmission distances prevent them from being capable of supplying the next-generation of broadband services.

1.4.1 Legacy Networks

The most widely deployed broadband connections currently are twisted-pair cables that were originally installed for telephone lines. While these lines were originally only intended to carry the 4 kHz plain-old-telephone service (POTS), service providers have recently used

11

many advanced transmission methods to maximize data throughput over these copper networks. These transmission technologies are generally termed as x digital subscriber loop (xDSL). Figure 1.6 shows an asymmetric digital subscriber loop (ADSL). In this type of network data sent from each customer premises is transmitted along its twisted pair copper cable to a remote digital-subscriber line-access multiplexer (DSLAM). This DSLAM is generally located in the central office of the service provider and is used to aggregate the multiple lower data rate streams into a higher speed signal for transmission over the network. For distances up to a maximum of 2.4 km ADSL can deliver about 8 Mb/s to each customer [52].

The second most deployed access network medium is coaxial copper cable used for the transmission of TV signals. Since an analog TV channel has a bandwidth of 8 MHz, it is almost impossible to transmit a TV signal over twisted pair copper cables for any significant distance. As a result, TV providers opted for coaxial cable due to the much larger bandwidths available since the electrical signal is guided between an inner conductor and a grounded outer shield. However there are limits on the transmission distances using coax cable resulting from the need for electrical amplifiers every 100 to 200 m. To overcome this distance limitation a combination of fibre and coax cables can be used to form a hybrid fibre-coax (HFC) network which can also be used as broadband connections [53]. A HFC network is shown in Figure 1.6. In this type of network data transmitted from each customer travels down the coax cable to a remote node. This remote node then multiplexes the electrical signals into a higher rate signal that is converted to the optical domain and transmitted down an optical fibre to the central office. The advantages of such a system are the removal of electrical amplifiers between the central office and the remote node and a reduced distance that the signal must travel while in the electrical domain, improving data rates. These networks typically use quadrature amplitude modulation (QAM) techniques that allow a maximum downstream data rate of 2.8 Gb/s and an upstream data rate of 150 Mb/s [54]. However since there are typically 500 – 1000 subscribers on a given node, the bandwidth per subscriber is 2.8 – 5.6 Mb/s for the downstream data and 0.15 – 0.3 Mb/s for the upstream data.

The major advantage to using either xDSL or a HFC network is that they leverage the existing legacy infrastructure to provide data transmission. However as bandwidth demands continue to increase, more complex technologies and modulation formats are required to increase data rates on these bandwidth limited networks. This results in high operational costs associated with the upgrading, powering and maintaining of mostly electrical equipment. Therefore, the logical step forward would be an all-optical network with fibre connections

TDMA PON
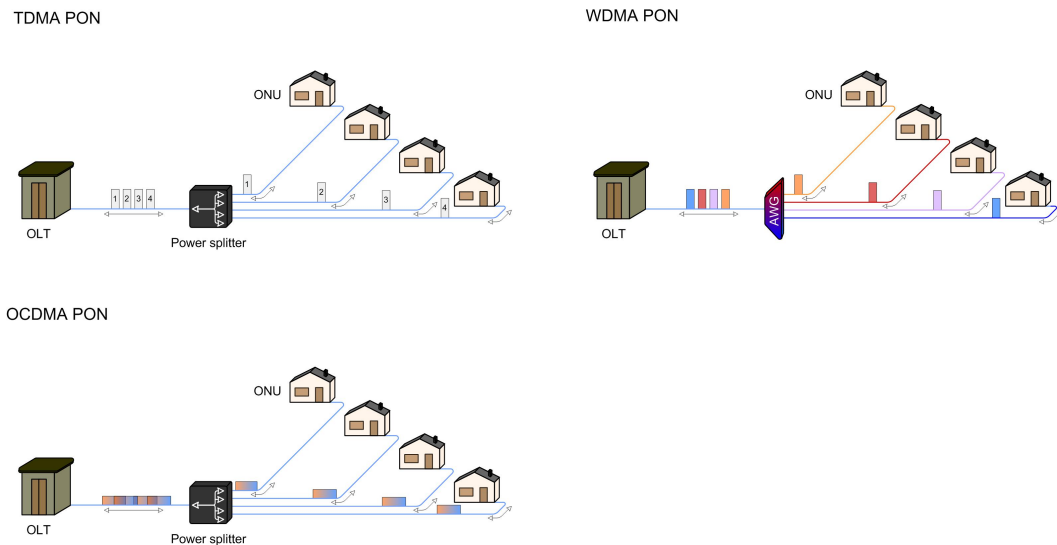
WDMA PON

OCDMA PON

Figure 1.7: Typical layout of TDMA-PON, WDMA-PON and OCDMA-PON.

provided to each consumer through deployments such as FTTH.

1.4.2   Passive Optical Networks

While advanced modulation technologies can be used to squeeze out every bit of bandwidth from current legacy networks, this practice can't continue to cope with the increasing demands for bandwidth. Passive optical networks (PONs) are seen as the only viable alternative that can cope with both the capacity demands while also providing these high data rates over transmission distances much larger than those achievable through DSL. In this architecture a feeder fibre runs from the central office to a remote node. This remote node contains a passive optical device that connects the fibre from the central office to the multiple fibres that run to each subscriber. An optical line termination (OLT) in the central office manages the transmissions from each subscriber. At the subscriber end, an optical network unit (ONU) is used to convert the incoming optical signals into the electrical domain. A PON infrastructure can be implemented using a number of schemes; time-division multiple access (TDMA), wavelength-division multiple access (WDMA) or code-division multiple access (CDMA). These schemes make use of the multiplexing techniques discussed in section 1.2 to provide access to the network for users.

1.4.2.1 Time-Division Multiple Access PON

The two most common PON variants which are currently being used in mass roll-outs are gigabit PON (GPON) and ethernet PON (EPON). Both of these networks make use of TDMA PON [55]. A typical TDMA PON layout is shown in Figure 1.7. In these PON infrastructures each subscriber is assigned a dedicated time slot in which they can access the available bandwidth. The passive power splitter couples $1/N$, where N is the number of subscribers, of the power from each subscriber into the feeder fibre which is transmitted back to the central office. The OLT at the central office is in charge of assigning the time slots used by each user to ensure that there are no collisions of the data streams. As a result the OLT requires precise time-delay information to each ONU to avoid packet overlap. This is achieved through ranging, however this ranging process needs to be repeated periodically since the time delays can change over time due to temperature effects on the individual fibres. This process is only important for upstream transmission as the OLT controls how the multiple signals are multiplexed together for downstream transmission.

TDMA PONs also require a burst-mode receiver at the OLT that needs to adjust its clock synchronisation and receiver gain for each transmission from the different subscribers [56]. These receivers can be technically challenging due to the requirement of a wide dynamic range for the different incoming burst signals and a short guard time for the clock synchronisation process. In a TDMA PON, unused capacity resulting from some ONUs not transmitting, can be reassigned through dynamic bandwidth allocation, however this adds to the complexity of the control algorithm for the PON. Due to the nature of TDMA PONs, it is believed that they cannot cope with the requirements of future network evolution with respect to aggregated bandwidth and that the insertion losses associated with the splitting ratio will limit the attainable link length [55]. One solution that could mitigate these problems is a WDMA PON.

1.4.2.2 Wavelength-Division Multiple Access PON

In a WDMA PON, similar to that shown in Figure 1.7, each subscriber is assigned a pair of dedicated wavelengths, one for the upstream data and one for the downstream data. This is opposed to a TDMA PON where a pair of wavelengths are shared among the subscribers for the up and downstream transmissions. As a result, each subscriber in a WDMA PON is independent and can transmit at any time without interfering with other channels, eliminating the management issues associated with sharing the network. In comparison to TDMA, WDMA employs a WDM multiplexer, such as an arrayed waveguide grating (AWG), at the remote node instead of a power splitter. An advantage of this is the insertion loss at the

node is considerably smaller and independent of the splitting ratio. Another advantage of a WDMA PON is there is no requirement for burst-mode receivers or a control algorithm to manage transmissions, resulting in simpler network operation. There are however a number of challenges associated with a WDMA PON. Firstly, each ONU requires a wavelength specific source that matches the wavelength profile of the AWG at the remote node. This is difficult to implement in a cost-effective manner as both the wavelength profile of the AWG and the lasing wavelength of the source in the ONU can vary due to environmental changes. A second disadvantage of a WDM PON is that the OLT requires a separate transceiver for each subscriber. Therefore $2N$ transceivers are required for the subscribers ONU's and the OLT compared to $N + 1$ transceivers for a TDMA PON.

Despite the difficulties associated with a practical implementation of a WDMA PON, a successful field trail of a WDMA PON has been carried out in Korea [57]. This network uses a broadband light source at the OLT to wavelength lock the Fabry-Pérot (FP) laser in each ONU while also aligning it with the respective wavelength profile of the AWG, mitigating the problem of wavelength drift between the AWG and the ONU laser. Optical comb generation, in which a number of uniform wavelengths are generated a by single laser, has been proposed as a cost-efficient solution to generate the entire wavelength grid using a single source [58]. At the ONU, a shared-source solution has been investigated that aims to eliminate the optical source at the ONU, making it more cost efficient while also reducing the risk of the source wavelength deviating and interfering with adjacent channels. This solution uses a partially modulated signal in the downstream that is split at the ONU with half of the signal remodulated and used in the upstream. A semiconductor optical amplifier (SOA) can be used to both amplify and remodulate the data signal [59]. Although there are a number of challenges to be overcome, it is clear that through field trails and experimental demonstrations, WDMA PON variants have the potential for a unified optical access and backhaul network.

1.4.2.3   Optical Code-Division Multiple Access PON

Since the first experimental demonstration of OCDMA [60] it has been seen as an alternative multiplexing technique to both WDM and OTDM with a number of inherent advantages such as asynchronous transmission, fair division of bandwidth and quality of service control. However, it is only recently that the maturity of all-optical devices required for OCDMA have reached a point where OCDMA can be considered a viable method of transmission in access networks. Device technologies for optical encoding/decoding have demonstrated the ability to encode/decode record length sequences [61], while there has been significant progress in optical thresholding technologies [62, 63]. A typical OCDMA

PON is shown in Figure 1.7. In this network each ONU is assigned a unique optical code that allows them to share the same time slot and bandwidth asynchronously, ideally without interference. As in the case for the TDMA PON, a passive splitter is used at the remote node to combine the individual transmissions onto the feeder fibre back to the OLT.

Despite the interest in OCDMA, it has only recently been explored as a technology for PONs [64] with an analysis of a 32-node EPON that uses OCDMA presented in [65]. Although this network used synchronisation, a bit error rate (BER) of less than 1×10^{-9} was achievable for all 32 nodes. OCDMA has also been considered for use with a WDMA PON to form a hybrid network for FTTH [66]. In this architecture, OCDMA is overlaid on a coarse WDM (CWDM) system to provide symmetric gigabit channels. This network also takes advantage of the reflection spectrum notches present in the encoder/decoders to suppress WDM interchannel crosstalk. Other promising results have come from a field trial carried out on an 80.8 km link on the Boston-South Network (BOSSNET) [67]. This field trial utilized a compact, integrated multiport AWG-pair encoder/decoder that could support code lengths up to 64 chips. Error-free transmission for two-channels operating at 2.5 Gb/s over 80.8 km without forward error correction (FEC) was demonstrated.

The major drawback associated with OCDMA is the presence of multiple access interference (MAI) and optical beat noise (OBN) discussed briefly in section 1.2.4. These noise sources severely limit the performance of an OCDMA system meaning successful suppression or rejection of both is key to enabling future deployments. One promising technique for the suppression of MAI and OBN is the use of nonlinear effects present in semiconductor devices which could provide a compact, integrated, cost-effective solution for future OCDMA PONs. This technique of noise suppression using semiconductor devices form the main contribution of the work presented in this thesis.

1.5 Summary

The global demand for bandwidth continues to increase at pace with the growth of video and image-based services, HDTV and peer-to-peer services. These services are forcing networks to become more flexible and to accommodate higher bandwidths. While advances in core network technology mean that these networks can handle the increased traffic volume, operational bottlenecks may be shifted to the metro, and in particular the access network. In the next generation of all-optical metro networks, capacity demands will be meet with DWDM. However in the metro and access networks, factors such as cost efficiency, reconfigurability and network complexity become major determinants in the development of

these networks. It is envisaged that the final electrical bottleneck in the access layer can be removed by replacing current electrical networks with optical fibre-based technology through deployments such as FTTH. It is widely accepted that these optical access networks will take the form of passive optical networks for their simplicity and cost-effectiveness. OCDMA is one technique proposed for use in PONs due to its inherent advantages over others. However, it suffers from a number of disadvantages that can also limit the performance of such networks. In this thesis, nonlinear optical devices are presented as a possible solution to these drawbacks that could be used as an compact, integrated and cost-effective solution in future OCDMA PONs.

References

[1] T. H. Maiman, "Stimulated optical radiation in ruby," *Nature*, vol. 187, pp. 493–494, 1960.

[2] K. C. Kao and G. A. Hockham, "Dielectric fiber surface waveguides for optical frequencies," *Proceedings IEEE*, vol. 133, pp. 1151–1158, 1966.

[3] G. P. Agrawal, *Fiber-optic communication systems*, 3rd ed. John Wiley & Sons Inc., 2002.

[4] A. Sano, H. Masuda, T. Kobayashi, M. Fujiwara, K. Horikoshi, E. Yoshida, Y. Miyamoto, M. Matsui, M. Mizoguchi, H. Yamazaki, Y. Sakamaki, and H. Ishii, "69.1 Tb/s (432×171 Gb/s) C- and extended L-band transmission over 240 km using PDM-16-QAM modulation and digital coherent detection," in *Proceedings of Optical Fibre Communications (OFC)*, San Diego, CA., 2010, paper PDPB7.

[5] E. Lach and K. Schuh, "Recent advances in ultrahigh bit rate ETDM transmission systems," *IEEE Journal of Lightwave Technology*, vol. 24, no. 12, pp. 4455–4467, 2006.

[6] E. Lach, K. Schuh, B. Junginger, G. Veith, J. Lutz, and M. Moeller, "Challenges for 100 Gbit/s ETDM transmission and implementation," in *Proceedings of Optical Fibre Communications (OFC)*, Anaheim, California, 2007, paper OWE1.

[7] K. Schuh, B. Junginger, H. Rempp, P. Klose, D. Rosener, and E. Lach, "85.4 Gb/s ETDM transmission over 401 km SSMF applying UFEC," in *Proceedings of European Conference on Optical Communications (ECOC)*, Glasgow, Scotland, 2005, post-deadline paper Th4.1.4.

[8] H. Fukano, T. Yamanaka, M. Tamura, and Y. Kondo, "Very-low-driving-voltage electroabsorption modulators operating at 40 Gb/s," *IEEE Journal of Lightwave Technology*, vol. 24, no. 5, pp. 2219–2224, 2006.

[9] Y. Muramoto, K. Yoshino, S. Jodama, Y. Hirota, H. Ito, and T. Ishibashi, "100 and 160 Gb/s operation of uni-travelling carrier photodiode module," *Electronics Letters*, vol. 40, no. 6, pp. 378–380, 2004.

[10] M. Nakazawa, T. Yamamoto, and K. R. Tamura, "1.28Tb/s-70 km OTDM transmission using third- and fourth-order simultaneous dispersion compensation with a phase modulator," *Electronics Letters*, vol. 36, no. 24, pp. 2027–2029, 2000.

[11] H. G. Weber, S. Ferber, M. Kroh, C. Schmidt-Langhorst, R. Ludwig, V. Marembert, C. Boerner, F. Futami, S. Watanabe, and C. Schubert, "Single channel 1.28 Tbit/s and 2.56 Tbit/s DQPSK transmission," *Electronics Letters*, vol. 42, no. 3, pp. 178–179, 2006.

[12] H.-G. Weber, R. Ludwig, S. Ferber, C. Schmidt-Langhorst, M. Kroh, V. Marembert, C. Boerner, and C. Schubert, "Ultrahigh-speed OTDM-transmission technology," *IEEE Journal of Lightwave Technology*, vol. 24, no. 12, pp. 4616–4627, 2006.

[13] R. Ludwig, S. Diez, A. Ehrhardt, L. Kueller, W. Pieper, and H. G. Weber, "A tunable femtosecond modelocked semiconductor laser for applications in OTDM-systems," *IEICE Transactions on Electronics*, vol. E81-C, no. 2, pp. 140–145, 1998.

[14] M. D. Pelusi, Y. Matsui, and A. Suzuki, "Femtosecond optical pulse generation from an electro-absorption modulator with repetition rate and wavelength tuning," in *Proceedings of European Conference on Optical Communications (ECOC)*, Nice, France, 1999, pp. 26–27.

[15] H. Murai, M. Kagawa, H. Tsuji, and K. Fujii, "EA-modulator-based optical time division multiplexing/demultiplexing techniques for 160-Gb/s optical signal transmission," *IEEE Journal of Selected Topics in Quantum Electronics*, vol. 13, no. 1, pp. 70–78, 2007.

[16] S. L. Jansen, M. Heid, S. Splater, E. Meissner, C. J. Weiste, A. Schopflin, D. Khoe, and H. De Waarth, "Demultiplexing 160 Gb/s OTDM signal to 40 Gb/s by FWM in an SOA," *Electronics Letters*, vol. 38, no. 17, pp. 978–980, 2002.

[17] J. P. Sokoloff, P. R. Prucnal, I. Glesk, and M. Kane, "A terahertz optical asymmetric demultiplexer (TOAD)," *IEEE Photonics Technology Letters*, vol. 5, no. 7, pp. 787–790, 1993.

[18] H. T. Yamada, H. Murai, A. R. Pratt, and Y. Ozeki, "Scalable 80 Gb/s OTDM using a modular architecture based on EA modulators," in *Proceedings of European Conference on Optical Communications (ECOC)*, Munich, Germany, 2000, paper P3.31.

[19] J. Slovak, T. Tekin, C. Bornholdt, B. Sartorius, E. Lach, M. Schmidt, S. Vorbeck, and R. Leppla, "Self-pulsating laser based all-optical clock recovery applied in 421 km field experiment for 170.6 : 42.7 Gbit/s OTDM demultiplexing," in *Proceedings of European Conference on Optical Communications (ECOC)*, Glasgow, Scotland, 2005, paper Th. 3.1.3.

[20] E. Lach, K. Schuh, M. Schimdt, B. Junginger, G. Charlet, P. Pecci, and G. Veith, "7 × 170 Gbits/s (160 Gbits/s + FEC overhead) DWDM transmission with 0.53 bit/s/Hz spectral efficiency over long haul distance of standard SMF," in *Proceedings of European Conference on Optical Communications (ECOC)*, Rimini, Italy, 2003, pp. 68–69.

[21] L. Möller, Y. Su, X. Liu, J. Leuthold, and C. Xie, "Generation of 160 Gb/s carrier-suppressed return-to-zero signals," in *Proceedings of European Conference on Optical Communications (ECOC)*, Remini, Italy, 2003, pp. 50–51.

[22] S. Feber, R. Ludwig, C. Boerner, A. Wietfield, B. Schmauss, J. Berger, C. Schubert, G. Unterboersch, and H. G. Weber, "Comparision of DPSK and OOK modulation format in 160 Gb/s transmission system," in *Proceedings of European Conference on Optical Communications (ECOC)*, Remini, Italy, 2003, pp. 1004–1005.

[23] M. J. O'Mahony, "Optical multiplexing fibre networks: Progress in WDM and OTDM," *IEEE Communications Magazine*, vol. 33, no. 12, pp. 82–88, 1995.

[24] B. Nyman, M. Farries, and C. Si, "Technology trends in dense WDM demultiplexers," *Optical Fiber Technology*, vol. 7, no. 4, pp. 255–274, 2001.

[25] T. Li, "The impact of optical amplifiers on long-distance lightwave telecommunications," *Proceedings of the IEEE*, vol. 81, no. 11, pp. 1568–1579, 1993.

[26] J. Kani, K. Hattori, M. Jinno, T. Kanamori, and K. Oguchi, "Triple-wavelength-band WDM transmission over cascaded dispersion-shifted fibers," *IEEE Photonics Technology Letters*, vol. 11, no. 11, pp. 1506–1508, 1999.

[27] International Telecommunications Union, "ITU-T recommendation G.694.1 spectral grids for WDM applications: DWDM applications," *Series G: Transmission systems and media, digital systems and networks*, vol. Transmission media characteristics-Characteristics of optical components and subsystems, no. G.694.1, 2002.

[28] G.Varaille and J. F.Marcerou, "1.8 Tbit/s 6500 km transoceanic NRZ system assessment with industrial margins using 25 GHz channel spacing," in *Proceedings of Euro-*

pean Conference on Optical Communications (ECOC), Copenhagen, Denmark, 2002, paper 9.1.3.

[29] H. Suzuki, M. Fujiwara, and K. Iwatsuki, "Application of super-DWDM technologies to terrestrial terabit transmission systems," *IEEE Journal of Lightwave Technology*, vol. 24, no. 5, pp. 1998–2005, 2006.

[30] S. Kuwahara, A. Hirano, Y. Miyamoto, and K. Murata, "Automatic dispersion compensation for WDM system by mode-splitting of tone-modulated CS-RZ signal," in *Proceedings of European Conference on Optical Communications (ECOC)*, Copenhagen, Denmark, 2002, paper 6.1.3.

[31] M. Schmidt, M. Witte, F. Buchali, E. L. andE. Le Rouzic, S. Salaun, S. Vorbeck, and R. Leppla, "8 × 170 Gb/s DWDM field transmission experiment over 430 km SSMF using adaptive PMD compensation," in *Proceedings of European Conference on Optical Communications (ECOC)*, Stockholm, Sweden, 2004, paper Th4.1.2.

[32] J. Berthold, A. A. M. Saleh, L. Blair, and J. M. Simmons, "Optical networking: Past, present, and future," *IEEE Journal of Lightwave Technology*, vol. 26, no. 9, pp. 1104–1118, 2008.

[33] G. R. Cooper and R. W. Nettleton, "A spread spectrum technique for high capacity mobile communications," *IEEE Transactions on Vehicular Technology*, vol. 27, no. 4, pp. 264–275, 1978.

[34] H. J. Kochevar, "Spread spectrum multiple access communication experiment through a satellite," *IEEE Transactions on Communications*, vol. 25, no. 8, pp. 853–856, 1977.

[35] H. Sotobayashi, W. Chujo, and K. Kitayama, "Highly spectrally-efficient optical code-division multiplexing transmission system," *IEEE Journal of Selected Topics in Quantum Electronics*, vol. 10, no. 2, pp. 250–258, 2004.

[36] X. Wang and K. Kitayama, "Analysis of beat noise in coherent and incoherent time-spreading OCDMA," *IEEE Journal of Lightwave Technology*, vol. 22, no. 10, pp. 2226–2235, 2004.

[37] D. D. Sampson, G. J. Pencock, and R. A. Griffin, "Photonic code-division multiple-access communications," *Fiber and Integrated Optics*, vol. 16, no. 2, pp. 129–157, 1997.

[38] A. A. M. Saleh and J. M. Simmons, "Evoution toward the next-generation core optical network," *IEEE Journal of Lightwave Technology*, vol. 24, no. 9, pp. 3303–3321, 2006.

[39] J. M. Simmons, "On determining the optimal optical reach for a long-haul network," *IEEE Journal of Lightwave Technology*, vol. 23, no. 3, pp. 1039–1048, 2005.

[40] D. G. Foursa, C. R. Davidson, M. Nissov, M. A. Mills, L. Xu, J. X. Cai, A. N. Pilipetskii, Y. Cai, C. Breverman, R. R. Cordell, T. J. Carvelli, P. C. Corbett, H. D. Kidorf, and N. S. Bergano, "2.56 Tb/s (256 × 10 Gb/s) transmission over 11,000 km using hybrid Raman/EDFAs with 80 nm of continuous bandwidth," in *Proceedings of Optical Fibre Communications (OFC)*, Anaheim, California, 2002, paper FC3-2.

[41] C. R. Giles and E. Desurvire, "Propagation of signal and noise in concatenated erbium-doped fiber optical amplifier," *IEEE Journal of Lightwave Technology*, vol. 9, no. 2, pp. 147–154, 1991.

[42] J. P. Gordon and L. F. Mollenauer, "Effects of fiber nonlinearities and amplifier spacing on ultra-long distance transmission," *IEEE Journal of Lightwave Technology*, vol. 9, no. 2, pp. 170–173, 1991.

[43] N. S. Bergano, "Wavelength division multiplexing in long-haul transoceanic transmission systems," *IEEE Journal of Lightwave Technology*, vol. 23, no. 12, pp. 4125–4139, 2005.

[44] B. Bakhshi, M. Vaa, E. A. Golovchenko, W. W. Patterson, R. L. Maybach, and N. S. Bergano, "Comparison of CRZ, RZ and NRZ modulation formats in a 64 × 12.3 Gb/s WDM transmission experiment over 9000 km," in *Proceedings of Optical Fibre Communications (OFC)*, Anaheim, California, 2001, paper WF4-1.

[45] A. N. Pilipetskii, "High-capacity undersea long-haul systems," *IEEE Journal of Selected Topics in Quantum Electronics*, vol. 12, no. 4, pp. 484–496, 2006.

[46] N. Madampopulos, M. D. Vaugh, L. Nederlof, and R. E. Wagner, "Metro network architecture scenarios, equipment requirements and implications for carriers," in *Proceedings of Optical Fibre Communications (OFC)*, Anaheim, California, 2001, paper WL2-1.

[47] A. A. M. Saleh and J. M. Simmons, "Architectural principles of optical regional and metropolitan access networks," *IEEE Journal of Lightwave Technology*, vol. 17, no. 12, pp. 2431–2448, 1999.

[48] N. Antoniades, A. Boskovic, I. Tomkos, N. Madamopoulos, M. Lee, I. Roudas, D. Pastel, M. Sharma, and M. J. Yadlowsky, "Performance engineering and topological design of metro WDM optical networks using computer simulation," *IEEE Journal on Selected Areas in Communications*, vol. 20, no. 1, pp. 149–165, 2002.

[49] K. Okamoto, K. Takiguchi, and Y. Ohmori, "16-channel optical add/drop multiplexer using silica-based arrayed-waveguide gratings," *Electronics Letters*, vol. 31, no. 9, pp. 723–724, 1995.

[50] "Europe breaks one million barrier FTTH council Europe," 2008. [Online]. Available: http://www.ftthcouncil.eu

[51] M. Kawahata, "Hi-OVIS (Higashi Ikoma optical visual information system) development project," in *Proceedings of Integrated Optics and Optical Communications (IOOC)*, 1977, pp. 467–471.

[52] P. E. Green Jr., *Fiber to the home: The new empowerment.* Hoboken, New Jersey: John Wiley & Sons, Inc., 2006.

[53] A. Paff, "Hybrid fiber/coax in the public telecommunications infrastructure," *IEEE Communications Magazine*, vol. 33, no. 4, pp. 40–45, 1995.

[54] X. Lin and O. Sneizko, "The evolution of cable TV networks," in *Optical Fiber Communications IVB*, I. Kaminow and T. Li, Eds. San Diego, California: Academic Press, 2002.

[55] K. Grobe and J.-P. Elbers, "PON in adolescence: From TDMA to WDM-PON," *IEEE Communications Magazine*, vol. 46, no. 1, pp. 26–34, 2008.

[56] C.-H. Lee, W. V. Sorin, and B. Y. Kim, "Fiber to the home using a PON infrastructure," *IEEE Journal of Lightwave Technology*, vol. 24, no. 12, pp. 4568–4583, 2006.

[57] C.-H. Lee, S.-M. Lee, K.-M. Choi, J.-H. Moon, S.-G. Mun, K.-T. Jeong, J. H. Kim, and B. Kim, "WDM-PON experiences in Korea," *Journal of Optical Networking*, vol. 6, no. 5, pp. 451–464, 2007.

[58] W. Mao, P. A. Andrekson, and J. Toulousse, "Investigation of a spectrally flat multi-wavelength DWDM source based on optical phase- and intensity-modulation," in *Proceedings of Optical Fibre Communications (OFC)*, Los Angeles, California, 2004, paper MF78.

[59] P. Healy, P. Townsend, C. Ford, L. Johnston, P. Townley, I. Lealman, L. Rovers, S. Perrin, and R. Moore, "Spectral slicing WDM-PON using wavelength-seeded reflective SOAs," *Electronics Letters*, vol. 37, no. 19, pp. 1181–1182, 2001.

[60] P. R. Prucnal, M. A. Santoro, and T. R. Fan, "Spread spectrum fiber-optic local area network using optical processing," *IEEE Journal of Lightwave Technology*, vol. LT-4, no. 5, pp. 547–554, 1986.

[61] X. Wang, K. Matsushima, A. Nishiki, N. Wada, F. Kubota, and K.-I. Kitayama, "Experimental demonstration of 511-chip 640 Gchip/s superstructured FBG for high performance optical code processing," in *Proceedings of European Conference on Optical Communications (ECOC)*, Stockholm, Sweden, 2004, paper Tu1.3.7.

[62] Z. Jiang, D. S. Seo, S.-D. Yang, D. E. Leaird, R. V. Roussev, C. Langrock, M. M. Fejer, and A. M. Weiner, "Four-user, 2.5-Gb/s, spectrally coded OCDMA system demonstration using low-power nonlinear processing," *IEEE Journal of Lightwave Technology*, vol. 23, no. 1, pp. 143–158, 2005.

[63] X. Wang, N. Wada, T. Hamanaka, K. Kitayama, and A. Nishiki, "10-user, truly-asynchronous OCDMA experiment with 511-chip SSFBG en/decoder and SC-based optical thresholder," in *Proceedings of Optical Fibre Communications (OFC)*, Anaheim, California, 2005, postdeadline paper PDP33.

[64] A. Stok and E. H. Sargent, "The role of optical CDMA in access networks," *IEEE Communications Magazine*, vol. 40, no. 9, pp. 83–87, 2002.

[65] J. Wu, F. R. Gu, and H.-W. Tsao, "Jitter performance analysis of SOCDMA-based EPON using perfect difference codes," *IEEE Journal of Lightwave Technology*, vol. 22, no. 5, pp. 1309–1319, 2004.

[66] X. W. Ken-Ichi Kitayama and N. Wada, "OCDMA over WDM-PON-solution path to gigabit-symmetric FTTH," *IEEE Journal of Lightwave Technology*, vol. 24, no. 4, pp. 1654–1662, 2006.

[67] R. P. Scott, V. J. Hernandez, N. K. Fontaine, F. M. Soares, R. Broeke, K. Perry, G. Nowak, C. Yang, W. Cong, K. Okamoto, B. H. Kolner, J. P. Heritage, and S. J. B. Yoo, "80.8-km BOSSNET SPECTS O-CDMA field trial using subpicosecond pulses and a fully integrated, compact AWG-based encoder/decoder," *IEEE Journal of Selected Topics in Quantum Electronics*, vol. 13, no. 5, pp. 1455–1462, 2007.

Chapter 2

Optical Code Division Multiple Access

2.1 Introduction

Code division multiple access (CDMA) principles have been investigated in the context of satellite and mobile radio communications since the late 1970's [1–4]. Since then CDMA has been successfully deployed in cellular telephony networks along with the global positioning system (GPS) satellite broadcast link. The success of CDMA in the wireless domain has inspired research on optical CDMA (OCDMA) with the aim of transferring the inherent advantages associated with CDMA technology to the optical domain. These advantages include flexible access to wide bandwidth, code-based dynamic reconfiguration, decentralized networking, passive code translation and a measure of security through data obscurity [5]. These benefits are particularly advantageous in an optical access network that is required to be flexible, scalable, reconfigurable and cost-efficient. OCDMA technology also allows asynchronous access to each user which is beneficial when considering traffic in an access network tends to be bursty in nature i.e. internet data. As a result, OCDMA provides a more efficient use and fairer division of bandwidth between the users in comparison to other multiplexing techniques.

OCDMA is a spread-spectrum technology where multiplexing is accomplished by encoding each data transmission with an optical code rather than assigning a wavelength or time-slot. This optical code is impressed upon the data to be transmitted with each optical code being unique to a given transmitter. This optical code requires a bandwidth much larger than that required for the transmitted data. As a result, the spectrum of the optical signal is broadened hence the term spread-spectrum. By assigning each transmitting channel with its own

unique optical code, OCDMA systems allow all transmitting channels overlap both temporally and spectrally, ideally without interfering. A copy of all transmitted signals added together is passed to all of the receivers. With the knowledge of the code used to encode the desired optical signal, a receiver extracts the desired data from the aggregate signal by comparing the coded multiuser stream with a copy of the desired code. If the codes match, the original data is recovered while codes that do not match are rejected.

The earliest demonstration of optical CDMA (OCDMA) was given in 1986 [6]. In that experimental demonstration, the CDMA concepts from radio frequency (RF) communications were directly applied to the optical domain using fibre delay lines to construct a temporal coding sequence. Since the publication of that paper, there has been significant progress in OCDMA in terms of the number of coding schemes that have been demonstrated [7–10] as well as the development of the all-optical technologies that enable such coding operations [11–13]. New families of optical code sequences were also developed to provide greater discrimination between the desired code and unwanted codes [14–17].

Despite the developments in related technologies to date, OCDMA systems suffer from a phenomenon known as multiple access interference (MAI) which limits the overall system performance as the number of active channels increases. MAI arises from the fact that a receiver receives a copy of all transmitted signals and not just the intended signal. Although the decoding operation recovers the desired signal with the remaining unwanted channels improperly decoded, these unwanted channels are still incident on the photodetector resulting in a background noise that scales as the number of users increases. To combat MAI, various optical time gating [18, 19] and optical thresholding [20–22] techniques have been experimentally demonstrated. Since all users share the same bandwidth, OCDMA also suffers from optical beat noise (OBN) which arises when all the incoming electric fields are mixed in the photodetector. OBN is a severe limitation in OCDMA as it scales with the square of the number of users [23]. Beat noise has been studied in relation to coherent and incoherent OCDMA [24] where it is determined that beat noise can be overcome through the use of a low-coherence source, longer optical codes or through the use of some form of synchronisation.

In this chapter, OCDMA encoding/decoding schemes and their enabling technologies are discussed in more detail while also discussing a number of popular optical code sequences. The main OCDMA impairments of MAI and OBN are also presented followed by the main mitigation techniques that are currently used.

2.2 OCDMA Encoding/Decoding

OCDMA is a multiplexing technique where each channel is distinguished by a unique optical code rather than by a wavelength or time-slot. Before transmission each data bit must undergo an encoding operation that optically encodes the data with the desired optical code. At the receiver, the data bit undergoes a decoding process that recovers the original data bit from the optical code sequence. OCDMA systems can be broadly categorized into two areas; incoherent OCDMA and coherent OCDMA. In an incoherent OCDMA system, encoding/decoding typically relies on intensity modulation and uses an incoherent optical source. In comparison, a coherent OCDMA system encodes/decodes the optical signal by manipulating the phase of the optical signal whose source is generally a highly coherent source such as a mode-locked laser. These two broad categories of OCDMA coding are discussed in more detail in the following sections.

2.2.1 Incoherent OCDMA Coding

In an incoherent OCDMA scheme the encoding/decoding process is based on the summation of optical powers. In the most basic implementation, unipolar codes that are long and sparsely weighted with optical pulses are used. Since the processing is done using the optical power of the pulses, the phase, frequency and spectral content of the codes are not important. As a result, incoherent OCDMA can generally be implemented more easily than coherent OCDMA and can also utilize lower cost wide-band incoherent sources. Incoherent OCDMA can be further divided up into temporal spreading, spectral-amplitude coding, spatial coding and two-dimensional (2D) wavelength hopping/time spreading (WHTS) depending on how exactly the intensity modulated code is applied. In this section the main incoherent encoding/decoding schemes are discussed in more detail.

2.2.1.1 Temporal Spreading Coding

Temporal spreading was the first encoding/decoding scheme experimentally demonstrated for OCDMA in 1986 [6]. In this scheme, each bit period is divided into N_T smaller time intervals, called chips, with N_T being the length of the code used. The optical code is then formed by placing short optical pulses at different chip positions where the number of pulses used in the optical code is the weight of the code. Two examples of these temporally spreading codes are shown in Figure 2.1 (a). A general implementation of a temporal spreading scheme is shown in Figure 2.1 (b) utilizing tapped delay lines and modulators to generate the optical code. Decoding of a temporally spreading optical code is achieved by using the conjugate version of the code in the decoder, which can also be realised using fibre delay lines. In the decoder, the intensities of the chip pulses are summed together at a
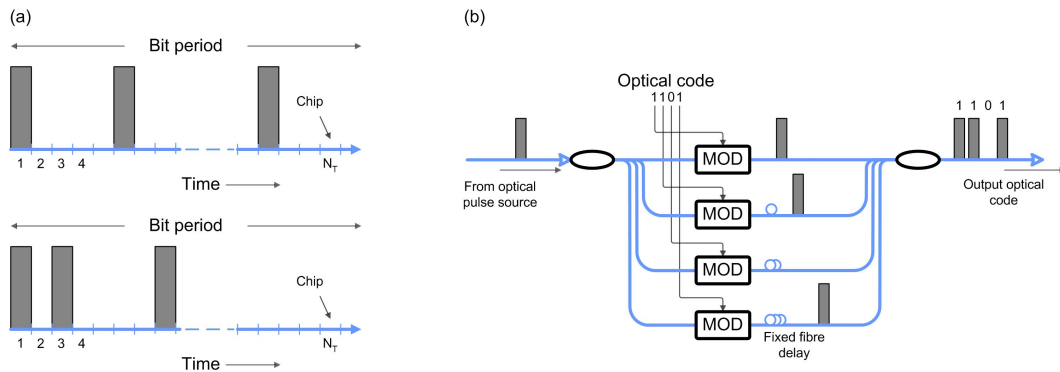
Figure 2.1: (a) Examples of two temporally spread code sequences and (b) One method for the implementation of the code sequences shown in (a).

single chip slot, giving an auto-correlation peak representing the original data pulse.

Time spreading optical codes can be implemented quite easily but are limited due to a number of factors. Firstly due to the fact that processing is performed using optical intensities, long code lengths are required to ensure a satisfactory level of discrimination between the desired and unwanted codes. This requirement for long optical codes sequences leads to a trade-off between optical pulse widths used and the data rate of the channel. If the data rate of the channel is set, meaning the given bit period is a set value, then a longer code must use narrower optical pulses to accommodate the longer code sequence. Conversely, if the optical pulse widths remain constant, then the highest achievable data rate for the channels must drop to allow enough space for a longer optical code.

Temporal spreading OCDMA can be implemented using prime codes [6, 16] or using optical orthogonal codes (OOCs) [15, 25]. OOCs are a set of code sequences that are designed to provide the optimal auto- and cross-correlation responses. However, these codes require large code lengths to support a moderate number of users while also using a sparse code weight.

2.2.1.2   Spectral Amplitude Coding

Spectral amplitude encoding (SAE) was first investigated in [8, 26]. In spectral amplitude OCDMA (SA-OCDMA) coding is performed in the wavelength domain rather than the time domain. The advantage of this is that the spectral nature of the codes is decoupled from the temporal nature of the data resulting in the code length being independent of the data rate. This is in direct contrast with time domain coding where the code length used and
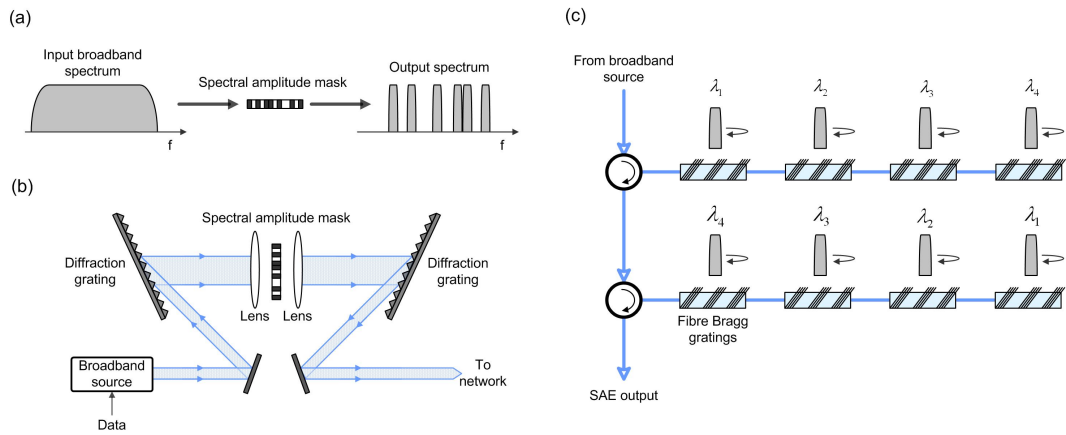
Figure 2.2: (a) Spectral amplitude encoding principle (b) Implementation of spectral amplitude encoding using diffraction gratings and spatial masks and (c) Implementation using fibre Bragg gratings.

the highest achievable data rate are connected. The principle of SA-OCDMA is shown in Figure 2.2 (a) where a large broadband spectrum is passed through an amplitude mask that encodes the incoming spectrum according to the given optical code. This spectral mask is divided up into frequency bins that modulate the amplitude of the frequency components. The number of frequency bins that can be resolved by the encoder dictate the code length used. Figure 2.2 (b) shows how this principle can be implemented using a bulk 4-f optical system. A broadband optical source is modulated with the data signal before the frequency content of the signal is spatially dispersed using a uniform diffraction grating and a lens. The spatially dispersed signal is then amplitude modulated by a suitable mask that contains the optical code. Finally a second lens and diffraction grating are used to recombine the filtered spectrum.

An alternative to using the bulk 4-f system for spectral amplitude filtering is to use fibre Bragg gratings (FBGs) to filter select wavelengths from a broadband spectrum according to a given code [27]. This implementation using FBGs is shown in Figure 2.2 (c). A linear array of FBGs can be used with each one centered at a particular wavelength as designated by the optical code. The reflected spectrum from each FBG in the array corresponds to a "1" bit in the code with the transmitted spectrum corresponding to the complementary code. However, due to the physical separation of the gratings, the wavelengths will also be separated in time, similar to the effects of chromatic dispersion. One solution is to use an identical array of FBGs but in reverse order to compensate the time delays incurred. At the receiver, two spectral filters and two photodetectors in a balanced configuration are em-

ployed. One of the spectral filters has the same spectral amplitude response as the filter used in the encoder while the second has the complementary response of the optical code. By using specially designed codes in conjunction with balanced detection, MAI can be cancelled.

Experimental demonstrations of SA-OCDMA have shown that eight channels operating at a data rate of 155 Mb/s can achieve bit error rates of less than 1×10^{-9} using inexpensive transmitters and without any spectral control [28]. Superimposed FBGs have also been shown to be suitable candidates for encoding/decoding in an SA-OCDMA system [29]. Good MAI rejection was achieved through the use of M sequences and balanced detection. However, the SA-OCDMA system presented still suffered significantly from beat noise limitations that are inherent to this coding scheme.

2.2.1.3   Wavelength-Hopping Time-Spreading Coding
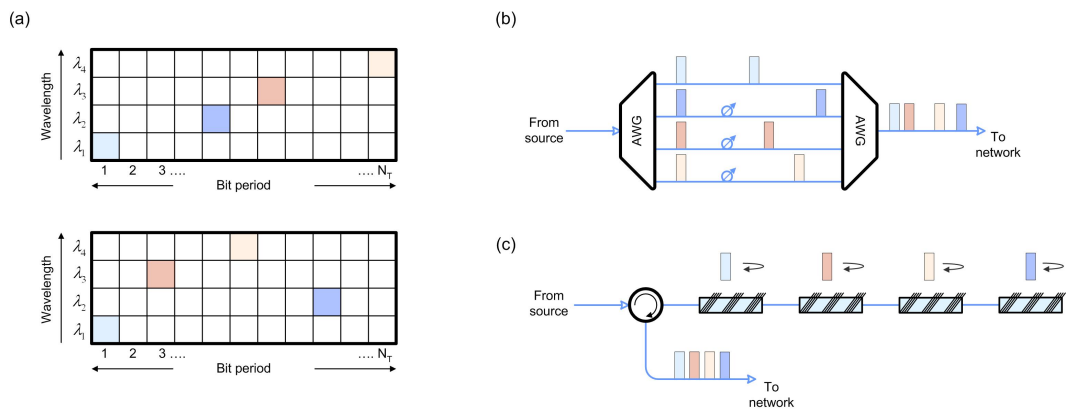
Figure 2.3: (a) Two example codes sequences for WHTS OCDMA (b) Implementation of a WHTS OCDMA encoder using AWGs and tuneable optical delays and (c) using an array of FBGs.

Wavelength-hopping time-spreading (WHTS) coding, first proposed in [9], is a 2-D scheme where the optical code used is spread in both the time domain and the wavelength domain simultaneously. It is similar to the time-spreading techniques discussed in section 2.2.1.1 whereby optical pulses are placed at different chip positions according to the given optical code, however in this case these optical chip pulses now have an assigned wavelength. As a result, the encoder essentially creates a combination of two patterns: a wavelength-hopping pattern and a time-spreading pattern. Therefore WHTS codes can be represented as a code matrix with time on one axis and wavelength on the second. Two examples of such codes are shown in Figure 2.3 (a). The wavelength domain is divided up into N_λ channels and

the time domain is divided up into N_T chips. A code consists of w short pulses of different wavelength and temporal position, where w is the weight of the code. The advantage of using a WHTS OCDMA system comes at the coding level. Firstly, they can exhibit better correlation properties; zero auto-correlations side lobes can be obtained with bounded cross correlations. Also shorter codes are required for good performance in comparison to 1-D schemes. As a result, scalability at higher data rates can be increased as can the number of potential users [34].

A number of technologies have been proposed for encoding/decoding a WHTS OCDMA signal. These include arrayed waveguide gratings (AWGs) [35], FBGs [36], thin-film filters (TFFs) [37] and holographic Bragg reflectors (HBRs) [38]. Figure 2.3 (b) and (c) show two implementations using AWGs and FBGs respectively. Depending on the choice of encoding technology, dynamic variation of the optical codes can be achieved. For example, encoders based on AWGs and TFFs create the desired wavelength-hopping pattern before applying the time-spreading pattern, allowing the use of tuneable optical delays to providing a degree of reconfigurability to the encoders. However encoders based on FBGs and HBRs apply both the wavelength and time patterns simultaneously, preventing independent control of the optical code. The decoder has the same architecture as the encoder with complementary time delays to those used during encoding. During decoding all wavelengths are aligned in time to create an auto-correlation peak of height w. All unwanted codes remain spread both temporally and spectrally.

Various experimental demonstrations of WHTS OCDMA have been presented in literature. In [39], 16 users, operating at a data rate of 1.25 Gb/s and encoded using FBGs were transmitted over 80 km of fibre. It was shown that the desired channel could be successfully decoded in the presence of interference from the remaining 15 unwanted channels. Error-free operation for a four-channel WHTS OCDMA system, operating at 2.5 Gb/s per channel, was presented in [40]. Encoding was performed using TFFs with a super-continuum spectrally sliced to create the desired wavelength channels. However, an ultrafast all-optical sampling gate was required at the receiver to remove multiple access interference. This demonstration was quickly followed by a 16-user Gigabit ethernet OCDMA system [41]. In this system, each channel operated at 1.25 Gsymbols/s with bit error rates of 1×10^{-11} achievable for the correctly decoded signal. Encoding was performed using an AWG and fibre delays. This system also required the use of an optical time gate, in the form of a 13 Gb/s D flip-flop, to suppress MAI. This paper also describes the significant limitation that beat noise has on system performance and the number of channels that can be supported.

2.2.2 Coherent OCDMA Coding

The second category used to classify OCDMA encoding/decoding schemes is coherent OCDMA. In coherent OCDMA an optical code is applied by phase coding the optical field rather than the intensity. Operating on the phase allows the use of bipolar orthogonal codes such as maximal-length sequences and Walsh codes, that result in better system performance due to the close to zero cross-correlations of these types of code sequences. Coherent OCDMA can be divided into temporal phase coding or spectral phase coding depending on whether the coding operation is performed in the time or spectral domain respectively. These two forms of coherent OCDMA are discussed in detail in this section.

2.2.2.1 Temporal Phase Coding
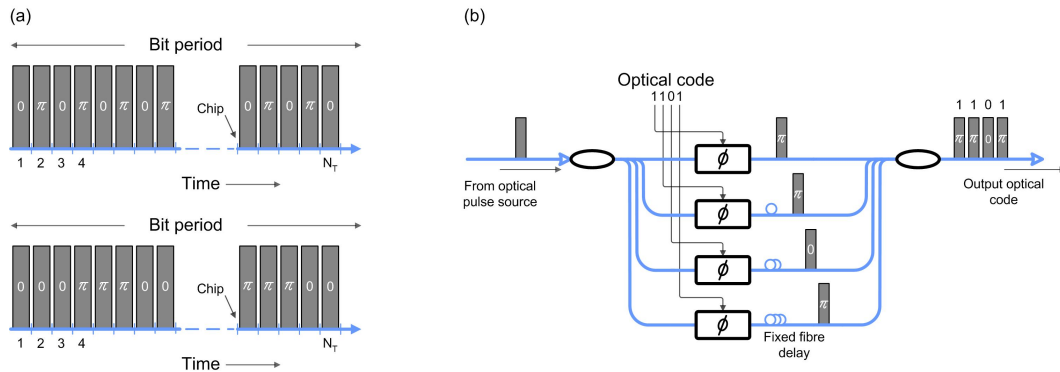
Figure 2.4: (a) Examples of two temporal phase codes (b) Implementation of temporal phase coding using fibre delay lines and optical phase modulators.

The system architecture for temporal phase coding OCDMA is quite similar to that of a temporally spread OCDMA (TS-OCDMA) system. In both cases the bit slot is divided up into N_T chip slots where N_T is the chip length. However, unlike TS-OCDMA that generally has a small code weight, a short optical pulse is placed at every chip slot in temporal phase coding. Coding is then performed on the phase of each chip pulse according to the coding sequence used. The applied phase shifts can be simple binary shifts between 0 and π or can be more advanced multilevel shifts. Two examples of temporal phase codes are shown in Figure 2.4 (a). In these codes each optical pulse is assigned a 180° phase shift relative to the other pulses. This combination of phase shifts becomes the unique identifier for each channel rather than the position of the pulses within the code sequence. Figure 2.4 (b) shows an implementation of a temporal phase encoder using fibre delay lines and phase modulators. The input pulse is split into N copies which are each phase modulated by an

optical phase modulator. Fibre delay lines are then used to align the pulses temporally to form the optical code. The decoder at the receiver follows the same architecture with complementary time delays that realign a number of optical pulses with the same phase at one chip slot, resulting in an auto-correlation peak.

Temporal phase coding for OCDMA systems was originally proposed in [42] using fibre ladder networks. Since then various technologies have been proposed for use with temporal phase coding such as planar lightwave circuits (PLCs) with monolithically integrated tapped delay lines, tuneable taps and optical phase shifters [10], AWG-based multi-port encoder/decoders [13] and superstructured fibre Bragg gratings (SSFBGs) [11, 43, 44]. The longest code lengths to date in OCDMA has been provided by SSFBGs [45]. Both AWG and SSFBGs based encoding schemes have been employed in a large number of experimental demonstrations due to their compact nature and general stability.

Temporal phase coding has received a lot of attention in literature due to its overall superior performance over incoherent OCDMA [13, 46, 47]. In [48], up to ten active channels could be supported while maintaining bit error rates less than 1×10^{-9}. Each channel operated at a data rate of 1.25 Gb/s and was encoded using a 511-chip code sequence applied by a SSFBG. A field trial over a 111 km span using a hybrid WDM/OCDMA scheme has also been presented in [49]. The hybrid system employed 10 OCDMA channels each operating at 10.71 Gb/s transmitted over 3 WDM channels. Encoding was performed using a multi-port AWG encoder/decoder with DPSK modulation and balanced detection. It is reported that bit error rates lower that 1×10^{-9} were achieved with 10 active OCDMA channels on 3 WDM wavelengths. Such a field trial highlights the potential offered by temporal phase OCDMA as a candidate for next-generation networks.

2.2.2.2 Spectral Phase Coding

Spectral phase coding is the second coherent OCDMA technique for encoding data. Spectral phase coding is similar to spectral amplitude coding in that the code sequence is applied to the spectrum of the optical signal. However, as the name suggests, spectral phase OCDMA modulates the phase relationship of the spectrum rather than the amplitude. The operating principle of spectral phase coding is shown in Figure 2.5 (a). A short optical pulse, typically from a mode-locked laser, is used as the input signal. A mode-locked laser is generally used because it is highly coherent from a frequency perspective; a requirement for a spectrally phase coded system. The spectral content of the optical pulse is then divided into discrete spectral bins with a distinct phase shift applied to each bin. As was the case with temporal phase coding in section 2.2.2.1, these phase shifts can be binary in nature,

33
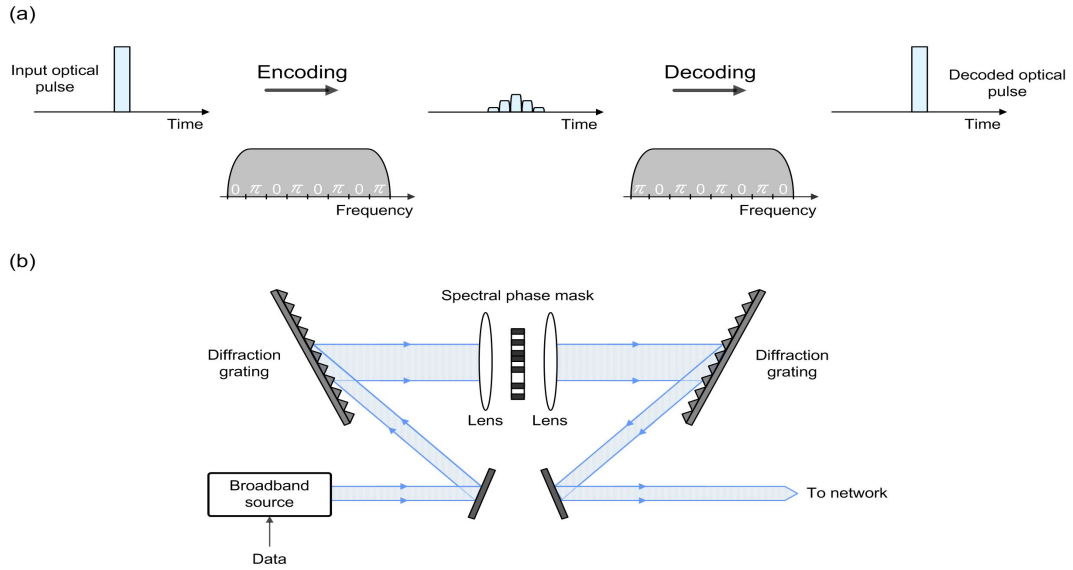
Figure 2.5: (a) Principle of spectral phase coding (b) Implementation using diffraction gratings, lenses and a spectral phase mask.

such as a 0 or π phase shift or they can be a more advanced multilevel format. The spectral phase encoding has the effect of temporally spreading the short optical pulse into a pseudo-noise-like signal. The encoded signals from each transmitter are then multiplexed together and sent across the network. The decoder at the receiver is identical in construction to the encoder, the only change is that the spectral phase mask in the decoder is the conjugate of that used in the encoder. When the incoming coded signal and the phase mask in the decoder match, the phase shifts applied to each spectral bin are removed, resulting in the optical pulse temporally reforming to its original state. Figure 2.5 (b) shows the implementation of a spectral phase encoder using diffraction gratings and a spectral phase mask. The architecture of the encoder is identical to the one used for spectral amplitude coding, with the only difference being the mask used to apply the code sequence.

The first successful demonstration of spectral phase OCDMA was presented in [7]. This paper demonstrated that a dispersion-free grating apparatus could be used to disperse the spectral content of a femtosecond optical pulse, allowing a phase code sequence to be applied to the spectrum of the optical pulse. For longer pulses with a reduced bandwidth, such as the bandwidth of a typical WDM channel, the maximum number of chips that can be used may be limited. A virtually imaged phase array (VIPA) has been shown to provide improved resolution ($\sim$1 GHz) in spectral phase OCDMA [50]. While free-space techniques for applying spectral phase codes are useful, a practical system would require

a compact, integrated low cost device. As a result, guided-wave devices were investigated for use in spectral phase OCDMA. One example of such a device is a micro-ring resonator, which has been successfully demonstrated as a spectral phase coder [51]. AWGs fabricated in silica and InP have also been developed for such a purpose [52].

A number of experimental demonstrations of spectral phase OCDMA have been undertaken since its original proposal. In [21], a four channel system operating at 2.5 Gb/s per channel was presented. Each spectral code was applied using a liquid-crystal modulator and a diffraction grating. The paper shows that bit error rates less than 1×10^{-11} could be achieved, however, nonlinear thresholding was required to suppress MAI from the unwanted channels. This experiment also used a slot level coordination scheme to intentionally separate the four users in the time domain to mitigate optical beat noise. A four channel spectral phase OCDMA testbed was presented in [53]. This testbed examined the worst-case scenarios for four channel operation i.e. when all channels are aligned temporally. It is shown that error-free operation was achievable with four simultaneous users, each operating at 10 Gb/s. Again, a nonlinear thresholder was required to suppress MAI. This testbed was later expanded in [54] to 32 channels, each operating at 10 Gb/s. This was achieved by time and polarization multiplexing eight OCDMA channels. By using time-gating, a nonlinear thresholder and forward error correction, bit error rates lower than 1×10^{-11} were possible. The same authors have also demonstrated a two-channel OCDMA link over 80.8 km of BOSSNET in Boston, Massachusetts [55]. The experimental system employed AWG devices to provide the spectral coding. Error free performance was possible for the desired channel in the presence of the interferer through the use of a nonlinear thresholder.

2.3 OCDMA Codes

OCDMA is a technique whereby each channel is distinguished by an optical code rather than an assigned wavelength or time slot. Therefore the choice of optical code used is vital to ensure that correct detection of the desired channel is maximized. The choice of the optical code sequence used also has implications for the maximum number of channels that can be supported. Hence the chosen code sequences are ideally orthogonal so that inter-channel interference is kept to a minimum allowing the maximum number of channels to be supported.

Optical codes can be divided up into two categories, incoherent and coherent codes, with the choice of code dependent on whether the coding scheme used is incoherent or coherent, as discussed in section 2.2. These two categories can be further divided up according to the

code family. The following sections discuss the most common code families that exist for both incoherent and coherent OCDMA.

2.3.1 Incoherent Codes

In an incoherent OCDMA system, decoding of an optical code sequence is based on the summation of optical intensities. Since optical intensities are unipolar $(0, +1)$ in nature, bipolar code sequences $(-1, +1)$ that have been studied with respect to RF systems may not be optimal in an incoherent OCDMA system. In an incoherent system, the auto-correlation peak is equal to the number of 1's in the code sequence. The peak of the cross-correlation is equal to the maximum number of coincidences of 1's in all shifted versions of the two code sequences [6]. Therefore code sequences that minimize the number of 1's in the code while maintaining a large discrimination between the auto-correlation and the cross-correlation are required. The most common code families used in incoherent systems are prime codes, optical orthogonal codes and carrier hopping prime codes.

2.3.1.1 Prime Codes

Prime codes are a set of sequences that have been considered for use in OCDMA networks since the first demonstrations of OCDMA [6, 16]. These codes are time-spread codes that must exhibit a large auto-correlation peak, indicating a matching code at the receiver, and low cross-correlation functions which indicates an incorrect code. The construction of these code sequences are described in [6, 14, 16]. When K users are transmitting simultaneously, the total interference at a given receiver is the superposition of $K - 1$ different cross-correlation functions. The signal-to-noise ratio (SNR) for prime codes is given by [6],

$$SNR \approx \frac{P^2}{0.29(K - 1)} \qquad (2.1)$$

From equation 2.1 it can be seen that the SNR is directly proportional to the number of chips per code sequence. For a given number of chips, the SNR gradually degrades as the number of simultaneous channels increases. This degradation of the SNR results in an increase in the probability of errors, resulting in poorer system performance for a larger number of users. It has been shown in [16] that to accommodate 31 subscribers on OCDMA system employing prime codes with a probability of error less than 1×10^{-9} would require a code length of $N = 961$. This code length severely limits the achievable data rate per channel without placing a strict limit on the optical pulse width of the chip pulses.

2.3.1.2 Optical Orthogonal Codes

Optical orthogonal codes (OOCs), proposed in [25], are a family of $(0, 1)$ sequences with desired auto- and cross-correlation properties that are designed to provide asynchronous transmission and good performance in OCDMA networks. OOCs are designed such that each sequence can be easily distinguished from a shifted version of itself and each sequence can be easily distinguished from a possibly shifted version of every other sequence in the set of codes [15]. In general, an $(F, K, \lambda_a, \lambda_c)$ optical orthogonal code C, is a family of $(0, 1)$ sequences of length F and weight K where λ_a and λ_c are the auto and cross correlation constraints respectively. When $\lambda_c = \lambda_a = 1$, it has been shown that the number of optical codes is upper-bounded by [15],

$$|C| \leq \left\lfloor \frac{(F-1)}{K(K-1)} \right\rfloor \tag{2.2}$$

where $\lfloor x \rfloor$ is the integer portion of the real number x. If an OOC is given by $(13, 3, 1, 1)$ then the maximum number of sequences that can be supported is two, with the two code sequences being,

$$C = \{1100100000000, 1010000100000\} \tag{2.3}$$

This demonstrates the main disadvantage associated with OOCs; while the code sequences are designed to provide the maximum auto-correlation while minimizing the cross correlation peaks, this is achieved at the expense of a relatively long code length that supports only a small number of users. It is shown in [16] that for an OOC with a code length of 43 and a weight of three, only seven users can be supported. An extensive treatment of OOCs and their performance analysis is given in [56].

2.3.1.3 Carrier Hopping Prime Codes

Carrier hopping prime codes (CHPCs) are a code family that are used in 2-D wavelength-hopping time-spreading OCDMA systems. As described in [57], a $(N_\lambda, N_T, w, \lambda_a, \lambda_c)$ CHPC is a set of $N_T \times N_\lambda$ $(0, 1)$ matrices or code words, where N_λ is the number of wavelengths and N_T is a prime number representing the code length. Each matrix has a weight w with each row of the matrix containing a single 1 element, resulting in each 1 chip in the code being sent on a distinct wavelength. The performance of a multi-wavelength OCDMA system employing $(N_\lambda, N_T, w, 0, 1)$ CHPCs is examined in [57]. It is shown that the probability that one of the pulses in a signature matrix lining up with a pulse in another signature matrix can be determined. If the decision threshold and the number of simultaneous users is known, then the error probability of a wavelength-time OCDMA system employing CHPCs and hard limiting can be calculated. In general, the error probability can be improved if the

number of wavelengths, N_λ, and/or the number of chips, N_T are increased. Also CHPCs allow for the adjustment of the number of wavelengths, the number of chips, or both, in order to achieve a given bit error rate performance for a set number of simultaneous users.

2.3.2 Coherent Codes

In a coherent OCDMA system, coding is performed by modulating the phase of the optical signal. While a coherent system can be more difficult to implement than incoherent systems because of the need to provide adequate optical phase control and stability, it offers the ability to implement bipolar codes $(-1, +1)$ that have been shown to have superior performance compared to unipolar codes used in incoherent systems [58]. This performance improvement stems from the autocorrelation peak being equal to P^2, where P is the code weight, for coherent systems which is an increase by a factor of P over incoherent systems. The most common code sequences proposed for coherent OCDMA are maximal-length sequences, Walsh codes and Gold sequences.

2.3.2.1 Maximal-Length Sequences

A maximal-length sequence or m-sequence is a pseudorandom sequence that is commonly found in RF and cellular spread spectrum networks. M-sequences are defined as a set of m sequences of length $N = 2^m - 1$, with a detailed discussion on m-sequences is given in [57, 59]. One of the main advantages for using m-sequences is that the correlation function between different shifts of the sequences are always equal to -1, thus allowing them to be used as different codes that have excellent correlation properties. It has been shown that with a relatively short code length, bipolar coding using m-sequences exhibits clear benefits in terms of contrast between the correlation peak and the background, in comparison to unipolar coding [11]. While the number of orthogonal codes for a seven-bit m-sequence is two, this number increases rapidly with code length.

2.3.2.2 Walsh Codes

Walsh codes are a set of code sequences that have been employed in wireless CDMA networks to improve bandwidth efficiency due to their zero cross correlation functions when they are synchronized in time [59]. Walsh functions are generated by mapping codeword rows of special square matrices called Hadamard matrices. These matrices contain one row of all $+1$'s with the remaining rows each having an equal number of $+1$'s and -1's. Walsh codes are defined as a set of N sequences of length $N = 2^n$ and are generated using a recursive procedure. For example, taking the code set W_2, the two code sequences are given by $[+1 \; +1]$ and $[+1 \; -1]$. 64-chip Walsh codes have been successfully demonstrated in

a 32 channel spectral phase OCDMA network testbed [54]. In this case, Walsh codes were chosen since they are ideally orthogonal signals when used synchronously. Also the MAI produced by Walsh codes ideally does not coincide with the auto correlation peak of the decoded signal but occurs before or after it.

2.3.2.3 Gold Sequences

Gold sequences are a family of bipolar codes that are useful in CDMA networks because of the large number of codes that they supply. A set of $N+2$ Gold sequences with length $N = 2^m - 1$ can be obtained by using a preferred pair of maximal-length sequences of identical length N. The construction of Gold code sequences is discussed in more detail in [59]. The auto correlation function of a Gold code exhibits side lobes that are dependent on the pair of code sequences used. However, the advantage of using Gold code is that the cross correlation between the codes is bounded. When K users are transmitting simultaneously, the total interference generated is given by the superposition of $K - 1$ cross correlation functions. Assuming the interferers are uncorrelated, the variance of the total interference is equal to the sum of the variances of the $K - 1$ cross correlation functions, which are assumed to be identical. It has been shown that the SNR for Gold codes is given by [60],

$$SNR = 4 \left[\frac{N^3}{(K-1)(N^2 + N - 1)} \right] \qquad (2.4)$$

From this equation it can be seen that the variance of the amplitude of the cross correlation function increases with the both the number of users K and the number of chips N. Therefore, it is apparent that while the number of simultaneous users can be increased by increasing the number of chips per bit, this increase in the number of chips also provides a larger contribution to the overall interference, limiting the improvement in the SNR.

2.4 OCDMA Network Impairments

OCDMA networks can be implemented through various coding techniques and can employ a number of coding sequences which have been discussed in sections 2.2 and 2.3. However, OCDMA networks suffer from two noise sources that can severely limit the number of channels that the system can support. These noise sources are multiple access interference (MAI) and optical beat noise (OBN). The two noise sources arise due to each channel on the network sharing the same bandwidth and time slot equally. Since each channel can transmit asynchronously, two or more channels can overlap in both the temporal and spectral domains. At the receiver, this overlap in both domains results in MAI and OBN. Both noise sources are discussed in more detail in the following sections.

2.4.1 Multiple Access Interference

Multiple access interference is present in OCDMA systems due to the fact that each receiver receives an aggregate signal that contains the data transmitted from each channel. The optical decoder at the receiver correlates the incoming signal with a stored version of the desired code that is to be detected. The desired channel is decoded correctly and generates an auto correlation peak representing the original data pulse that was transmitted and is detected by the receiver's photodetector. The remaining unwanted channels also pass through the decoder but remain temporally/spectrally spread. However, these unwanted channels are also incident on the photodetector and result in a degradation of the SNR of a desired signal. This degradation scales as the number of simultaneous transmitting channels increases, limiting the performance of the system. The level of MAI has been shown in section 2.3 to be dependent on the length of the optical code used, with longer code sequences performing better due to lower levels of MAI. However, there is generally a trade-off between the practicality of implementing larger code lengths and the level of MAI generated.

An eye diagram similar to that of a correctly decoded OCDMA signal with no interfering channels is shown in Figure 2.6 (a). It clearly shows a large eye opening that allows the decoded data to be successfully thresholded and recovered. In comparison, Figure 2.6 (b) shows the same decoded channel, this time in the presence of an interfering channel. This interfering channel introduces a third intensity level to the eye opening that effectively reduces the 'correct' portion of the eye opening, increasing the probability of error after detection. Both optical signals in Figure 2.6 were detected using 50 GHz photodiode, hence there is a clear distinction between the correctly decoded optical pulse, that has a narrow pulse width and high optical peak power, and the incorrectly decoded MAI that is spread over the entire bit slot and has a low optical peak power. However, the energy in both the desired and unwanted channel is the same, with both signals having a temporal duration that is equal to or below the bit period, meaning that they appear essentially identical to a photodetector that is band-limited to the data rate. This would result in a three-level eye diagram and an optical signal that cannot be correctly recovered without errors since the band-limited receiver cannot distinguish between the desired channel and the interfering channel. Consequently, either a fast receiver that has a bandwidth greater than the data rate of the desired channel must be used, or some form of optical thresholding or time gating is required to remove MAI.
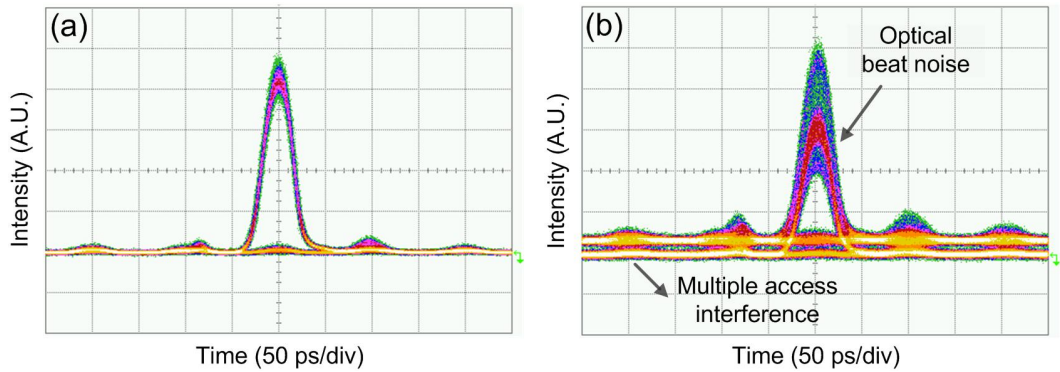
Figure 2.6: Output pulses from an OCDMA decoder for (a) Single correctly decoded channel (b) Correctly decoded channel with MAI and optical beat noise.

2.4.2 Optical Beat Noise

Optical beat noise is the second major impairment to OCDMA networks. Beat noise arises when different optical signals with identical (or nominally different) frequencies are incident on a given photodetector simultaneously. Since a photodetector has a square-law detection characteristic, optical beating will occur between the optical signals incident on the detector. When two optical signals are incident on a photodetector, the total intensity, I, is given by [34],

$$I = I_1 + I_2 + 2\sqrt{I_1 I_2} \, cos(\delta\phi) \qquad (2.5)$$

where I_1 and I_2 are the intensities of the two optical signals and $\delta\phi$ is the phase difference between the two signals. From equation 2.5 the total intensity can beat from a minimum value of $I_{min} = I_1 + I_2 - 2\sqrt{I_1 I_2}$, if the two waves are out of phase, to a maximum of $I_{max} = I_1 + I_2 + 2\sqrt{I_1 I_2}$ if the two waves are in phase. This variation in the intensity of the optical signal can severely degrade the performance of an OCDMA system.

Figure 2.6 (b) highlights the intensity variation caused by optical beating between two OCDMA signals. It can be seen that OBN introduces a large amount of noise to the top of the eye diagram in comparison to the single channel eye diagram shown in Figure 2.6 (a). The limits on the performance of OCDMA systems as a result of OBN are often larger than those resulting from MAI. This is due to beat noise scaling with the square of the number of detected fields, which is proportional to the number of channels [23].

Optical beat noise has been examined both theoretically and experimentally in a number of publications [24, 61–64]. In these papers, it is shown that beat noise severely limits

system performance, especially in a coherent OCDMA system where it becomes the main impairment. A number of methods for suppressing beat noise are presented in [24]. These include reducing the level of interference between the OCDMA channels through either using a longer code sequence or introducing some form of synchronisation to the system. Implementing a longer code sequence can increase hardware cost and/or limit the transmission data rate depending on the OCDMA scheme employed. Introducing synchronisation to the system has the effect of lowering the bandwidth efficiency and increasing the overall complexity of the network. A second option is to use a low-coherence source such as a wide-band light emitting diode (LED) or amplified spontaneous emission (ASE). Such a solution can be effective in an incoherent OCDMA system at reducing beat noise but is not suitable for a coherent system that requires an optical source that has a coherence length of at least the chip length.

2.5 OCDMA MAI Suppression Techniques

In the previous section, MAI and optical beat noise were discussed as the two main sources of noise in an OCDMA system. These two noise sources scale with the number of simultaneous users on the system, reducing the overall performance. While increasing the length of the code sequences used can lower the amount of interference generated, this technique is only successful if the receiver has a bandwidth greater than the data rate of the transmitted signal. Therefore, further processing techniques are required to eliminate the interference. In principle, it is possible to use a high bandwidth photodetector and remove the interference in the electrical domain. However, this technique would be impractical due to the cost of both a high-speed photodetector and the subsequent electronics. As a result, MAI rejection is mostly performed in the optical domain. The two main techniques for OCDMA MAI suppression are optical time gating and optical thresholding.

2.5.1 Optical Time Gating

The purpose of optical time gating is to extract a decoded OCDMA signal at a given time interval in the presence of unwanted MAI noise. Through the careful selection of an appropriate code set it is possible to design a synchronous system such that the auto correlation peak occurs in a given time slot while the energy of the MAI generated falls outside of this time interval. Therefore, by optically gating the incoming data signal at the desired time interval, it is possible to retrieve the desired data signal while suppressing the unwanted noise. The use of an optical time gate requires an optical clock train that is used to open the switching window of the time gate. While the use of an optical clock train does not require global synchronisation across the network, optical clock recovery at the receiver is required
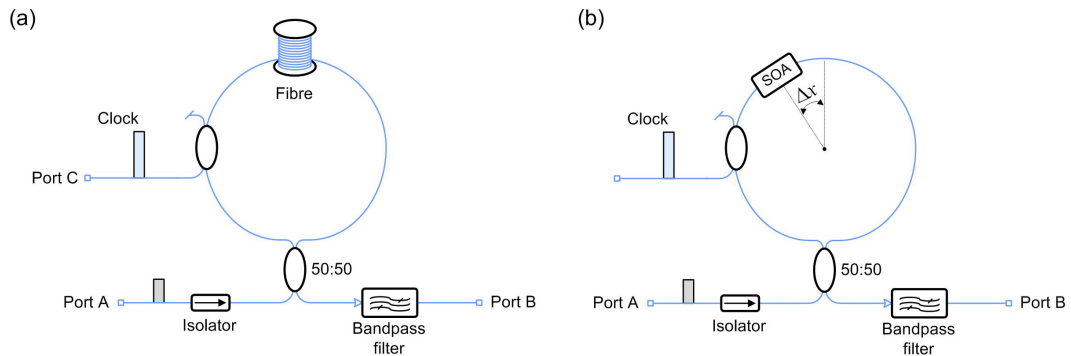
Figure 2.7: Optical time gating using (a) A nonlinear optical loop mirror and (b) A terahertz optical asymmetric demultiplexer.

for synchronisation with the auto correlation peaks. In this section, two of the most common forms of optical time gate are discussed; the nonlinear optical loop mirror (NOLM) and the terahertz optical asymmetric demultiplexer (TOAD).

2.5.1.1 Nonlinear Optical Loop Mirror

A nonlinear optical loop mirror can be used as an optical time gate by using an optical clock pulse to alter the effective phase shift through one arm of the mirror. This phase shift can be accomplished by nonlinear propagation through a length of optical fibre. Figure 2.7 (a) illustrates a typical configuration of a NOLM as an optical time gate. Assuming for simplicity that only a single pulse is present at the input port A, the operation of the NOLM is as follows. The incoming pulse at port A is split using a 50 : 50 coupler into two counter-propagating replicas. When no clock signal is present at port C, the input pulses simply counter-propagate around the loop and recombine at the coupler. The interference condition at the coupler is such that the signals interfere destructively at the output port B and interfere constructively at the input port A, thereby reflecting the input pulse. Typically an isolator is used on the input port to prevent the reflected pulse from propagating back through the receiver. If a large amplitude optical clock pulse, with a wavelength close to but distinguishable from the data pulse wavelength, is injected at port C, it is possible to overlap the clock pulse and the co-propagating data pulse and introduce a nonlinear phase shift of π. As a result, the interference condition at the coupler has changed such that constructive interference occurs, with the data pulse now appearing on the output port B. An optical bandpass filter is then used to filter out the clock signal.

Optical time gating using a NOLM has been successfully employed in a temporal phase

43

coded OCDMA system [18]. However, the NOLM does have a number of disadvantages. A NOLM requires high optical peak powers and long interaction lengths due to the low nonlinear coefficient in fibre. This can be problematic for optical signals that have a broad optical spectrum as fibre dispersion becomes a problem for these signals and can limit the functionality of NOLMs that employ long lengths of fibre. These lengths of fibre can also become susceptible to changes in environmental conditions which can also affect the operation of the time gate.

2.5.1.2 Terahertz Optical Asymmetric Demultiplexer

An terahertz optical asymmetric demultiplexer [19] is a form of interferometer that can be used for optical time gating purposes. In a TOAD, the variation of the gain and phase of a semiconductor optical amplifier (SOA) due to optical signals is employed to generate an optical gate. The typical implementation of a TOAD for optical time gating is shown in Figure 2.7 (b). It can be seen that the configuration of a TOAD is quite similar to that of a NOLM. However, where a NOLM uses nonlinear propagation in fibre to generate the required phase shift, a TOAD uses an SOA that is offset from the centre of the loop by Δx.

The operation of a TOAD is as follows. The input pulse at port A is split into a clockwise (CW) and counterclockwise (CCW) traveling pulse. In Figure 2.7 (b) the CW pulse reaches the SOA before the CCW pulse. If there is no clock pulse present at port C then both pulses counter-propagate around the loop, experiencing a similar effective medium, and recombine at the coupler. The interference condition is such that the pulses combine destructively at the output port B and combine constructively at port A, reflecting back the input pulse. However, if a high power clock pulse is present at port C, it saturates the SOA, changing it's refractive index. The clock pulse is timed so that it arrives before the CCW pulse and after the CW pulse, resulting in a differential phase shift between the two pulses. This differential phase shift changes the interference condition at the coupler resulting in the input pulse being gated out to the output port B. A bandpass filter is then used to filter out the clock pulse, leaving only the desired data. The duration of the switching window, τ_{win}, is determined by the offset of the SOA, Δx, from the midpoint of the loop, given by,

$$\tau_{win} = 2\Delta x / c_{fibre} \tag{2.6}$$

By controlling the offset position of the SOA, short switching windows can be achieved. WHTS OCDMA systems employing TOADs have been successfully demonstrated [65, 66], with a 2 ps switching window achieved in [66].

2.5.2 Optical Thresholding
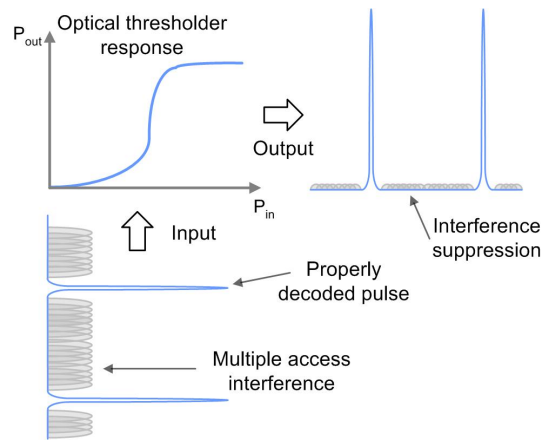
Figure 2.8: Operating principle of optical thresholding for MAI rejection.

Optical thresholding is another approach that can be used to suppress MAI noise in OCDMA systems. The principle behind optical thresholding relies on using a device that has a non-linear power-transfer response. This idea is illustrated in Figure 2.8. For pulses with a large amplitude, such as correctly decoded OCDMA signals, they pass through the optical thresholder while experiencing a relatively low loss. However, lower power pulses such as MAI noise, experience a large loss as they pass through the optical thresholder and are effectively suppressed. One of the advantages of using optical thresholding is that the clock pulse required in an optical time gate is not needed, simplifying the receiver. A number of optical thresholders has been been proposed and are discussed in the following sections.

2.5.2.1 NOLM and TOAD-Based Thresholding

Both a NOLM and a TOAD can be used as an optical thresholder by slightly changing their configuration from those shown in Figure 2.7. When used as an optical thresholder, both devices no longer require the clock pulse input port, so this coupler is removed. The only other change is that the splitting ratio of the input coupler is changed from a $50 : 50$ ratio to an asymmetric ratio. This asymmetry allows one counter-propagating high power pulse to undergo a differential phase shift relative to the other, allowing the input pulse to be sent to the output port rather than get reflected back out the input port. In comparison, if the input pulse is low power, then neither counter-propagating pulse will have sufficient energy to induce a phase shift, resulting in the pulses being reflected back at the input.

A NOLM-based optical thresholder has been experimentally shown to provide a signifi-

cant performance improvement in OCDMA systems [18, 20, 67]. In these demonstrations, a 70 : 30 splitting ratio is used at the input coupler of the NOLM. A TOAD-based optical thresholder in a WHTS OCDMA system was presented in [68].

2.5.2.2 Fibre-Based Thresholding

A number of fibre-based optical thresholders have been proposed for OCDMA systems. These optical thresholders use nonlinear effects in various types of fibre to discriminate between the desired signal and MAI noise. The types of fibre used include highly nonlinear fibre (HNLF) [53], holey fibre [69] and dispersion-flattened fibre (DFF) [22]. Each of these fibre-based thresholders uses a nonlinear effect in the fibre, typically self-phase modulation (SPM), to suppress MAI. For high power optical pulses, SPM in the fibre has the effect of broadening it's spectrum. These additional portions of the spectrum only contain the desired OCDMA signal, as the accompanying MAI does not have sufficient power to generate SPM. As a result, these SPM portions of the spectrum can be filtered out using an optical bandpass filter after the fibre thresholder, giving only the desired signal and effectively removing MAI. A periodically poled lithium-niobate waveguide (PPLN) has also been demonstrated as an optical thresholder in a spectral phase OCDMA system [21]. This type of thresholder uses second harmonic generation (SHG) to suppress MAI, since the output power is strongly dependent on the input signal intensity.

2.6 Summary

Optical code division multiple access is a promising multiplexing technique that is particularly suited for future all-optical access networks. OCDMA has a number of inherent advantages such as asynchronous transmission, quality of service control and a large degree of flexibility and scalability. Various demonstrations of enabling technologies have been presented in literature allowing a number of different OCDMA coding techniques to be achieved. These include coding in both the temporal and spectral domains, or through a combination of both. Coding can either be performed on an amplitude or phase basis with advantages and disadvantages associated with both. However, all OCDMA systems suffer from two main impairments that limit the overall system performance, multiple access interference and optical beat noise. Both noise sources scale with the number of simultaneous users, resulting in the need for some form of rejection and/or suppression to ensure that a given performance level can be achieved.

Numerous experimental demonstrations of optical time gates and nonlinear optical thresholders have shown that they can significantly improve the performance of an OCDMA sys-

tem, in the presence of MAI. However these devices either require a synchronised clock pulse, thus requiring optical clock recovery, in the case of time gating, or either a long length of fibre or a speciality fibre, in the case of the optical thresholder. An alternate to these fibre-based solutions is the nonlinear optical-to-electrical conversion process of two-photon absorption (TPA) present in semiconductor devices. TPA is a nonlinear process that can be used for simultaneous optical thresholding and detection in a single device. Due to the semiconductor nature of the device, it offers a number of advantages such as a low cost, a small form factor and the potential for integration with a number of other devices. Therefore, TPA and its potential for optical thresholding in OCDMA systems is the primary focus of the next chapter.

References

[1] G. R. Cooper and R. W. Nettleton, "A spread spectrum technique for high capacity mobile communications," *IEEE Transactions on Vehicular Technology*, vol. 27, no. 4, pp. 264–275, 1978.

[2] H. J. Kochevar, "Spread spectrum multiple access communication experiment through a satellite," *IEEE Transactions on Communications*, vol. 25, no. 8, pp. 853–856, 1977.

[3] L. B. Milstein, "Interference rejection techniques in spread spectrum communications," *Proceedings of the IEEE*, vol. 76, no. 6, pp. 657–671, 1988.

[4] K. S. Gilhousen, I. M. Jacobs, R. Padovani, A. J. Viterbi, L. A. Weaver, Jr., and C. E. Wheatley, III, "On the capacity of a cellular CDMA system," *IEEE Transactions on Vehicular Technology*, vol. 40, no. 2, pp. 303–312, 1991.

[5] J. P. Heritage and A. M. Weiner, "Advance in spectral optical code-division multiple-access communications," *IEEE Journal of Selected Topics in Quantum Electronics*, vol. 13, no. 5, pp. 1351–1369, 2007.

[6] P. R. Prucnal, M. A. Santoro, and T. R. Fan, "Spread spectrum fiber-optic local area network using optical processing," *IEEE Journal of Lightwave Technology*, vol. LT-4, no. 5, pp. 547–554, 1986.

[7] A. M. Weiner, J. P. Heritage, and J. A. Salehi, "Encoding and decoding of femtosecond pulses," *Optics Letters*, vol. 13, no. 4, pp. 300–302, 1988.

[8] D. Zaccarin and M. Kavegard, "An optical CDMA system based on spectral amplitude encoding of an LED," *IEEE Photonics Technology Letters*, vol. 5, no. 4, pp. 479–482, 1993.

[9] L. Tancĕvski and I. Andonovic, "Wavelength hopping/time spreading code division multiple access systems," *Electronics Letters*, vol. 30, no. 17, pp. 1388–1390, 1994.

[10] N. Wada and K. Kitayama, "A 10Gb/s optical code division multiplexing using 8-chip optical bipolar code and coherent detection," *IEEE Journal of Lightwave Technology*, vol. 17, no. 10, pp. 1758–1765, 1999.

[11] P. C. Teh, P. Petropoulos, M. Ibsen, and D. J. Richardson, "A comparative study of the performance of seven and 63-chip optical code-division multiple-access encoders and decoders based on superstructured fiber Bragg gratings," *IEEE Journal of Lightwave Technology*, vol. 19, no. 9, pp. 1352–1365, 2001.

[12] C. Tian, Z. Zhang, M. Ibsen, P. Petropoulos, and D. J. Richardson, "A 16-channel reconfigurable OCDMA/DWDM system using continuous phase-shift SSFBGs," *IEEE Journal of Selected Topics in Quantum Electronics*, vol. 13, no. 5, pp. 1480–1486, 2007.

[13] X. Wang, N. Wada, G. Cincotti, T. Miyazaki, and K. Kitayama, "Demonstration of over 128 Gb/s capacity (12-user $\times$ 10.71-Gb/s/user) asynchronous OCDMA using FEC and AWG-based multiport optical encoder/decoders," *IEEE Photonics Technology Letters*, vol. 18, no. 15, pp. 1603–1605, 2006.

[14] A. A. Shaar and P. A. Davies, "Prime sequences: Quasi-optimal sequences for OR channel code division multiplexing," *Electronics Letters*, vol. 19, no. 21, pp. 888–889, 1983.

[15] J. A. Salehi, "Code division multiple-access techniques in optical fiber networks—Part I: Fundamental principles," *IEEE Transactions on Communications*, vol. 37, no. 8, pp. 824–833, 1989.

[16] W. C. Kwong, P. A. Perrier, and P. R. Prucnal, "Performance comparison of asynchronous and synchronous code-division multiple-access techniques for fiber-optic local area networks," *IEEE Transactions on Communications*, vol. 39, no. 11, pp. 1625–1634, 1991.

[17] R. M. H. Yim, L. R. Chen, and J. Bajcsy, "Design and performance of 2-D codes for wavelength-time optical CDMA," *IEEE Photonics Technology Letters*, vol. 14, no. 5, pp. 714–716, 2002.

[18] H. Sotobayashi, W. Chujo, and K. Kitayama, "1.6-b/s/Hz 6.4 Tb/s QPSK-OCDM/WDM (4OCDM $\times$ 40WDM $\times$ 40Gb/s) transmission experiment using optical hard thresholding," *IEEE Photonics Technology Letters*, vol. 14, no. 4, pp. 555–557, 2002.

[19] J. P. Sokoloff, P. R. Prucnal, I. Glesk, and M. Kane, "A terahertz optical asymmetric demultiplexer (TOAD)," *IEEE Photonics Technology Letters*, vol. 5, no. 7, pp. 787–790, 1993.

[20] J. H. Lee, P. C. Teh, P. Petropoulos, M. Ibsen, and D. J. Richardson, "Reduction of interchannel interference noise in a two-channel grating-based ocdma system using a nonlinear optical loop mirror," *IEEE Photonics Technology Letters*, vol. 13, no. 5, pp. 529–531, 2001.

[21] Z. Jiang, D. S. Seo, S.-D. Yang, D. E. Leaird, R. V. Roussev, C. Langrock, M. M. Fejer, and A. M. Weiner, "Four-user, 2.5-Gb/s, spectrally coded OCDMA system demonstration using low-power nonlinear processing," *IEEE Journal of Lightwave Technology*, vol. 23, no. 1, pp. 143–158, 2005.

[22] X. Wang, T. Hamanaka, N. Wada, and K. Kitayama, "Dispersion-flattened-fiber based optical thresholder for multiple-access-interference suppression in OCDMA system," *Optics Express*, vol. 13, no. 14, pp. 5499–5505, 2005.

[23] D. D. Sampson, G. J. Pencock, and R. A. Griffin, "Photonic code-division multiple-access communications," *Fiber and Integrated Optics*, vol. 16, no. 2, pp. 129–157, 1997.

[24] X. Wang and K. Kitayama, "Analysis of beat noise in coherent and incoherent time-spreading OCDMA," *IEEE Journal of Lightwave Technology*, vol. 22, no. 10, pp. 2226–2235, 2004.

[25] F. R. K. Chung, J. A. Salehi, and V. K. Wei, "Optical orthogonal codes: Design, analysis and applications," *IEEE Transactions on Information Theory*, vol. 35, no. 3, pp. 595–604, 1989.

[26] M. Kavehard and D. Zaccarin, "Optical code-division-multiplexed systems based on spectral encoding of noncoherent sources," *IEEE Journal of Lightwave Technology*, vol. 13, no. 3, pp. 534–545, 1995.

[27] Z. Wei, H. M. H. Shalaby, and H. Ghafouri-Shiraz, "Modified quadratic congruence codes for fiber Bragg-grating-based spectral-amplitude-coding optical CDMA systems," *IEEE Journal of Lightwave Technology*, vol. 19, no. 9, pp. 1274–1281, 2001.

[28] T. Pfeiffer, B. Deppisch, M. Witte, and R. Heidemann, "Operational stability of a spectrally encoded optical CDMA system using inexpensive transmitters without spectral control," *IEEE Photonics Technology Letters*, vol. 11, no. 7, pp. 916–918, 1999.

[29] J. Magné, D.-P. Wei, S. Ayotte, L. A. Rusch, and S. LaRochelle, "Experimental demonstration of frequency-encoded optical CDMA using superimposed fiber Bragg gratings," in *Proceedings of Bragg Gratings, Photosensitivity, and Poling in Glass Waveguides (BGPP)*, Monterey, California, 2003, paper WD4.

[30] J. Y. Hui, "Pattern code modulation an optical decoding — A novel code-division multiplexing technique for multifiber networks," *IEEE Journal on Selected Areas in Communications*, vol. 3, no. 6, pp. 916–927, 1985.

[31] E. Park, A. J. Mendez, and E. M. Garmire, "Temporal/spatial optical CDMA networks—Design, demonstration, and comparison with temporal networks," *IEEE Photonics Technology Letters*, vol. 4, no. 10, pp. 1160–1162, 1992.

[32] K. Kitayama, "Novel spatial spread spectrum based fiber optic CDMA networks for image transmission," *IEEE Journal on Selected Areas in Communications*, vol. 12, no. 4, pp. 762–772, 1994.

[33] S. Kim, K. Yu, and N. Park, "A new family of space/wavelength/time spread three-dimensional optical code for OCDMA networks," *IEEE Journal of Lightwave Technology*, vol. 18, no. 4, pp. 502–511, 2000.

[34] C. S. Brès, Y. K. H. nd I. Glesk, and P. R. Prucnal, "Scalable asynchronous incoherent optical CDMA," *Journal of Optical Networking*, vol. 6, no. 6, pp. 599–615, 2007.

[35] S. Yegnanarayanan, A. S. Bhushan, and B. Jalali, "Fast wavelength-hopping time-spreading encoding/decoding for optical CDMA," *IEEE Photonics Technology Letters*, vol. 12, no. 5, pp. 573–575, 2000.

[36] L. R. Chen and P. W. E. Smith, "Demonstration of incoherent wavelength-encoding/time-spreading optical CDMA using chirped Moiré gratings," *IEEE Photonics Technology Letters*, vol. 12, no. 9, pp. 1281–1283, 2000.

[37] V. Baby, I. Glesk, R. J. Runser, R. Fischer, Y.-K. Huang, C.-S. Brès, W. C. Kwong, T. H. Curtis, and P. R. Prucnal, "Experimental demonstration and scalability analysis of a four-node 102-Gchip/s fast frequency-hopping time-spreading optical CDMA network," *IEEE Photonics Technology Letters*, vol. 17, no. 1, pp. 253–255, 2005.

[38] Y.-K. Huang, V. Baby, P. R. Prucnal, C. M. Greiner, D. Iazikov, and T. W. Mossberg, "Integrated holographic encoder for wavelength-hopping/time-spreading optical CDMA," *IEEE Photonics Technology Letters*, vol. 17, no. 4, pp. 825–827, 2005.

[39] H. B. Jaafar, S. LaRochelle, P.-Y.Cortès, and H. Fathallah, "1.25 Gbit/s transmission of optical FFH-OCDMA signals over 80 km with 16 users," in *Proceedings of Optical Fibre Communications (OFC)*, Anaheim, California, 2001, paper TuV3-1.

[40] I. Glesk, V. Baby, C.-S. Brès, L. Xu, D. Rand, and P. R. Prucnal, "Experimental demonstration of a 2.5 Gbps incoherent 2D OCDMA system," in *Proceedings of Conference on Lasers and Electro-Optics (CLEO)*, San Jose, California, 2004, paper CWH1.

[41] V. J. Hernandez, A. J. Mendez, C. V. Bennett, R. M. Gagliardi, and W. J. Lennon, "Bit-error-rate analysis of a 16-user gigabit ethernet optical-CDMA (O-CDMA) technology demonstrator using wavelength/time codes," *IEEE Photonics Technology Letters*, vol. 17, no. 12, pp. 2784–2786, 2005.

[42] R. A. Griffin, D. D. Sampson, and D. A. Jackson, "Optical phase coding for code-division multiple access networks," *IEEE Photonics Technology Letters*, vol. 4, no. 12, pp. 1401–1402, 1992.

[43] A. Grunnet-Jepsen, A. E. Johnson, E. S. Maniloff, T. W. Mossberg, M. J. Munroe, and J. N. Sweetser, "Demonstration of all-fiber sparse lightwave CDMA on temporal phase encoding," *IEEE Photonics Technology Letters*, vol. 11, no. 10, pp. 1283–1285, 1999.

[44] P. C. Teh, P. Petropoulos, M. Ibsen, and D. J. Richardson, "Phase encoding and decoding of short pulses at 10 Gb/s using superstructured fibre Bragg gratings," *IEEE Photonics Technology Letters*, vol. 13, no. 2, pp. 154–156, 2001.

[45] X. Wang, K. Matsushima, K. Kitayama, A. Nishiki, N. Wada, and F. Kubota, "High-performance optical code generation and recognition by use of a 511-chip, 640-Gchip/s phase shifted superstructured fibre Bragg grating," *Optics Letters*, vol. 30, no. 4, pp. 355–357, 2005.

[46] X. Wang, K. Matsushima, A. Nishiki, N. Wada, F. Kubota, and K.-I. Kitayama, "Experimental demonstration of 511-chip 640 Gchip/s superstructured FBG for high performance optical code processing," in *Proceedings of European Conference on Optical Communications (ECOC)*, Stockholm, Sweden, 2004, paper Tu1.3.7.

[47] X. Wang, N. Wada, T. Hamanaka, K. Kitayama, and A. Nishiki, "10-user, truly-asynchronous OCDMA experiment with 511-chip SSFBG en/decoder and SC-based optical thresholder," in *Proceedings of Optical Fibre Communications (OFC)*, Anaheim, California, 2005, postdeadline paper PDP33.

[48] X. Wang, N. Wada, T. Miyazaki, G. Cincotti, and K. Kitayama, "Asynchronous multiuser coherent OCDMA system with code-shift-keying and balanced detection," *IEEE Journal of Selected Topics in Quantum Electronics*, vol. 13, no. 5, pp. 1463–1470, 2007.

[49] ——, "Field trial of 3-WDM×10-OCDMA×10.71-Gb/s asynchronous WDM/DPSK-OCDMA using hybrid E/D without FEC and optical thresholding," *IEEE Journal of Lightwave Technology*, vol. 25, no. 1, pp. 207–215, 2007.

[50] S. Etemad, P. Toliver, R. Menendez, J. Young, T. Banwell, S. Galli, J. Jackel, P. Delfyett, C. Price, and T. Turpin, "Spectrally efficient optical CDMA using coherent phase frequency coding," *IEEE Photonics Technology Letters*, vol. 17, no. 4, pp. 929–931, 2005.

[51] A. Agarwal, P. Toliver, R. Menendez, S. Etemad, J. Jackel, J. Young, T. Banwell, B. E. Little, S. T. Chu, W. Chen, W. Chen, J. Hryniewicz, F. Johnson, D. Gill, O. King, R. Davidson, K. Donovan, and P. J. Delfyett, "Fully programmable ring-resonator-based integrated photonic circuit for phase coherent applications," *IEEE Journal of Lightwave Technology*, vol. 24, no. 1, pp. 77–87, 2006.

[52] H. Tsuda, H. Takenouchi, T. Ishii, K. Okamoto, T. Goh, K. Sato, A. Hirano, T. Kurokawa, and C. Amano, "Spectral encoding and decoding of 10 Gbit/s femtosecond pulses using high resolution arrayed-waveguide grating," *Electronics Letters*, vol. 35, no. 14, pp. 1186–1188, 1999.

[53] R. P. Scott, K. Li, V. J. Hernandez, B. H. Kolner, J. P. Heritage, and S. J. Ben Yoo, "Demonstration of an error-free 4×10 Gb/s multiuser SPECTS O-CDMA network testbed," *IEEE Photonics Technology Letters*, vol. 16, no. 9, pp. 2186–2188, 2004.

[54] V. J. Hernandez, W. Cong, J. Hu, C. Yang, N. K. Fontaine, R. P. Scott, Z. Ding, B. H. Kolner, J. P. Heritage, and S. J. Ben Yoo, "A 320-Gb/s capacity (32-user $\times$ 10 Gb/s) SPECTS O-CDMA network testbed with enhanced spectral efficiency through forward error correction," *IEEE Journal of Lightwave Technology*, vol. 25, no. 1, pp. 79–86, 2007.

[55] V. J. Hernandez, R. P. Scott, N. K. Fontaine, F. M. Soares, R. Broeke, K. Perry, G. Nowak, C. Yang, K. Okamoto, J. P. Heritage, B. H. Kolner, and S. J. B. Yoo, "SPECTS O-CDMA 80.8-km BOSSNET field trial using a compact, fully integrated, AWG-based encoder/decoder," in *Proceedings of Optical Fibre Communications (OFC)*, Anaheim, California, 2007, paper OMO7.

[56] J. A. Salehi and C. A. Brackett, "Code division multiple-access techniques in optical fiber networks—Part II: Systems performance analysis," *IEEE Transactions on Communications*, vol. 37, no. 8, pp. 834–842, 1989.

[57] G. C. Yang and W. C. Kwong, *Prime codes with applications to CDMA optical and wireless networks*. Norwood, MA: Artech House, 2002.

[58] M. E. Marhic, "Coherent optical CDMA networks," *IEEE Journal of Lightwave Technology*, vol. 11, no. 5, pp. 854–864, 1993.

[59] E. H. Dinan and B. Jabbari, "Spreading codes for direct sequence CDMA and wideband CDMA cellular networks," *IEEE Communications Magazine*, vol. 36, no. 9, pp. 48–54, 1988.

[60] S. Tamura, S. Nakano, and K. Akazaki, "Optical code-multiplex transmission by Gold sequences," *IEEE Journal of Lightwave Technology*, vol. 3, no. 1, pp. 121–127, 1985.

[61] L. Tancĕvski and L. A. Rusch, "Impact of the beat noise on the performance of 2-D optical CDMA systems," *IEEE Communications Letters*, vol. 4, no. 8, pp. 264–266, 2000.

[62] T. Bazan, D. Harle, I. Andonovic, and M. Meenakshi, "Effect of beat noise on the performance of two-dimensional time-spreading/wavelength-hopping optical code-division multiple-access systems," *Journal of Optical Networking*, vol. 4, no. 3, pp. 121–129, 2005.

[63] C. S. Brès, Y.-K. Huang, D. Rand, I. Glesk, P. R. Prucnal, T. Bazan, C. Michie, D. Harle, and I. Andonovic, "On the experimental characterization of beat noise in 2-D time-spreading wavelength-hopping OCDMA systems," *IEEE Photonics Technology Letters*, vol. 18, no. 21, pp. 2314–2316, 2006.

[64] C. Michie, I. Andonovic, R. Atkinson, Y. Deng, J. Szefer, C.-S. Brès, Y.-K. Huang, I. Glesk, P. Prucnal, K. Sasaki, and G. Gupta, "Interferometric noise characterization of a 2-D time-spreading wavelength-hopping OCDMA network using FBG encoding and decoding," *Journal of Optical Networking*, vol. 6, no. 6, pp. 663–676, 2007.

[65] C.-S. Brès, I. Glesk, and P. R. Prucnal, "Demonstration of an eight-user 115-Gchip/s incoherent OCDMA system using supercontinuum generation and optical time gating," *IEEE Photonics Technology Letters*, vol. 18, no. 7, pp. 889–891, 2006.

[66] I. Glesk, P. R. Prucnal, and I. Andonovic, "Incoherent ultrafast OCDMA receiver design with 2 ps all-optical time gate to suppress multiple-access interference," *IEEE Journal of Selected Topics in Quantum Electronics*, vol. 14, no. 3, pp. 861–867, 2008.

[67] J. H. Lee, P. C. Teh, P. Petropoulos, M. Ibsen, and D. J. Richardson, "A grating-based ocdma codingdecoding system incorporating a nonlinear optical loop mirror for improved code recognition and noise reduction," *IEEE Journal of Lightwave Technology*, vol. 20, no. 1, pp. 36–46, 2002.

[68] L. Xu, I. Glesk, V. Baby, and P. R. Prucnal, "Multiple access interference (MAI) noise reduction in a 2D optical CDMA system using ultrafast optical thresholding," in *Lasers and Electro-Optics Society*, Puerto Rico, 2004, paper WP4.

[69] J. H. Lee, P. C. Teh, Z. Yusoff, M. Ibsen, W. Belardi, T. M. Monro, and D. J. Richardson, "A holey fiber-based nonlinear thresholding device for optical CDMA receiver performance enhancement," *IEEE Photonics Technology Letters*, vol. 14, no. 6, pp. 876–878, 2002.

Chapter 3

Nonlinear Optical Thresholding Using Two-Photon Absorption

3.1 Introduction

A number of fibre-based optical time gating and optical thresholding solutions have been experimentally proposed for noise suppression in optical code division multiple access (OCDMA) systems, however these devices generally require lengths of nonlinear fibre and/or a synchronised clock pulse to successful recover the desired data signal in the presence of MAI noise. Another candidate for nonlinear thresholding in OCDMA systems is two-photon absorption (TPA). TPA is a nonlinear optical-to-electrical conversion process present in semiconductor devices that could be used to provide a nonlinear optical thresholder that is low-cost, compact in size and can offer the potential for integration with other devices. Since TPA is a optical-to-electrical conversion process, a TPA-based device also simultaneously optically thresholds and detects an optical signal, eliminating the need for an additional photodetector.

TPA-based devices have been used in a number of different optical signal processing applications to date. These include auto correlation measurements [1, 2], all-optical sampling [3, 4], optical clock recovery [5] and all-optical demultiplexing in OTDM systems [6, 7]. It has also been experimentally demonstrated that a TPA-based microcavity device can be used for dispersion monitoring in WDM systems [8] and optical signal-to-noise ratio (OSNR) monitoring in transmission systems employing NRZ-PSK modulation [9]. TPA in GaAs p-i-n waveguide photodetectors was investigated with respect to optical thresholding in [10, 11]. These demonstrations show the dependence of the TPA photocurrent on the incoming pulse width, with larger photocurrents generated for narrow pulse widths with the same average

pulse power, and highlights the feasibility of TPA as a possible candidate for nonlinear optical thresholding.

This chapter investigates the use of a 1.3 μm Fabry-Pérot (FP) laser diode as a TPA-based optical thresholder and detector. The characterisation of this TPA-based detector in terms of photocurrent generated as a function of incident optical power is outlined in section 3.3. The response of this detector is used to generate an accurate simulation model of the TPA-based device. This model is used in a simulation of a four-channel OCDMA system to determine the feasibility of using a TPA-based device as a nonlinear optical thresholder in section 3.5. Finally, an experimental demonstration of a four-channel OCDMA system is demonstrated in section 3.6. This experiment highlights the performance improvement that is gained through the use of a TPA-based detector in comparison to a standard linear detector, with both devices band-limited to the data rate of the desired channel.

3.2 Two-Photon Absorption

Electrical current is generated in a standard semiconductor photodetector when incident photons with an energy greater than the band gap of the active region are absorbed. These absorbed photons each excite an electron from the ground state, or valance band, to the excited state, or conduction band, creating an electron-hole pair. When an electric field is present across the active region of the photodetector, each electron-hole pair is separated, resulting in a flow of photocurrent in an external circuit.

Incident photons that have an energy less than the band gap of the photodetector do not generate an electron-hole pair and as a result, do not contribute to the photocurrent generated. However, under certain operational conditions, two incident photons can be absorbed simultaneously to produce a single electron-hole pair. This nonlinear optical-to-electrical conversion process is called two-photon absorption and was proposed in 1931 [12] and experimentally demonstrated in 1961 [13].

The TPA process occurs when a photon with energy E_{ph} is incident on an active region with a band gap energy E_g, where $E_{ph} < E_g < 2E_{ph}$. Under these conditions, a single photon does not possess enough energy to produce an electron-hole pair. However, an electron-hole pair can be generated by the simultaneous absorption of two photons, were the combined energy of both photons is greater than the energy of the band gap. This two-photon absorption process can be explained through the use of a virtual state between the conduction band and the valence band and is shown in Figure 3.1. An incident photon with
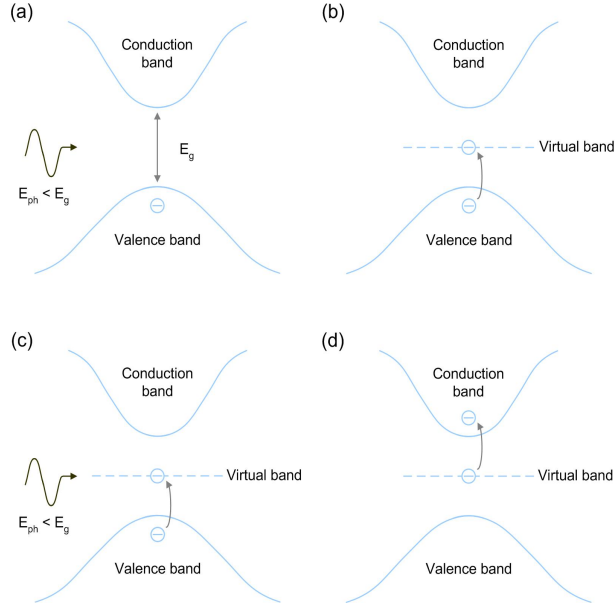
Figure 3.1: Illustration of the two-photon absorption process using an intermediate virtual state.

an energy of $E_{ph} < E_g$ is absorbed, causing an electron to be excited from the valence band to a virtual band somewhere in the band gap region, as shown in Figure 3.1 (a) and (b). This electron is then instantaneously moved to the conduction band by the absorption of a second electron as in Figure 3.1 (c) and (d). By increasing the intensity of the incident light, hence increasing the number of incident photons per second, the probability of two-photon absorption increases. It is this nonlinear response and the ultra-fast response time of 10^{-14} s at 1550 nm [14] that allow TPA to be used for nonlinear optical thresholding. Again it should be noted that the TPA process involves the simultaneous absorption of two photons via a virtual state, resulting in the generated photocurrent becoming proportional to the square of the incident optical power. In contrast a two-step absorption process would require a real intermediate state, with a finite lifetime, resulting in a different intensity-dependent absorption relationship [15].

3.2.1 TPA Photocurrent

Assuming the semiconductor active region has a linear or single photon absorption (SPA) coefficient α and a two-photon absorption coefficient β, the differential equation for the intensity propagation $I(z)$ along the z axis is given by,

$$\frac{dI(z)}{dz} = -\alpha I(z) - \beta I(z)^2 \tag{3.1}$$

Solving for $I(z)$ gives [16],

$$I(z) = I_0 \frac{e^{-\alpha z}}{1 + (\beta I_0/\alpha)(1 - e^{-\alpha z})} \tag{3.2}$$

Both the SPA and TPA contributions to the total absorption for a sample with length L can be derived as,

$$I^{\alpha}_{abs} = I_0 \left(1 - \frac{e^{-\alpha L}}{C} \right) \frac{\alpha L}{\alpha L + \ln C} \tag{3.3}$$

$$I^{\beta}_{abs} = I_0 \left(1 - \frac{e^{-\alpha L}}{C} \right) \frac{\ln C}{\alpha L + \ln C} \tag{3.4}$$

where $C = 1 + (\beta I_0/\alpha)(1 - e^{-\alpha L})$. It can be shown that the photocurrent due to two-photon absorption is given by,

$$J = \frac{eS}{h\upsilon} \left(A_1 I^{\alpha}_{abs} + \frac{1}{2} A_2 I^{\beta}_{abs} \right) \tag{3.5}$$

where e is the electron charge, S is the illuminated area, $h\upsilon$ is the photon energy and A_1 and A_2 are the probabilities of carrier generation due to one- or two-photon absorption respectively.

The generated photocurrent as a function of incident optical power for a semiconductor device is shown in Figure 3.2. The device has a length $L = 1$ μm, an illuminated area $S = 1$ μm^2, a TPA coefficient of $\beta = 2 \times 10^{-12}$ m/W and various values for the SPA coefficient α. The dynamic range over which TPA dominates can be clearly seen, with the TPA response characterised by having a slope of two. The TPA response is limited by SPA which becomes dominant for lower optical powers, with this linear response having a slope of one. TPA is also limited at higher powers by total absorption. It can be seen that the SPA contribution increases as the SPA coefficient is increased, resulting in a reduced dynamic range. Therefore, decreasing the α/β ratio ensures that the dynamic range increases. Increasing the length of the device can also increase the dynamic range, however, this increased length reduces the operating the speed of the device. The level of photocurrent generated by the device in Figure 3.2 is also quite large, with a photocurrent of 100 μA resulting from an incident optical power of 1 W. This is due to the fact that the quantum efficiency of both the SPA and TPA responses, A_1 and A_2 in equation 3.5 are assumed to be 100% and as a result of other simplification assumptions. Despite this however, the use of a TPA-based device for optical signal processing is still feasible, and combined with the advantages previously mentioned for using such a device, makes it a viable candidate for nonlinear optical thresholding.
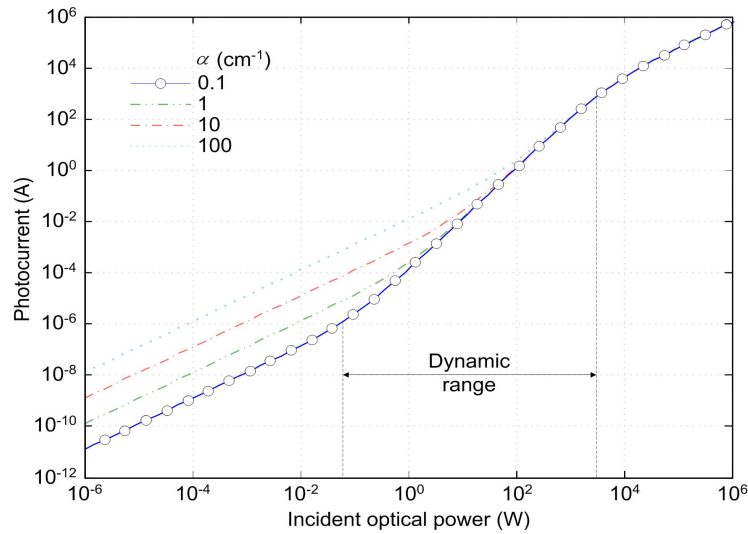
Figure 3.2: Photocurrent as a function of incident optical power for a semiconductor with $L = 1\ \mu$m, $S = 1\ \mu$m^2, $\beta = 2 \times 10^{-12}$ m/W, an incident wavelength of 1550 nm and various values of α.

3.3 Characterisation of a 1.3 μm FP Laser as a TPA-Based Device

It was discussed in the previous section that the nonlinear TPA response can be generated in a device that has a band gap energy greater than the energy of an incoming photon but less than twice the photon energy. If the incident optical signal has a wavelength of 1550 nm, this corresponds to a photon energy of 0.8 eV. Therefore a device that operates at a wavelength of 1310 nm, with a band gap energy of 0.954 eV, could generate a TPA response with sufficient incident optical intensities. As a result, a commercially available 1.3 μm FP laser diode was experimentally characterised as a TPA-based detector.

3.3.1 P-I Curve

A P-I curve is a basic characterisation experiment for a nonlinear device. The experimental setup for the characterisation of a P-I curve for a TPA-based device is shown in Figure 3.3. An optical pulse source is used to illuminate the TPA-based device with the resultant photocurrent generated measured using a picoammeter (pA). Three different optical sources with varying repetition rates and pulse widths were used to ensure that a range of optical peak powers were incident on the device, allowing a complete response for the device to be measured. This is due to the relationship between the peak power of an optical signal and
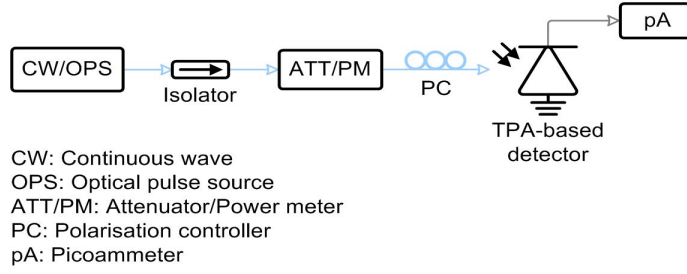
Figure 3.3: Experimental setup to characterise the P-I curve of a TPA-based device.

the average power, with this relationship given by,

$$P_{\text{Pk}} = \frac{T}{\tau} P_{\text{Avg}} \tag{3.6}$$

where T is the period of the optical signal and τ is the pulse width. From equation 3.6 it can be seen that the peak power of an optical signal can be increased by either increasing the period (lowering the repetition rate) of the signal, decreasing the pulse width or a combination of both. Therefore, by using a range of optical sources with varying repetition rates and pulse widths, a large range of optical peak powers can be accessed, ensuring a TPA response from the device under test.

The first source used was a continuous wave (CW) source operating at a wavelength of 1550 nm. An inline attenuator/power meter was used to vary the average optical power that reached the TPA-based device. A polarisation controller (PC) was used before the light was coupled into the device to optimise the polarisation of the signal. Figure 3.4 shows the instantaneous photocurrent generated by the device as a function of the input optical peak power. The triangles ($\triangle$) in Figure 3.4 show the response generated due to the CW source. This response is linear in nature as shown by it having a slope of one. This response also shows the noise floor introduced by the pA used to measure the output photocurrent. Since the duty cycle of the CW source is one, the peak power of the incident light is equal to the average power. As a result, the signal falling on the TPA-based device does not have sufficient energy to generate a nonlinear response.

The second optical source used was a 10 GHz tuneable mode-locked laser (TMLL) that generates an optical pulse train with pulse widths of 2 ps. Due to the pulsed nature of this source, the peak power incident on the TPA-based device was 50 times greater than the average power. Again, the inline attenuator was used to varying the power falling on the device. The diamonds ($\diamond$) in Figure 3.4 show the response due to this signal. Similar to the
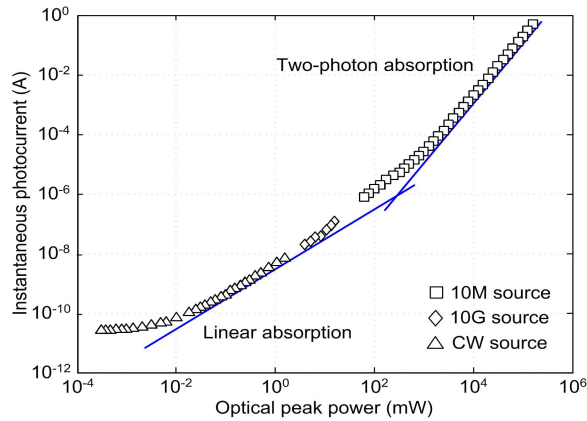
Figure 3.4: P-I curve measured for a 1.3 μm FP laser acting as a TPA-based device.

CW source, the response due to the 10 GHz signal is linear, however, at a peak power of $\sim$ 10 mW, the response starts to deviate towards a slope greater than one. The final source used generated a 10 MHz optical pulse train with a pulse width of $\sim$ 500 fs. This gives an optical peak power that is 250,000 times greater than the average power. The instantaneous photocurrent generated by the TPA-based device from this incident signal is shown by the squares ($\square$) in Figure 3.4. These data points clearly show a nonlinear response due to TPA, indicated by a slope of two. The SPA threshold occurs at an optical peak power of $\sim$ 1 W above which the TPA response becomes dominant.

Figure 3.4 demonstrates the feasibility of using a 1.3 μm FP laser as a nonlinear device. However, it can be seen that a relatively large optical peak power is required to generate TPA within the device. Therefore, to generate a significant amount of photocurrent either a large average power is required or the duty cycle must be decreased by either lowering the repetition rate and/or the optical pulse width. It should also be noted that while the photocurrent values in Figure 3.4 are quite large, these values are the instantaneous values of the photocurrent which were found by multiplying the average photocurrent values by the duty cycle. Therefore the average values are a factor of the duty cycle lower than the instantaneous values. This places a further limit on the repetition rate and pulse width of the optical signal that can be used, as the signal is required to generate an average photocurrent that can be successfully amplified by an electrical amplifier in order to be used in an optical system.

3.3.2 Demonstration of a TPA-Based Device as an Optical Receiver

In the previous section it was shown that a 1.3 μm FP laser could be used as a TPA-based device. However, if such a device is to be used as a simultaneous optical thresholder and detector in an optical system, it is important to determine the performance of the device when operating as an optical receiver. Therefore a bit error rate (BER) analysis is required to ensure that a TPA-based detector can successfully detect an optical data signal in a back-to-back scenario while remaining error-free. In this section, the P-I curve of the TPA-based device is characterised using an incident optical signal that has a repetition rate of 100 MHz and a pulse width of 2 ps. The BER performance of the device is measured as a function of incident average power for an optical data pattern of length $2^7 - 1$.

3.3.2.1 P-I Curve
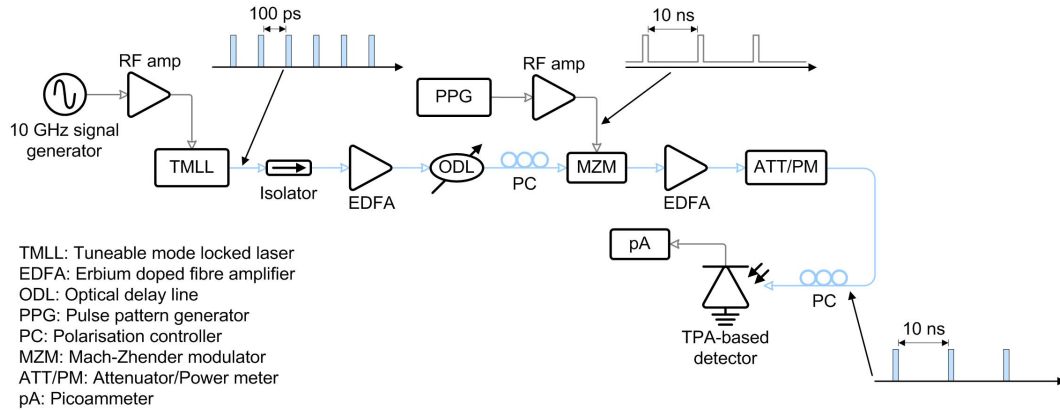
Figure 3.5: Experimental setup to characterise the output photocurrent from a TPA-based device as a function of incident optical power.

The experimental setup used to characterise the generated photocurrent from a TPA-based device with a 100 MHz optical signal is shown in Figure 3.5. A 10 GHz electrical signal generator was used to actively mode-lock a tuneable mode-locked laser (TMLL). This TMLL generates an optical pulse train at a repetition rate of 10 GHz with each optical pulse having a pulse width of 2 ps. This optical pulse train is then amplified using an erbium fibre-doped amplifier (EDFA) before passing through an optical delay line (ODL). This ODL before the MZM is used to ensure that the gated out optical pulse resides within the centre of the 100 ps gating window. The polarization of the signal is controlled using a polarization controller (PC) before it passes through a Mach-Zhender modulator (MZM). The purpose of the MZM is to gate down the optical signal from a repetition rate of 10 GHz to 100 MHz. This is achieved by programming a pulse pattern generator (PPG) with a

10 GHz user defined pattern. This pattern is 100 bits in length and consists of a single '1' bit followed by 99 '0' bits. As a result, the electrical signal that drives the MZM now has a repetition rate of 100 MHz with each '1' bit having a pulse width of 100 ps. As the 10 GHz optical signal passes through the MZM, the electrical signal only allows one in every one hundred optical pulses pass through, effectively gating the 10 GHz optical signal down to 100 MHz with the bit period extending from 100 ps to 10 ns.

The EDFA directly after the TMLL amplifies the 10 GHz optical pulse train to compensate for the power loss incurred in the MZM due to the gating process. After the MZM a second EDFA is used to ensure that the incident optical power on the TPA-based device is sufficient to generate a nonlinear response. An inline optical attenuator/power meter is used to adjust and record the average optical power that is incident on the TPA-based device at any given time. A second PC is also used to adjust the polarization of the optical signal. Finally, the electrical signal generated by the TPA device is measured using a picoammeter (pA).

The purpose of optically gating down the signal is related to equation 3.6 and the relationship between the peak power and the average power of an optical signal as discussed in section 3.3. By lowering the repetition rate to 100 MHz, the peak power of the optical signal is now 5,000 times the average power, assuming a pulse width of 2 ps in comparison to 50 times the average power for a 10 GHz signal. This increase in peak power is required to ensure that a nonlinear response is achieved in the TPA device. Figure 3.6 shows the photocurrent generated as a function of incident optical peak power for the TPA-based device when illuminated with the 100 MHz signal. Similar to Figure 3.4, it can be seen that at
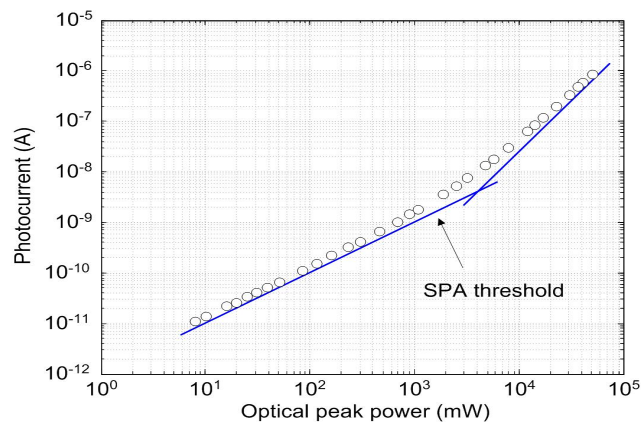
Figure 3.6: Plot of the P-I Curve for the TPA-based device using a 100 MHz optical signal.

low incident optical powers, the response from the TPA-based device is linear, again char-
acterised by a slope of one. The SPA threshold occurs at a peak power power of ~ 1 W,
after which the response moves into the TPA regime.

3.3.2.2 BER Analysis of a TPA-Based Detector
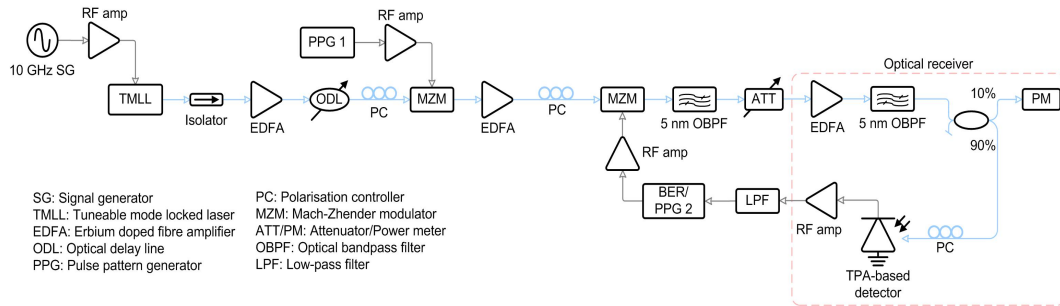
Figure 3.7: Experimental setup to characterise the BER performance of a TPA-based re-
ceiver.

In order for a TPA-based receiver to be used in an optical system, it is important to de-
termine the performance of such a nonlinear device in a back-to-back scenario. In such a
scenario, an optical data pattern is generated and is then immediately incident on the re-
ceiver under test, to determine the ability of the receiver to correctly detect the data signal.
The bit error rate for the receiver is then measured as a function of incident average power,
allowing the performance of the receiver to be assessed.

Figure 3.7 shows the experimental setup for determining the BER performance of a TPA-
based receiver. This setup is quite similar to that discussed in section 3.3.2.1, with a 10 GHz
optical source generating an optical pulse train of 2 ps pulses that are optically clocked down
to 100 MHz. This 100 MHz optical signal is then amplified using an EDFA to compensate
for the losses experienced in the MZM due to the clocking down process. A polarisation
controller is used to optimise the polarisation of the signal before being modulated by a
second MZM. This MZM is electrically driven by a pseudo-random bit sequence (PRBS)
of length $2^7 - 1$. The PRBS signal originates from a 3.3 GHz pulse pattern generator operat-
ing at a repetition rate of 100 MHz. A 5 nm optical bandpass filter (OBPF) centered on the
operating wavelength of 1550 nm follows the MZM to remove the amplified spontaneous
emission (ASE) generated by the two previous EDFAs. A variable attenuator is placed just
before the optical receiver to vary the received optical power.

Within the optical receiver, a final EDFA is used to ensure that sufficient optical power
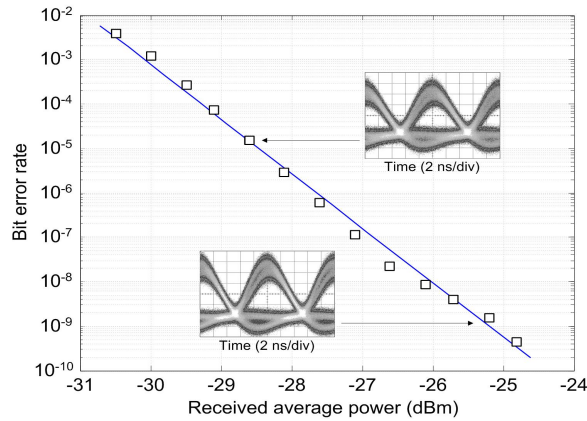
Figure 3.8: BER plot for the TPA-based detector in a back-to-back setup.

is incident of the TPA-based device. This EDFA is followed by a second 5 nm OBPF to remove unwanted ASE. The 10% arm of a 90 : 10 optical coupler is fed to an optical power meter to ensure that the power falling on the TPA device remains constant at 13 dBm, which is in the nonlinear region of the detector. This ensures that any degradation in the measured BER is a result of the changing OSNR due to the changing attenuation before the optical receiver and is not due to a change in response of the TPA device. The remaining 90% from the optical coupler passes through a polarisation controller before falling on the TPA detector. The resultant photocurrent is electrically amplified and passed through an electrical low-pass filter with a bandwidth of 117 MHz. Finally, the electrical signal is analyzed by a BER tester that compares the received signal to the original PRBS sequence and determines the number of errors between the two.

The BER measured as a function of received average power for the TPA-based detector is shown in Figure 3.8. This plot shows that error free performance, defined here as a BER of less than 1×10^{-9}, is achievable using the TPA-based device. It can be seen that the additional power required to change the BER from 1×10^{-2} to 1×10^{-10} is ~ 6 dB. The two insets in Figure 3.8 shows the eye diagrams measured at the respective BER points. These eye diagrams show a largely open eye in which the data can be correctly recovered. However, there is a large amount of noise on both levels of the eye. This is possibly due to in-band ASE generated by the three EDFAs used in the setup that can reduce the amount of TPA generated. The extinction ratio in the first MZM is also important when examining the output of the TPA device. Since this MZM is used to clock down the original 10 GHz signal, the extinction ratio in this modulator is required to be as high as possible to suppress the unwanted optical pulses in this signal. If these unwanted pulses are not suppressed

sufficiently, they form a background noise to the gated optical pulse. At the receiver, this background noise has the effect of increasing the level of SPA and as a result reducing the performance of the receiver. Despite this, however, these results show the feasibility of using a TPA-based device as an optical detector.

3.4 Two-Channel OCDMA System using TPA-Based Detection

To determine the feasibility of a TPA-based optical thresholder and detector in an OCDMA system, a simple two-channel back-to-back OCDMA system was investigated in [17]. This OCDMA system employed a temporal phase coding scheme using fibre Bragg gratings (FBGs). The decoded signal was detected using either a standard linear detector or a TPA-based detector with the output electrical signal from both devices then being analysed.

3.4.1 Experimental Setup

The experimental setup of the two-channel OCDMA system is shown in Figure 3.9. Optical pulses with a duration of 28 ps were generated at repetition rate of 10 GHz at a wavelength of 1561 nm. This operating wavelength corresponds to the operational wavelength of the FBGs used for the encoding/decoding of the optical signal. This optical pulse train was gated down to 155 MHz and encoded with a PRBS data signal before being split by a $50 : 50$ optical coupler. The first arm of the OCDMA encoding stage consists of a 150 m reel of single-mode fibre (SMF), an EDFA, an optical circulator and a super-structured fibre Bragg grating (SSFBG) optical encoder. The SMF was used to ensure that the two copies of the signal that propagate through the first and second arms of the encoding stage are uncorrelated and are not coherently interfering when recombined. The encoding/decoding process was achieved using SSFBGs, with the SSFBG encoders applying two 31-chip, 40 Gchip/s quaternary phase shift keyed codes, similar to those presented in [18]. The second arm of the encoding stage consists of an optical delay line (ODL), a second EDFA, an optical circulator and a second SSFBG for channel two. The ODL allows the relative timing between the two codes to be adjusted at the output of the transmitter. The two encoded signals were then combined before entering the decoding stage. The decoder stage used in the experiment consisted of an EDFA and a single SSFBG, with the SSFBG designed to match that which is used to encode data for channel one. Once decoded, the signal is then detected using either linear detection or TPA-based detection.

The optical receiver consists of two detection subsystems, a nonlinear thresholder and detector and a linear detector. The output signals from these detectors are passed to a digital communications analyzer (DCA) which allowed the production of optical eye diagrams.
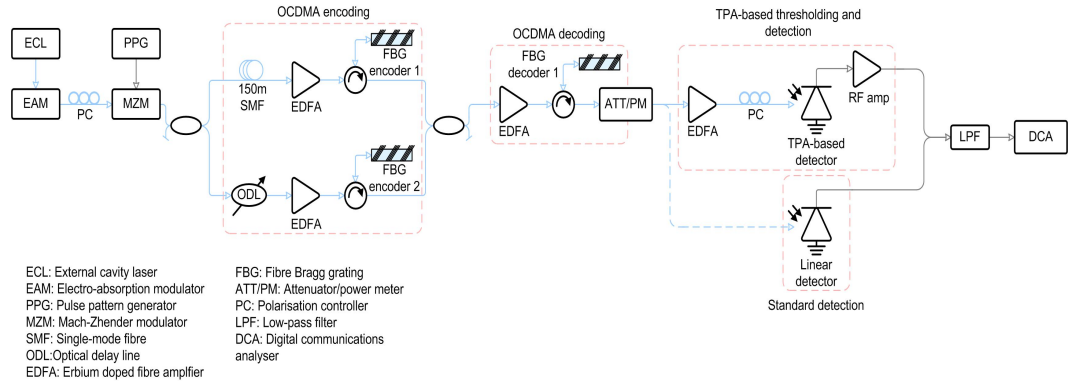
Figure 3.9: Experimental setup of a two-channel OCDMA system employing both linear and TPA-based detection.

The output of the optical decoder enters an inline power meter/attenuator which allowed the average power of the optical signal to be constantly monitored. The nonlinear thresholding and detection subsystem consisted of an EDFA, polarization controller, a 1.3 μm laser diode (InGaAsP, bandwidth $\sim$1 GHz) acting as a TPA detector and a low noise RF amplifier. The linear detector used was the optical input of the DCA. To match the bandwidths of the two detection schemes, the outputs from both detection schemes were passed through a low-pass filter with a bandwidth of 155 MHz prior to entering the DCA. The bandwidth of the DCA was 622 MHz.

3.4.2 Experimental Results

The TPA-based device used was characterised in terms of the average photocurrent generated as a function of incident peak power using a femtosecond laser pulse source generating pulses at a repetition rate of 100 MHz with pulse widths of 5 ps at a wavelength of 1550 nm. The resultant plot is shown in Figure 3.10 (a) for both the experimental characterisation data, given by the squares ($\square$) in the figure, and for the TPA simulation model, given by the dashed line, which is discussed in more detail in section 3.5.1. From this plot it can be seen that the TPA-based device starts to exhibit a nonlinear response at incident peak powers greater than $\sim$ 1 W.

Figure 3.10 (b) and (c) show the traces obtained for the back-to-back two-channel OCDMA system using standard linear detection and TPA-based nonlinear detection, respectively. In Figure 3.10 (b) the overlaid traces for each transmitting channel are shown. The large response corresponds to the correctly decoded pulse while the second response is that of the interfering channel generated by the unmatched encoder/decoder pair. In comparison, Fig-

68
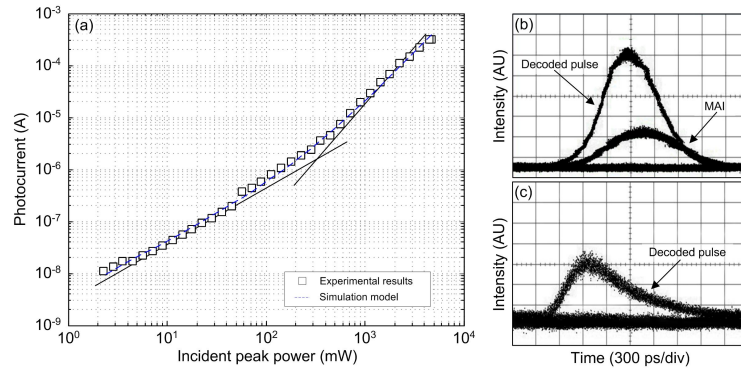
Figure 3.10: Experimental results for the two-channel OCDMA system (a) Plot of photocurrent as a function of optical peak power for the TPA-based detector (b) Received eye diagram using a linear detector (c) Received eye diagram using a TPA-based detector.

ure 3.10 (c) shows only the correctly decoded pulse while suppressing any noise generated by the interfering channel. Using the linear detector, the extinction ratio between the decoded pulse and the MAI was 5.3 dB. This value was improved to ~ 10 dB using the TPA detector, an improvement of ~ 5 dB. From these results, the performance improvement gained through the use of a TPA-based detector is clearly visible, with a significant level of suppression of MAI achieved when compared to standard detection methods.

3.5 Simulation Model of a Four-Channel OCDMA System Using TPA Detection

In the previous section it was shown that a TPA-based detector can increase the extinction ratio of an OCDMA signal compared to a standard linear detector, demonstrating the viability of using a TPA-based device as a receiver in an optical system. In this section, a simulation model is generated to examine the overall system performance of a four-channel OCDMA system, based on the experimental results shown in the previous section. In particular, the performance improvement gained through the use of a TPA-based detector is analysed in comparison to the performance of a system using standard detection techniques.

3.5.1 Four-Channel OCDMA Simulation Model

To assess the performance improvement achieved through the use of a TPA-based detector in an OCDMA system quantitively using bit error rate analysis, a simulation model of the TPA detector characterised in Figure 3.10 (a) was generated. From the measured experimental data in this figure, the SPA and TPA coefficients, α and β, for the TPA detector were

69
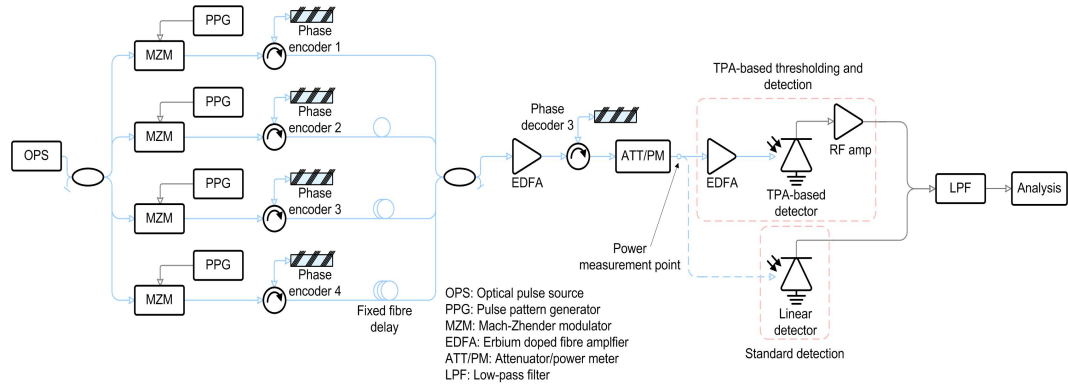
Figure 3.11: Simulation model of a four-channel OCDMA system employing temporal phase coding and TPA-based detection.

found to be 1.36×10^{-4} m^{-1} and 2.35×10^{-16} m/W assuming an effective area of 9.6 μm^2 and a diode length of 600 μm. Using these values and equations (3.3)–(3.5), a TPA detector model was created. The nonlinear response of the simulation model is shown in Figure 3.10 (a) by the dashed line. It can be seen that there is excellent agreement between the response of the physical device and the simulation model.

To directly compare the performance of standard linear detection with the TPA model, a simulation model of a four-channel OCDMA system was created using VPI network simulation software package. The simulation model is shown in Figure 3.11. A 155 MHz optical pulse train with a pulse width of 2 ps was split into four copies that were each modulated by four separate PRBS signals. These signals were encoded using eight-chip temporal phase codes. The four codes used were eight-chip Walsh codes given as $(0, 0, 0, 0, \pi, \pi, \pi, \pi)$, $(0, \pi, 0, \pi, 0, \pi, 0, \pi)$, $(0, 0, \pi, \pi, 0, 0, \pi, \pi)$ and $(0, 0, 0, 0, 0, 0, 0, 0)$ for encoders one to four respectively. In these codes, 0 represents no phase shift on the given optical chip pulse while π represents a 180° phase shift. These codes were chosen due to the minimum amount of interference they generate when passing through a given optical decoder.

The simulation model employs simple slot-level coordination, similar to that described in [19], to prevent optical beat noise between the signals. This slot-level coordination results in each optical signal being delayed by 70 ps with respect to the previous signals. The decoded signal is then either incident on a standard linear detector or the nonlinear TPA model. Throughout all simulation results presented, the phase decoder present corresponds to the optical code used in encoder three. Both detector models pass through a low-pass filter with a bandwidth of 155 MHz. The responsivity of the linear detector was 1 A/W.

70

An additional EDFA with a gain of 25 dB was used before the TPA model to overcome the inherent inefficiency of the TPA process. The optical power incident on the device is measured before the second EDFA and is shown in Figure 3.11 by the power measurement point. The output electrical signal was then analysed in terms of the generated eye diagrams and the BER measurements as a function of incident power as each additional channel was added to the system.

3.5.1.1   Simulation Results using Standard Detection
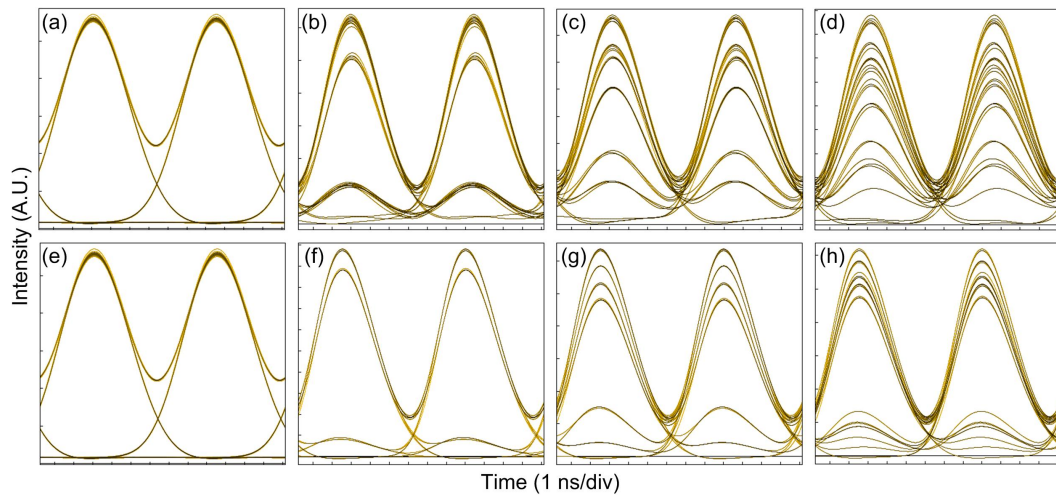
Figure 3.12: (a)–(d) Electrical eye diagrams after detection using a standard detector for one, two, three and four transmitting channels respectively (e)–(h) Electrical eye diagrams after detection using a TPA-based detector for one, two, three and four transmitting channels respectively.

Figure 3.12 (a)–(d) shows the eye diagrams for decoder three using a linear detector for four different cases; only one channel present (a), two channels (b), three channels (c), and when all four channels (d) are present. The multiple eye levels clearly seen in the two, three and four-channel cases can be explained due to the interference from the incorrectly decoded channels. As these channels pass through the decoder, the phase nature of the codes results in constructive and destructive interference occurring in the signal. This results in each channel having a different average power after passing through the decoder, which is subsequently detected by the linear detector. Thus, examining the eye diagram generated for two channels in Figure 3.12 (b), four different levels are present. These levels are (0, 0), (0, 1), (1, 0) and (1, 1), where (x, y) corresponds to the data bit transmitted by the desired channel and the interfering channel respectively. This eye diagram highlights the problem associated with using a linear detector with a bandwidth equal to the data rate of the desired

71

Figure 3.13: BER plot as a function of received average power for a standard linear detector used in a four-channel OCDMA simulation model.

signal. Since the detector integrates the entire incident energy over the bit period, additional levels are introduced when interfering channels are transmitting. If both the desired and unwanted signal possessed the same average power when incident on the detector, then the eye levels (0,1) and (1,0) would merge together in the centre of the eye due to the detectors inability to differentiate between the two signals, thus making correct detection of the desired signal impossible. This problem is further exacerbated with the addition of further channels, resulting in the eye diagram closing quite severely. Again, it should be noted that in this simulation model each channel has a different average power after passing through the decoder and as a result a small portion of the eye opening remains, albeit with a large amount of noise present.

Figure 3.13 shows the simulated bit-error rate plot as a function of incident average power for decoder 3 using a linear detector. As shown, error-free performance, corresponding to a BER of 1×10^{-9}, using a linear detector can only be achieved for systems having at most two channels. Even for the two-channel case, incident average optical power falling on the linear detector must be of the order of –8 dBm in order to ensure error-free performance. This results in a power penalty of 18 dB when the system increases the number of channels from one to two. The two other cases presented containing three and four-channel systems are unable to achieve error-free performance, with a four-channel system having an error floor at a BER of 1×10^{-2}. This error floor is due to the increased levels of MAI generated by the unwanted optical signals falling on the detector. The level of MAI noise increases proportionally with the number of users within the network, limiting overall system performance. From the results presented in Figure 3.13 it is obvious that when a linear detector is

employed in this particular system, the maximum number of users is limited to two. Therefore, if the number of channels is to be increased, some form of nonlinear thresholding is required.

3.5.1.2 Simulation Results using a TPA-Based Detector

As previously mentioned, in order to allow more channels to transmit data across the network, some form of noise suppression is required to reduce the impact of MAI on the overall performance. In this section, the results measured for the four-channel OCDMA system using the model of a TPA-based detector are discussed. These results allow a direct comparison in performance between the two different detection schemes.

Figure 3.12 (e)–(h) show the eye diagrams for the same four transmission scenarios discussed in section 3.5.1.1. As was the case for the linear detector results, the addition of interfering channels results in multiple eye levels being present in the eye diagram. However, the eye openings when using the TPA-based detector are significantly improved when compared to the corresponding eye diagrams for a linear detector. This is due to the TPA-based detectors nonlinear response that suppresses the amount of MAI that is being generated by the improperly decoded optical signals incident on the detector, thus improving overall system performance. The amount of improvement gained is clearly demonstrated by the BER plots for the TPA-based detector shown in Figure 3.14.

Figure 3.14 shows the simulated BER plots obtained for the TPA-based detector. It can be clearly seen that the performance of the TPA detector differs greatly from the performance of the linear detector shown in Figure 3.13. The performance improvement gained through the TPA-based detector allows a BER of 1×10^{-9} to be achieved in all four transmitting scenarios. For a one channel system, error-free performance can be achieved when the incident average power is around -13 dBm. When a second transmitting channel is added to the OCDMA system, a power penalty of approximately 3 dB is incurred. The addition of a third channel incurs a further penalty of $\sim$8 dB, while the addition of the fourth channel incurs a further 3 dB penalty. As a result, there is an overall power penalty of 14 dB when the number of channels is varied from a single channel to a four-channel system. While 14 dB is a significant power penalty, the benefit of such an increase in the incident power is that error-free performance can be achieved with four-channels transmitting data simultaneously using TPA detection. Again this is in comparison to the same situation for linear detection using higher incident optical powers, where error rates of only 1×10^{-2} could be achieved with four channel operation.
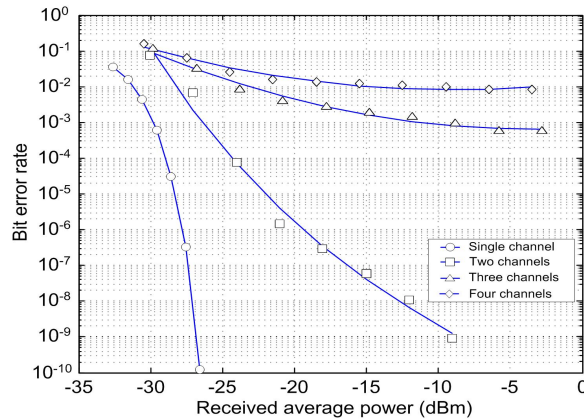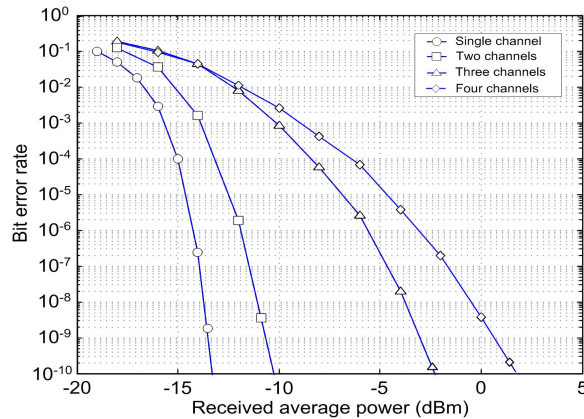
Figure 3.14: BER plot as a function of received average power for a TPA-based detector used in a four-channel OCDMA simulation model.

3.6 Four-Channel OCDMA System Experiment Using a TPA-Based Detector

In the preceding section, a simulation model of a four-channel OCDMA system was presented. This model used both a standard linear detector and a TPA-based detector in the receiver. With both detectors operating with a bandwidth equal to the data rate of the transmitted signal, it was shown that in the case of the linear detector, a large amount of MAI was present on the recovered electrical signal due to the interfering channels. This MAI placed significant limits on the system performance that could be achieved. In the case of the TPA-based detector, it was clear that the nonlinear response present in the device allowed for a large amount of suppression of the MAI noise, hence improving the overall performance. In this section, an experimental demonstration of a four-channel OCDMA system employing both linear and TPA-based detection is presented. The performance of the system using both forms of detection is analysed quantitively using BER results and electrical eye diagrams.

3.6.1 Four-Channel OCDMA System Experimental Setup

The experimental setup of a four-channel OCDMA system is shown in Figure 3.15. The optical pulse source used was an electro-absorption modulator (EAM) based pulse carver that generated a train of 25 ps optical pulses at 10 GHz. The wavelength of these optical pulses was 1559.22 nm. This wavelength was chosen to match the operational wavelength of the FBGs that were used as the OCDMA encoders. The 10 GHz optical pulses were then gated down to 100 MHz using the same method discussed in section 3.3.2.1. This 100 MHz signal
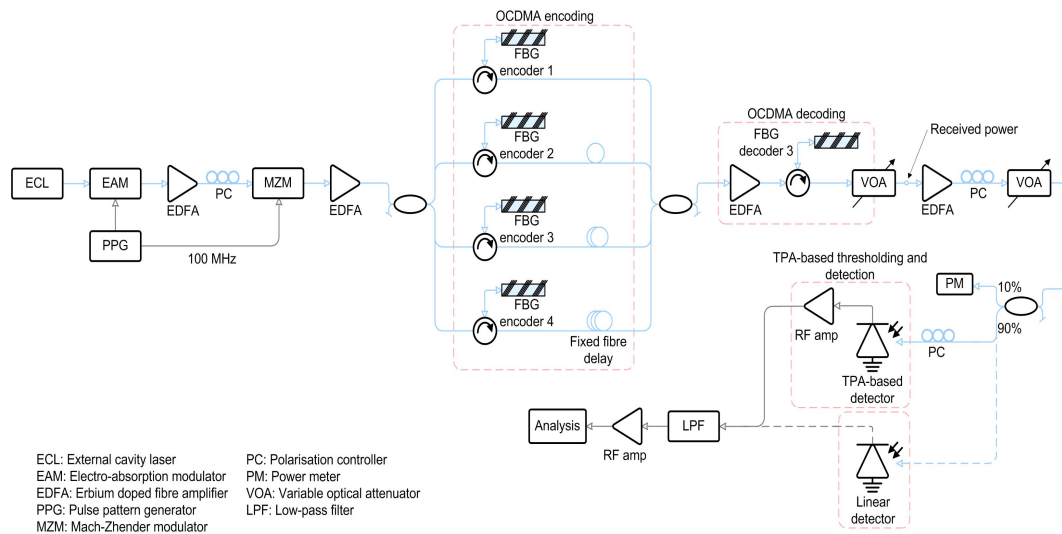
Figure 3.15: Experimental setup of a four-channel OCDMA system using both standard and TPA-based detection methods.

was then data-modulated with a PRBS data signal using an MZM. The modulated signal was then amplified using an EDFA before being split using a one-to-four optical coupler. Each path from the optical coupler is reflected off an FBG encoder which applies an optical code to the signal corresponding to a particular channel. The FBG encoders apply a 31-chip, 40 Gchip/s quaternary phase-shift keyed codes, similar to those discussed in [18], to each data signal. The coded channels, reflected from the FBG encoders, are passed through varying lengths of SMF to ensure that the data signals are uncorrelated. The lengths of SMF are also used to roughly overlap the encoded signals in the time domain. The aggregate signal was amplified using an EDFA before being reflected off an FBG decoder that is matched to the code sequence used in encoder three. A variable optical attenuator (VOA) was used to vary the optical power that entered the optical receiver.

The optical receiver consists of an EDFA, a polarisation controller, a second VOA and either a standard linear photodetector or a TPA-based detector. The VOA in the receiver was used to ensure that the optical power falling on either detector remained constant. Due to the inefficiency of the TPA process, an electrical amplifier is required directly after the TPA detector. This amplifier limits the bandwidth of the detector to roughly 70 MHz. A low-pass filter is used to ensure that the bandwidth of the linear detector is limited to 117 MHz. The output electrical signals were then amplified again before being analysed by a DCA and a bit error rate tester.
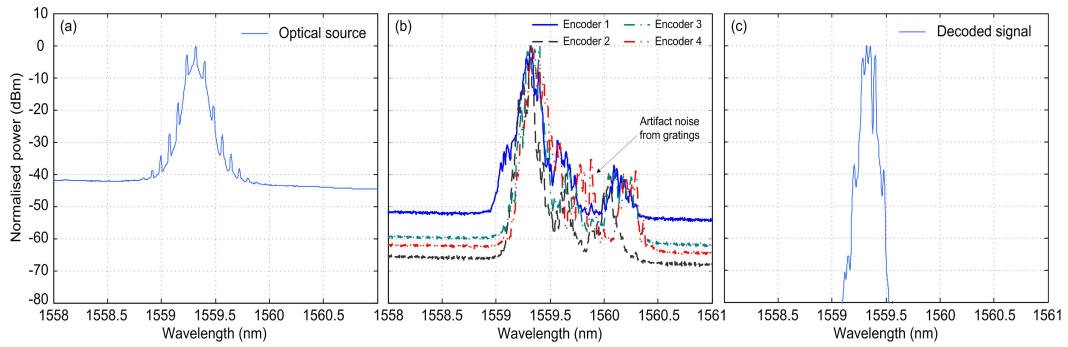
Figure 3.16: Measured optical spectra for (a) the input optical source (b) each optical encoder operating in the reflection mode (c) the output of decoder three operating in the reflection mode.

3.6.1.1 Fibre Bragg Grating Encoders/Decoders

As previously mentioned, the gratings used to apply the optical codes carry 31-chip, 40-Gchip/s quaternary phase codes that offer optimal correlation characteristics [20]. The chip length of the gratings is 2.5 mm, corresponding to a chip duration of 25 ps, hence the pulse width of the optical source was chosen to be 25 ps to match the chip duration of the gratings. The total length of the grating is 77.5 mm. The four code sequences are given as,

Code sequence 1 = [3 2 0 2 3 3 0 3 3 1 2 1 2 3 2 2 0 2 1 2 0 1 2 1 3 0 2 3 3 1 3]

Code sequence 2 = [3 1 2 1 1 3 2 1 2 1 0 2 2 0 3 2 2 1 0 1 3 0 2 1 3 1 1 3 0 2 2]

Code sequence 3 = [2 3 2 3 0 2 2 0 1 2 2 3 0 3 1 0 2 3 1 3 3 1 0 2 2 1 3 2 3 3 1]

Code sequence 4 = [3 3 1 2 2 2 3 3 0 1 3 1 0 1 0 1 2 2 2 0 3 0 2 1 2 1 1 2 2 1 1]

where each number in the sequence is a factor times $\pi/2$, giving the desired phase shifts. Figure 3.16 (b) shows the reflected spectra from the four FBG encoders used in the experimental setup. From these traces it can be clearly seen that there is a pattern dependent structure on the top of each reflected spectrum due to the applied optical code. These traces also highlight the spectral efficiency of the system since each channel occupies the same spectral width around 1559.2 nm. It is believed that the additional peaks at ∼1560 nm are due to ASE noise from the EDFA before the one-to-four optical coupler in Figure 3.15 that is patterned by the wings of the FBG gratings and are not a part of the applied code sequence. This noise occurs 40 dB down from the peak of the main signal.

The filtering property of the FBGs is demonstrated in the spectral traces of both the optical source and the decoded OCDMA signal in Figure 3.16 (a) and (c) respectively. A clear

76
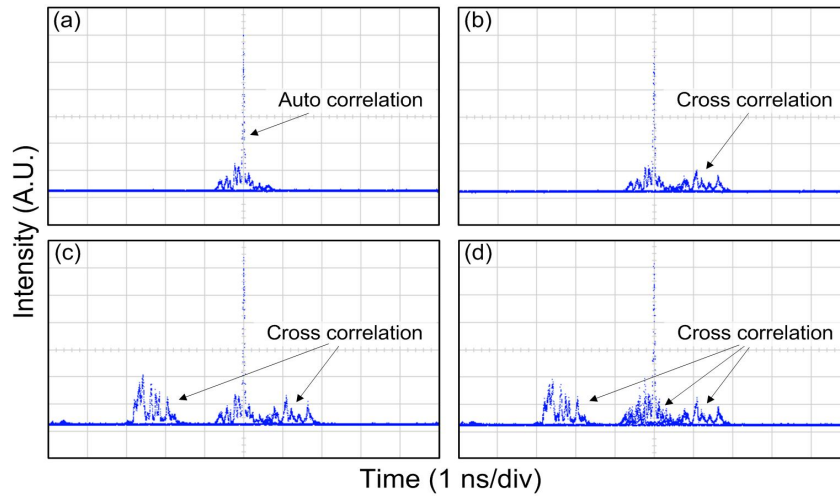
Figure 3.17: Correlation traces measured after decoder three for (a) the matched code (b)–(d) the matched code and each additional unwanted channel added sequentially.

noise floor is visible 40 dB down from the peak on the trace for the optical source, however after passing through the FBG encoders, this noise floor is now between 50 and 65 dB below the main peaks. Finally after the decoding FBG, this noise floor is at least 80 dB below the peak of the main signal. This filtering property is advantageous as it reduces the need for additional band-pass filters in the system and also allows for in OCDMA/WDM hybrid system, as demonstrated in [18]. Figure 3.17 shows the measured correlation traces after the decoder as each channel is added to the system sequentially. Figure 3.17 (a) is the auto correlation trace measured when the encoded data signal from encoder three is correctly decoded by the decoder. The finer elements of the correlations traces are clearly seen due to the high-speed photodetector that was used to detect the optical signal. This auto correlation waveform exhibits a large peak at the centre of the decoded waveform with relatively small auto correlation side lobes. Figure 3.17 (b)–(d) show the combination of the auto correlation and the cross correlation waveforms generated as each additional transmitting channel is added to the system. The additional channels are slightly offset in time due to the varying lengths of fibre that were used to de-correlate the data signals. There is also a clear discrimination between the correctly decoded channel and the remaining unwanted channels as they pass through the optical decoder. However, it should be noted once again that this is only true when using a photodetector with a bandwidth equal to or greater than the chip rate of the OCDMA signal. A lower speed detector that is band-limited to the data rate of a given channel is unable to distinguish between the different channels due to them all having the same amount of optical power, as is demonstrated in the next section.

3.6.2 System Performance Using Standard Detection

Figure 3.18: Plot of the BER as a function of received average power for encoder three using a standard detector as each OCDMA channel is added to the system.

Figure 3.18 shows the BER curves measured as a function of incident average power when channel three is decoded and detected using a standard linear detector. This detector was band-limited to ~ 117 MHz. It can be seen that error rates less than 1×10^{-9} can be achieved, with an incident average power of –24 dBm, with a single channel transmitting. There is a power penalty of 3.5 dB with the addition of an interfering channel. The electrical eye diagrams measured after the photodetector for the single and two channels scenarios are shown in Figure 3.19 (a) and (b) respectively. For the single channel case a clear eye opening is seen, allowing the electrical data to be successfully recovered. However, with the addition of the interfering channel the eye opening is significantly degraded with the addition of multiple eye levels. The four eye levels visible in Figure 3.19 (b) are similar to those discussed in section 3.5.1.1. It can be seen that the peaks of these multiple levels are slightly offset from each other. This is again due to the length of the fibre used after the encoders, which results in the correlation waveforms being offset temporally. This offset however, allows the correct data channel to be recovered from the electrical signal as this channel forms the eye opening to the left, as seen in Figure 3.19 (b). As a result, error rates approaching error free can be achieved with two transmitting channels.

The addition of a third transmitting channel further closes the eye opening as seen in Figure 3.19 (c). This third channel introduces more eye levels to the eye diagram and also introduce an eye opening to the left-hand side of the eye opening. By examining Figure 3.17 (c) it is clear that this eye opening is due to the third channel being temporally offset from the main eye opening by 2 ns. Therefore extracting the desired electrical data
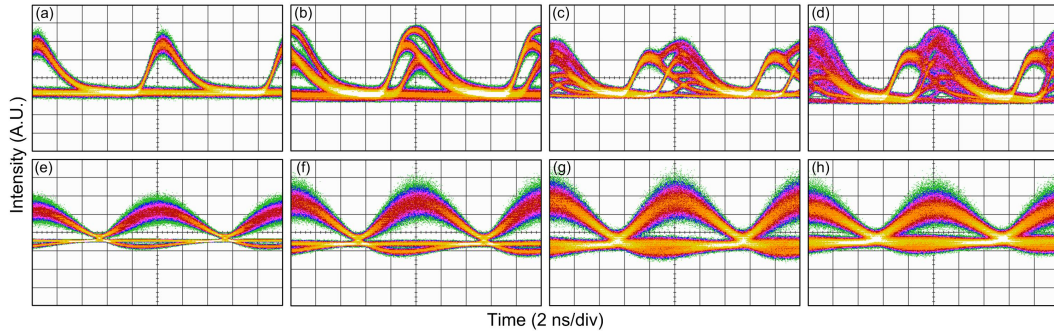
Figure 3.19: (a)–(d) Eye diagrams measured after linear detection for one to four channels transmitting respectively (e)–(h) eye diagrams measured after TPA-based detection for one to four channels.

pattern from this portion of the signal is not possible as it is not part of the desired signal. Figure 3.18 shows that an error floor at 1×10^{-3} is introduced with the addition of the third channel. This result is in good agreement with the simulation results for the four-channel OCDMA system with linear detection discussed in section 3.5.1.1. Finally, Figure 3.19 (d) shows the eye diagram obtained for all four channels simultaneously transmitting on the system. For this case, the main eye opening has been completely closed due to MAI from the interfering channels. This level of noise is so large that no BER data could be obtained for this four-channel scenario. In the next subsection, the performance of the same system is examined with the TPA-based detector used instead of the linear detector.

3.6.3 System Performance Using TPA-Based Detection

The bit error rates measured as a function of incident average power for the OCDMA system using TPA-based detection are shown in Figure 3.20. From this figure it can be seen that error free operation can be achieved for the single channel case at a received average power of –18 dBm. The addition of the second channel results in a power penalty of 3 dB with error free performance now achieved at a received power of –15 dBm. Figure 3.19 (e) and (f) show the eye diagrams obtained for the one and two-channel cases for the OCDMA system using a TPA-based detector respectively. When compared to the corresponding eye diagrams for the linear detector, it can be clearly seen that the additional eye levels cause by MAI have been suppressed by the nonlinear response of the TPA-based detector, giving a clear thresholding window in which the data pattern can be retrieved.

For the three-channel scenario, the best BER achieved was 5×10^{-8} at a received power of –10 dBm. Similarly, for the four-channel case, the lowest BER achieved was 6×10^{-6} at
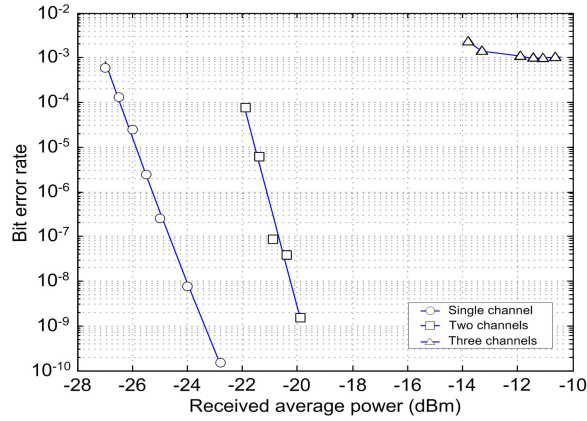
79
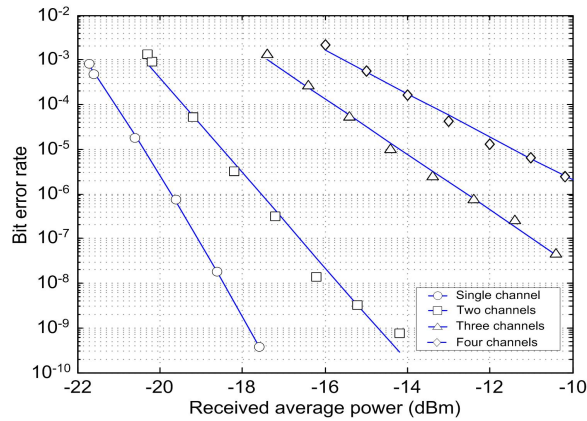
Figure 3.20: Plot of the BER as a function of received average power for encoder three using TPA-based detection as each OCDMA channel is added to the system.

a received power of –10 dBm. Examining the respective eye diagrams in Figure 3.19 (g) and (h), it can be seen that the addition of each interfering channel results in the eye opening gradually closing, accounting for the gradual degradation of performance as measured by the BERs in Figure 3.20. However, when these eye diagrams are compared to the same diagrams measured for the linear detector, a clear improvement can be seen for the TPA-based detector as the device suppresses the multiple eye levels generated by the MAI. The overall power penalty associated with the transition from a single channel system to a four channel system is 9 dB at an error rate of 1×10^{-5}. This value is in excellent agreement with the simulation model results in section 3.5.1.2 where a power penalty of 10 dB is incurred at the same error rate when moving from a single channel to a four channel system. It should be noted that for the BER curves, the optical power measured is the power present in all transmitting channels. Therefore if all channels in a four-channel system have the same average power then there is an inherent 9 dB power penalty incurred between the single channel and four channel case, assuming an ideal optical thresholder.

It is believed that better overall performance in terms of BER and receiver sensitivity could be achieved using the TPA-based detector by improving the optical signal-to-noise ratio (OSNR) of the generated optical pulses. An OSNR of 18 dB was measured for the optical pulses directly before the pulse train was split using the one-to-four optical coupler. This in-band noise results in a reduced level of TPA photocurrent generated by the device, increasing the required incident power. The effect of this low OSNR is visible in the eye diagram in Figure 3.19 (e). This eye diagram clearly shows a significant level of noise present on the one level of the eye, indicating a large level of noise within the incident op-

tical signal. By increasing the OSNR, a larger TPA photocurrent could be generated for a given received power, resulting in an improved receiver sensitivity. Despite this however, the performance improvement that can be achieved through the use of a TPA-based simultaneous thresholder and detector when compared to a standard detector can be clearly seen in the results presented in this section.

3.7 Summary

Due to the nature of an OCDMA system, the performance of the system is limited by the number of simultaneously transmitting channels in the form of MAI. It has been shown that using standard detection methods operating with a bandwidth equal to the data rate of a given channel, the performance of the OCDMA system is severely degraded when two or more channels are transmitting at the same time due as a result of the detector being unable to distinguish between the desired channel and the unwanted channels. One method that can be used to overcome this problem is to take advantage of the nonlinear optical-to-electrical conversion process of two-photon absorption that is present in semiconductor devices. This nonlinear response can be used to simultaneously optical threshold and detect an OCDMA signal. In this chapter, the feasibility of using a TPA-based device in an OCDMA system has been demonstrated by characterising its nonlinear response while determining its ability to correctly detected an optical data pattern. It is shown experimentally that a TPA-based device can improve the extinction ratio of an OCDMA signal by 5 dB in comparison to a standard detector, with this figure dependent on the initial extinction ratio. The performance of an OCDMA system using both a standard detector and a TPA-based device is examined both experimentally and through simulation models. In both instances, it is demonstrated that there is a significant performance improvement gained by using the TPA device over a standard detector. This improvement allows the number of simultaneous channels to be increased while still allowing error free operation.

References

[1] L. P. Barry, B. C. Thomsen, J. M. Dudley, and J. D. Harvey, "Autocorrelation and ultrafast optical thresholding at 1.5 μm using a commercial InGaAsP 1.3 μm laser diode," *Electronics Letters*, vol. 34, no. 4, pp. 358–360, 1998.

[2] T. Krug, M. Lynch, A. L. Bradley, J. F. Donegan, L. P. Barry, H. Folliot, J. S. Roberts, and G. Hill, "High-sensitivity two-photon absorption microcavity autocorrelator," *IEEE Photonics Technology Letters*, vol. 16, no. 6, 2004.

[3] K. Kikuchi, "Optical sampling system at 1.5 μm using two photon absorption in Si avalanche photodiode," *Electronics Letters*, vol. 34, no. 13, pp. 1354–1355, 1998.

[4] B. C. Thomsen, L. P. Barry, J. M. Dudley, and J. D. Harvey, "Ultra sensitive all-optical sampling at 1.5 μm using waveguide two-photon absorption," *Electronics Letters*, vol. 35, no. 17, pp. 1483–1484, 1999.

[5] R. Salem and T. E. Murphy, "Broad-band optical clock recovery system using two-photon absorption," *IEEE Photonics Technology Letters*, vol. 16, no. 9, pp. 2141–2143, 2004.

[6] B. C. Thomsen, L. P. Barry, and J. M. Dudley, "Ultrahigh speed all-optical demultiplexing based on two-photon absorption in a laser diode," *Electronics Letters*, vol. 34, no. 19, pp. 1871–1872, 1998.

[7] P. J. Maguire, L. P. Barry, T. Krug, M. Lynch, A. L. Bradley, J. F. Donegan, and H. Folliot, "Simulation of a high-speed demultiplexer based on two-photon absorption in semiconductor devices," *Optical Communications*, vol. 249, no. 4–6, pp. 415–420, 2005.

[8] K. Bondarczuk, P. J. Maguire, D. A. Reid, L. P. Barry, J. O'Dowd, W.-H. Guo, M. Lynch, A. L. Bradley, and J. F. Donegan, "Chromatic dispersion monitoring for high-speed WDM systems using two-photon absorption in a semiconductor microcavity," *IEEE Journal of Quantum Electronics*, vol. 45, no. 3, pp. 223–232, 2009.

[9] D. A. Reid, K. Bondarczuk, K. J. Dexter, K. Shi, P. M. Anandarajah, L. P. Barry, W.-H. Guo, J. O'Dowd, M. Lynch, A. L. Bradley, and J. F. Donegan, "Two-photon-absorption-based OSNR monitor for NRZ-PSK transmission systems," *IEEE Photonics Technology Letters*, vol. 22, no. 5, pp. 275–277, 2010.

[10] Z. Zheng, A. M. Weiner, J. H. Marsh, and M. M. Karkhanehchi, "Ultrafast optical thresholding based on two-photon absorption GaAs waveguide photodetectors," *IEEE Photonics Technology Letters*, vol. 9, no. 4, pp. 493–495, 1997.

[11] Z. Zheng, S. Shen, H. Sardesai, C.-C. Cheng, J. H. Marsh, M. M. Karkhanehchi, and A. M. Weiner, "Ultrafast two-photon absorption optical thresholding of spectrally coded pulses," *Optical Communications*, vol. 167, no. 1–6, pp. 225–233, 1999.

[12] M. Göppert-Mayer, "Über elementarakte mit zwei quantensprügen," *Annalen der Physik*, vol. 401, no. 3, pp. 273–294, 1931.

[13] W. Kaiser and C. G. B. Barrett, "Two-photon excitation in CaF_2:Eu^{2+}," *Physical Review Letters*, vol. 7, no. 6, pp. 229–231, 1961.

[14] J. Donegan, "Two-photon absorption speeds optical switching," *Lightwave Europe*, vol. 1, no. 5, p. 31, 2002.

[15] H. P. Weber, "Two-photon absorption laws for coherent and incoherent radiation," *IEEE Journal of Quantum Electronics*, vol. 7, no. 5, pp. 189–195, 1971.

[16] P. M. W. Skovgaard, R. J. Mullane, D. N. Nikogosyan, and J. G. McInerney, "Two-photon photoconductivity in semiconductor waveguide autocorrelators," *Optical Communications*, vol. 153, no. 1–3, pp. 78–82, 1998.

[17] P. J. Maguire, K. Bondarczuk, L. P. Barry, C. Tian, Z. Zhang, M. Ibsen, D. J. Richardson, and P. Petropoulos, "Reduction of multiple access interference in a DS-OCDMA system via two-photon absorption," in *Proceedings of Optical Fibre Communications (OFC)*, Anaheim, California, 2006, paper OWV6.

[18] C. Tian, Z. Zhang, M. Ibsen, P. Petropoulos, and D. J. Richardson, "A 16-channel reconfigurable OCDMA/DWDM system using continuous phase-shift SSFBGs," *IEEE Journal of Selected Topics in Quantum Electronics*, vol. 13, no. 5, pp. 1480–1486, 2007.

[19] Z. Jiang, D. S. Seo, S.-D. Yang, D. E. Leaird, R. V. Roussev, C. Langrock, M. M. Fejer, and A. M. Weiner, "Four-user, 2.5-Gb/s, spectrally coded OCDMA system demonstration using low-power nonlinear processing," *IEEE Journal of Lightwave Technology*, vol. 23, no. 1, pp. 143–158, 2005.

[20] S. Boztas, R. Hammons, and P. Y. Kumar, "4-phase sequences with near-optimum correlation properties," *IEEE Transactions on Information Theory*, vol. 38, no. 3, pp. 1101–1113, 1992.

Chapter 4

Noise Suppression using an SA-SOA-TPA-Based Receiver

4.1 Introduction

Multiple access interference suppression is a key element for increasing the number of channels in an OCDMA system while maintaining a high level of performance. It has been demonstrated in the previous chapter that the nonlinear optical-to-electrical conversion process of two-photon absorption can be used to simultaneously optically threshold and detect an OCDMA signal, providing a significant performance improvement in comparison to standard detection methods. In this chapter a saturable absorber is examined as an additional nonlinear optical device that can be used in conjunction with a TPA-based device for the suppression of MAI. It is shown that the use of a saturable absorber before a TPA-based detector can further improve the performance of an optical system in the presence of MAI. This improvement is due to the suppression of noise in the saturable absorber.

The degradation of performance due to optical beat noise is also examined in this chapter. It is shown that the beating between optical signals is a limiting factor on the number of channels that can be supported by a given OCDMA system. The nonlinear responses of both a saturable absorber (SA) and a TPA-based device intensify this beat noise, resulting in the need to clamp the peak of the optical signal. This is achieved through the use of a gain-saturated semiconductor optical amplifier (GS-SOA). This GS-SOA is used to clamp the peak of the optical signal to a single level after it has been reflected off a saturable absorber and before it is thresholded and detected using the TPA-based device. This SA-SOA-TPA-based receiver is experimentally demonstrated in an optical system that simulates the output of an OCDMA system. It is shown that this receiver can overcome the limitations imposed

85

on a given system by the effects of both MAI and optical beat noise.

4.2 Nonlinear Optical Thresholding using a Saturable Absorber and a TPA-Based Device

It was shown in chapter three that a TPA-based device can be employed as an optical thresholder to improve the performance of an OCDMA system. In this section, a nonlinear receiver consisting of a saturable absorber directly before a TPA-based device is tested to determine the performance improvement that can be gained from such a receiver when used in an OCDMA system in the presence of MAI.

4.2.1 Saturable Absorber

A saturable absorber is an optical device that exhibits an intensity-dependent transmission characteristic. This means that the device behaves differently depending on the intensity of the light passing through it [1]. When the device is illuminated with an optical signal with an instantaneous peak power below some threshold P_{sat}, the photonic absorption of the saturable absorber is high, resulting in a low transmittance of the signal. Above the threshold value, the absorption of the device begins to saturate resulting in the transmittance of the absorber rapidly increasing towards a level near unity excluding the insertion loss. This nonlinear transfer curve of the saturable absorber allows it to be used in a number of applications such as passive mode-locking of lasers [2, 3] and optical regeneration [4, 5]. Figure 4.1 shows the typical construction of a resonant saturable absorber mirror (RSAM).
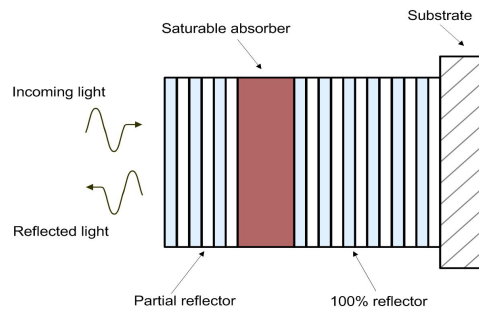
Figure 4.1: Typical construction of a resonant saturable absorber mirror.

These devices are typically made up of a InGaAs/InP quantum well structure embedded in a microresonator. The front mirror of the microresonator is a dielectric multilayer mirror made of TiO_2/SiO_2 while the back mirror is a high-reflectivity metallic based mirror of $Ag+SiO_2$. This resonator structure reduces the device saturation threshold and increases

the saturation contrast [6]. The saturable absorber presented in this chapter is an RSAM mounted on an optical circulator. This RSAM has a strong nonlinear reflectance with a low and high intensity transmittance of 3 and 45% respectively. The resonance wavelength of the device is 1556 nm with a temperature dependent resonance wavelength shift of $\Delta\lambda = 6$ nm for a temperature change of between $10 - 70$ °C. This device is designed specifically for optical noise suppression with the main applications being the suppression of ASE after optical amplification.

Figure 4.2 shows the reflection profile of the saturable absorber. This reflection profile was characterised by illuminating the device with ASE generated by an EDFA and measuring the reflected optical signal using an optical spectrum analyser. From the figure a clear dip can be seen at a wavelength of 1556 nm corresponding to the resonance wavelength of the device and the resultant absorption of the incident light at this wavelength. A saturable absorber has a number of factors that determine the level of suppression that can be achieved through the use of the device. Firstly, the reflectance of the device is dependent on the fluence of the incoming optical pulses. Since the pulse fluence is given by the energy of the pulse per incident area, the spot size on which the light is focused into the device becomes important. Secondly, the factor by which the signal-to-noise ratio (SNR) is improved depends on the input signal-to-noise ratio. If the SNR of the input is high, then the suppression ratio is larger than if the SNR of the input signal was small. Finally, it has been shown in [7] that a temperature increase in the device due to an optical signal depends on the repetition rate and the pulse width of the optical signal. The main consequence of this temperature change is a shift in the reflectivity spectrum of the device towards higher wavelengths reducing the contrast ratio.
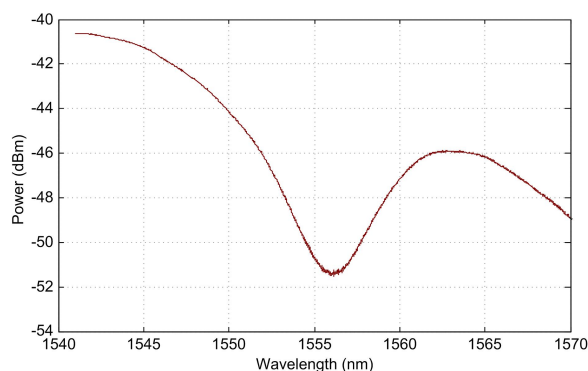
Figure 4.2: The reflection profile of a saturable absorber using ASE generated by an EDFA.
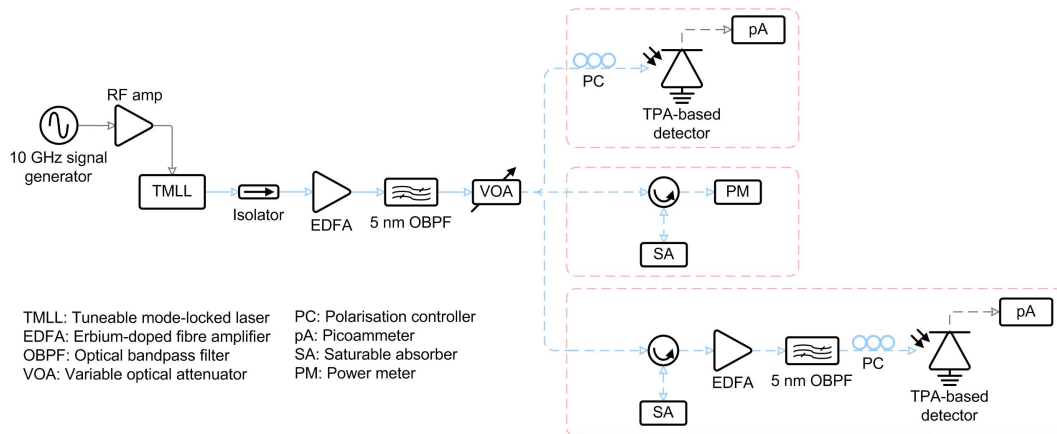
Figure 4.3: Experimental setup used to characterise a nonlinear receiver consisting of a saturable absorber and a TPA-based detector.

4.2.2 Characterisation of an SA-TPA-Based Receiver

The nonlinear responses of both the saturable absorber and the TPA-based device were characterised using the experimental setup shown in Figure 4.3. In this setup both the saturable absorber and the TPA-based detector were characterised individually before the combined nonlinear response of both devices operating in series was measured. The experimental setup was as follows. A tuneable mode-locked laser (TMLL) laser source was actively mode-locked using an RF signal generator operating at 10 GHz. The resultant 10 GHz optical pulse train was amplified using an EDFA and passed through a 5 nm optical bandpass filter. A variable optical attenuator was used to vary the optical power that was then incident on one of three different devices under test (DUT) configurations. The first DUT consisted of a polarisation controller and a TPA-based device. The resultant photocurrent generated was measured using a picoammeter. The second DUT consisted of an optical circulator that reflected the incoming optical signal off the saturable absorber. The optical power of the reflected signal was then measured using a power meter. The final DUT configuration consisted of a circulator which reflected the incoming light off the saturable absorber. The reflected signal from the SA was then re-amplified using an EDFA to ensure that the optical power incident on the TPA-based device was sufficient to generate a nonlinear response. This second EDFA was followed by an additional 5 nm bandpass filter and a polarisation controller. The generated TPA photocurrent was measured using a picoammeter. Figure 4.4 shows the measured nonlinear responses for the TPA-based device, the saturable absorber and the saturable absorber in series with the TPA-based device. The photocurrent generated as a function of incident average power for the TPA-based device is shown in Figure 4.4 (a). From this plot it can be seen that the output of the device becomes dominated by TPA at an
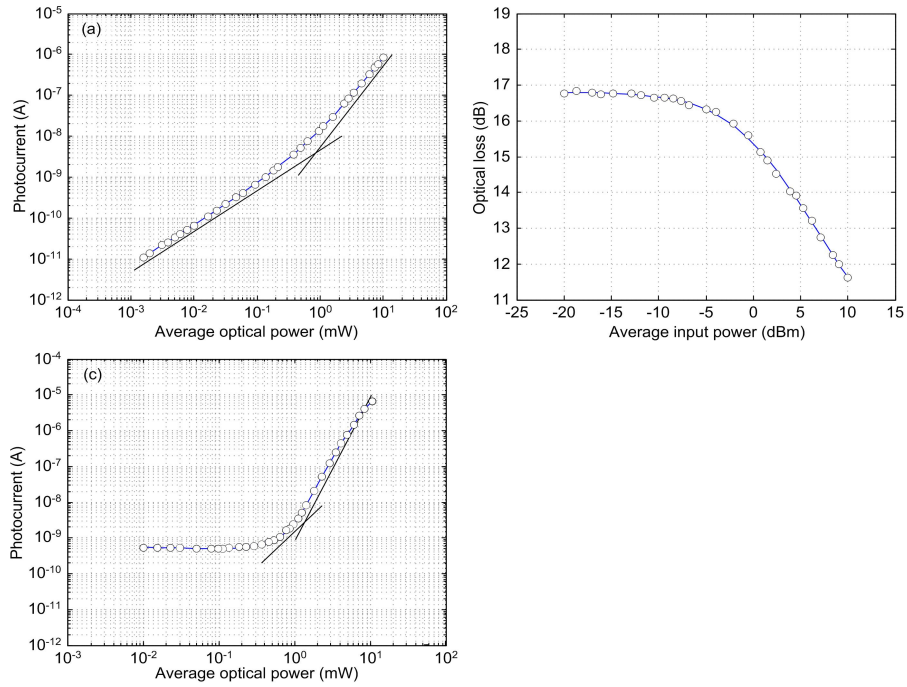
Figure 4.4: The measured (a) photocurrent as a function of average optical power for a TPA-based device (b) optical loss as a function of average incident optical power for the saturable absorber and (c) photocurrent as a function of incident average power for the saturable absorber in series with the TPA-based device.

average power of ~ 0.25 mW. Below this value the response is linear due to SPA being the dominant contributor. The optical loss measured as a function of input average power for the saturable absorber is shown in Figure 4.4 (b). It can be seen that for low optical powers below –7 dBm, the optical loss experienced upon reflection from the device was measured as 16.8 dB. The optical loss of the device is reduced by 5.1 dB to 11.7 dBm at an average input power of 10 dBm.

Figure 4.4 (c) shows the measured photocurrent from the TPA-based device with the saturable absorber directly before it. From this plot, it can be seen that at input optical powers less than 0.3 mW, the output photocurrent from the TPA-based device is constant at a value of $\sim 6 \times 10^{-10}$ A. This is due to the large losses experienced in the saturable absorber at low powers, resulting in only a small amount of the optical signal being reflected off the device and reaching the following EDFA. Therefore ASE dominates the output signal from the EDFA, operating in constant output power mode, which is incident on the TPA-based device. This ASE signal remains relatively constant for low input signals hence a constant output photocurrent from the TPA device. As the input power increases above 0.3 mW the
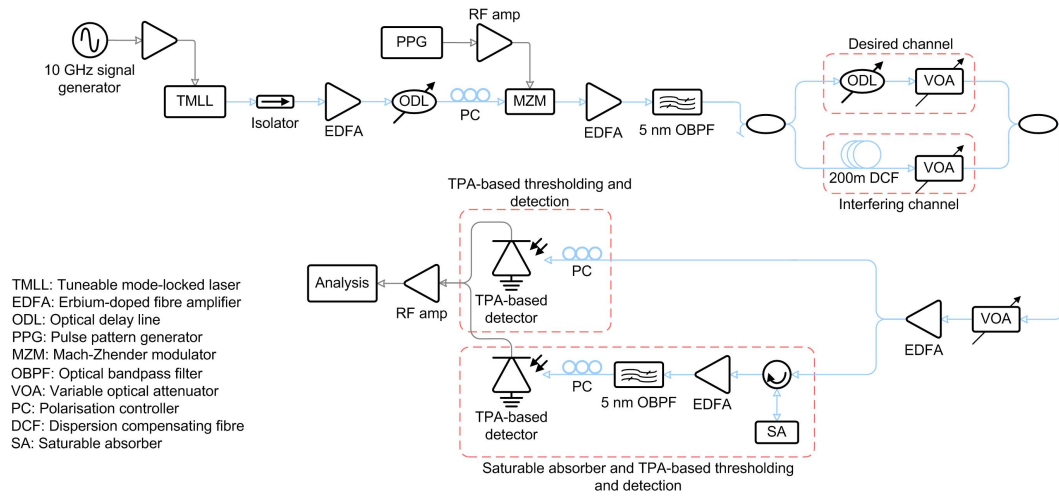
Figure 4.5: Experimental setup to demonstrate using a combination of a saturable absorber and a TPA-based detector to suppress MAI.

photocurrent moves into a nonlinear regime. It can be seen that this nonlinear response gives a steeper slope than either the nonlinear response from the TPA-based device or the saturable absorber, providing better thresholding discrimination. Therefore the nonlinear characteristics of both devices combine to produce a significantly steeper nonlinear response. This combined response can result in a greater suppression of MAI present in a decoded OCDMA signal.

4.2.3 Experimental Setup

Figure 4.5 shows the experimental setup used to test the performance of a two-channel system using a saturable absorber and a TPA-based detector. In this system, the OCDMA encoding and decoding operations are not performed. Instead this system simulates a typical decoded OCDMA signal consisting of a correctly decoded signal and an unwanted interfering signal that would be encountered after a given optical decoder. This is achieved as follows. A 10 GHz optical pulse train with a pulsewidth fo 2 ps was generated using a tuneable mode-locked laser. This pulse train was amplified using an EDFA before is was optically gated down to a repetition rate of 100 MHz using a Mach-Zhender modulator. This same MZM applied a $2^7 - 1$ data signal to the 100 MHz pulses. The data signal was amplified by a second EDFA before being split by a 50 : 50 optical coupler. The first arm from the coupler consists of an optical delay line and a variable optical attenuator. This arm is intended to simulate a correctly decoded OCDMA signal. The 2 ps optical pulses represent the auto correlation peak that would be generated by an OCDMA decoder if the

matching encoded signal passed through it. The second arm from the coupler consists of 200 m of dispersion compensating fibre (DCF) and a second variable optical attenuator. The length of DCF is used to temporally broaden the 2 ps pulses in this arm to ~ 35 ps. The DCF also decorrelates the data patterns between the two arms. This second arm is intended to simulate the MAI generated by an interfering channel that has been incorrectly decoded in an OCDMA decoder. The attenuators in each arm are used to ensure that both channels have the same average power.

The optical signals from both arms are combined using a second coupler. The optical delay line in the first arm is used to offset the centre of both signals by 50 ps to eliminate beat noise. The combined optical signal with the 50 ps offset is shown in Figure 4.6. This signal was varied using a variable optical attenuator before passing to the receiver. Two receiver configurations were used. The first consisted of an EDFA followed by the TPA-based detector, and the second consisted of a saturable absorber, an additional EDFA, a 5 nm bandpass filter and the TPA-based detector. The TPA detector in both cases is bandwidth-limited to 100 MHz. The output electrical signals from both receivers were amplified before being analysed using a BER tester and an oscilloscope.
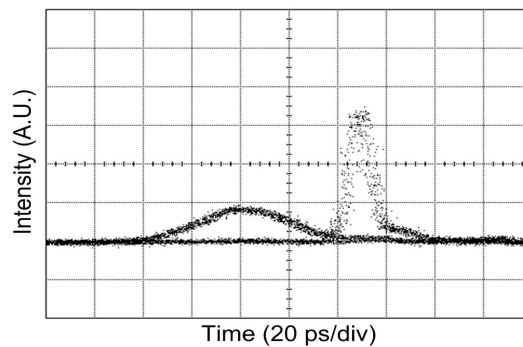
Figure 4.6: Measured optical signal with the desired channel and the interfering channel offset by 50 ps.

4.2.4 Experimental Results

Figure 4.7 (a) shows the measured BER plots and eye diagrams for the SA-TPA receiver and the TPA-based detector. The performance of the system was measured for each receiver with one and two-channel operation. It can be seen that error-free performance can be achieved using the TPA-based detector with only the desired channel transmitting, as shown in Figure 4.7 (a). A BER of 1×10^{-9} is possible for a received average power of
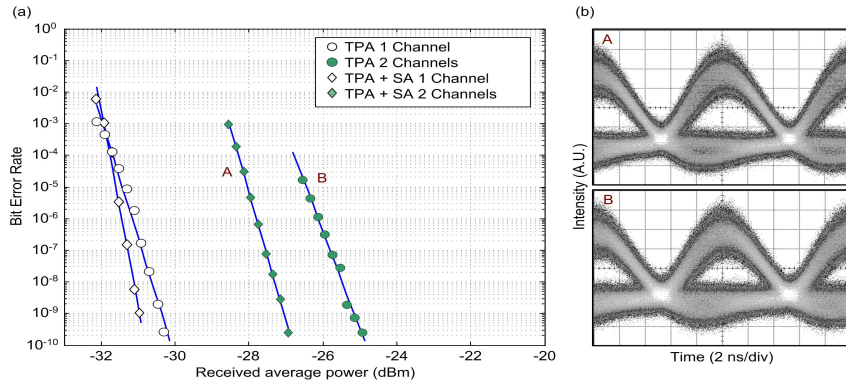
Figure 4.7: Measured BER plots as a function of average power and eye diagrams for the SA-TPA receiver.

– 30 dBm. When the interfering channel is added there is a power penalty of 5 dB when using the TPA-based detector. However, despite this addition penalty, error-free performance is still achievable at a received power of – 25 dBm.

Error-free performance can also be achieved using the SA-TPA receiver with a single channel transmitting. A BER of 1×10^{-9} is obtained for a received power of – 31 dBm. This is an improvement of 1 dB compared to the TPA-based detector only. The addition of the second transmitting channel results in a power penalty of 3 dB. However, as with the TPA-based detector, error-free operation is possible even with the interfering channel present. The improvement in the power penalty of 2 dB for the two-channel case is due to the saturable absorber improving the OSNR of the received signal. This improvement in the OSNR results in a larger TPA photocurrent and hence an improved receiver performance.

Two eye diagrams, A and B, are shown in Figure 4.7 (b). The points at which these eye diagrams were taken are shown on the BER plot. Both eye openings were taken for the two-channel case. It can be seen that the eye is largely open and does not contain the multiple levels that were evident for linear detection methods discussed in section 3.6.2. Again, it should be noted that while the interfering channel is offset from the desired channel by 50 ps, the TPA-based detector is bandwidth-limited to the data rate of the data signal. Therefore, both incoming optical channels are integrated over the bit period of the signal which would result in a three-level eye opening, due to both channels having the same average power, if a linear detector was used. However, in both cases the combined nonlinear responses of the saturable absorber and the TPA-based detector successfully suppress the interfering channel allowing the electrical data signal to be recovered.

An eye diagram measured after a TPA-based device with a temporal offset of 50 ps between the channels is shown in Figure 4.8 (a). It can be seen from the eye diagram that there is a minimal amount of beating occurring between the two signals due to the temporal offset. However, Figure 4.8 (b) shows the same eye diagram measured after the TPA-based device when the offset is reduced to 0 ps. From this eye diagram a large amount of beating is visible on the one level of the signal reducing the eye opening and hence reducing the performance of the system. This is because although the nonlinear response of both the saturable absorber and the TPA-based detector suppress noise on the zero level, they can increase the noise present on the one level. Therefore, some method for the suppression of optical beat noise combined with the suppression of MAI using an SA-TPA receiver is required for OCDMA systems that provide asynchronous transmission which can result in the presence of both MAI and optical beat noise.
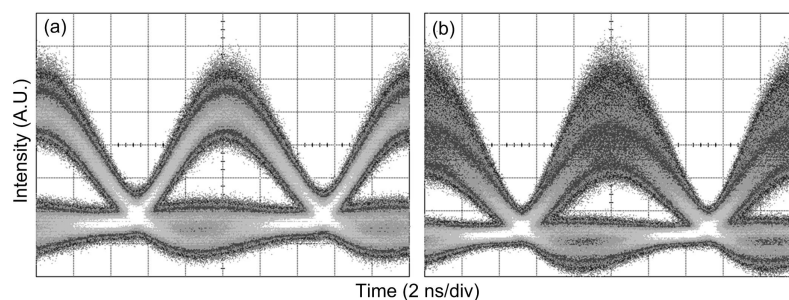
Figure 4.8: (a) Eye diagram obtained after the TPA-based detector with a temporal offset of 50 ps (b) Eye diagram obtained after the TPA-based detector with a temporal offset of 0 ps.

4.3 Reduction of MAI and Optical Beat Noise using an SA-SOA-TPA-Based Receiver

In the previous section, it was shown that an SA-TPA-based receiver can be used to successfully suppress MAI present on an OCDMA signal. However, even with the suppression of MAI, the presence of optical beat noise on an OCDMA signal can severely limit the performance of the system. This degradation caused by optical beat noise can be compounded by the nonlinear responses of a saturable absorber and a TPA-based device. Therefore, a method for clamping the one level of an OCDMA signal is required. One optical device that can be used for such a task is a semiconductor optical amplifier (SOA).

4.3.1 Semiconductor Optical Amplifier

A semiconductor optical amplifier is based on the same technology as a semiconductor laser diode with two types of SOA, the Fabry-Pérot amplifier (FPA) and the travelling wave amplifier (TWA). Both amplifiers have the same basic structure but have different mirror reflectivities. For an FPA, the reflectivities are around 0.3 [8] while a TWA uses anti-reflection coatings at the facets allowing only a single pass of the signal through the cavity [9]. At its most basic, a bulk SOA is a simple p-n junction. By applying a forward bias to the device, population inversion occurs in the active region where the number of atoms in an excited state far exceeds those in a ground state. The interaction between an incoming photon at the correct wavelength and the atoms in an excited state can cause these atoms to return to the ground state with the emission of a photon through the process of stimulated emission with the emitted photon having the same frequency, phase and direction as the incident photon. This process repeats for each photon resulting in overall gain of the incoming signal.

Efficient amplification can be obtained by confining the light and the injected carriers to the active layer. This is achieved by enclosing the active layer between two layers that have a larger band gap and a smaller refractive index than the active layer. As a result, the larger band gaps confine the carriers to the active layer while the lower refractive indices of the cladding layers act as an optical waveguide confining the light to the active layer. Typically an SOA is capable of providing a high internal gain of around 15 to 35 dB with a low power consumption. However, an SOA cannot maintain a fixed gain for an arbitrarily high input power signal as that would require adding arbitrary amounts of power to the optical signal. Since the amount of power that an SOA can supply is finite, the gain for high input power signals is reduced. This phenomenon is called gain saturation. For a small input optical power the gain of an SOA remains linear. However, the gain begins to saturate at higher input power levels with the decrease in the gain for increasing input powers becoming non-linear in nature. The saturated output power of the SOA occurs at the point where the gain of the amplifier is reduced by 3 dB.

It is generally preferred to have an SOA with a high value of saturated output power, however, the gain saturation phenomenon can be used in all-optical signal processing techniques. In [10], it was demonstrated that a gain-saturated SOA could be used for noise suppression of incoherent light in relation to spectrum-sliced WDM systems. A gain-saturated SOA was also experimentally demonstrated as a method for optical beat noise reduction in a wavelength division multiplexed/subcarrier multiplexed (WDM/SCM) passive optical network (PON) in [11]. In this section, a gain-saturated SOA is used to suppress optical beat noise that is present in an OCDMA system.

4.3.2 Experimental Setup
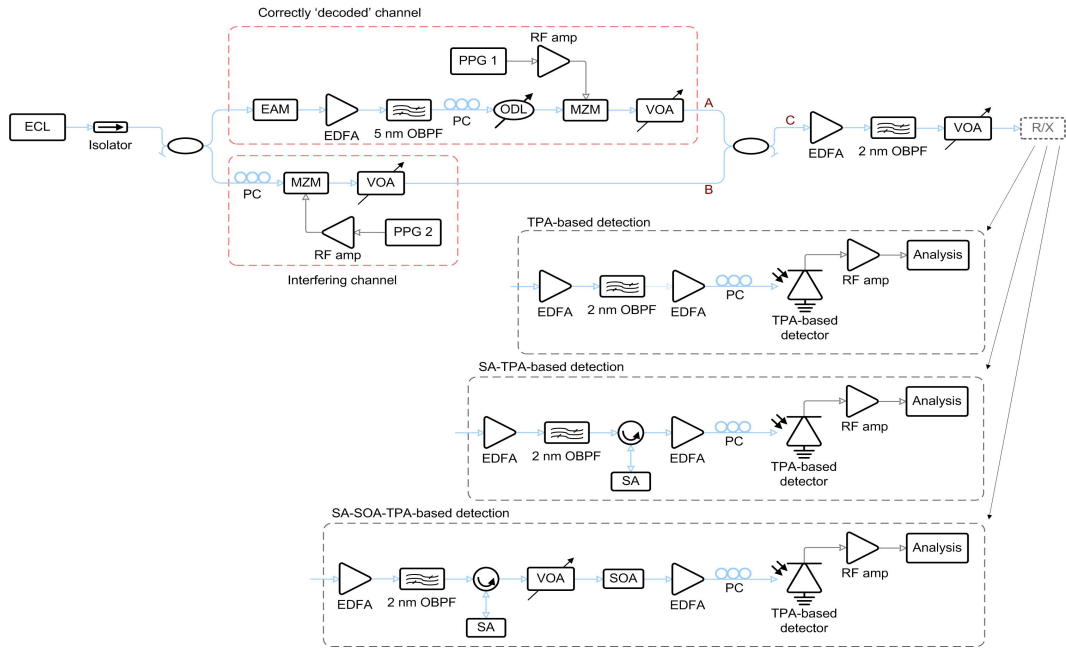
Figure 4.9: Experimental setup used to simulate the output signal from an OCDMA decoder with MAI and optical beat noise. The three different receiver structures used are also shown.

In section 3.6 it was shown that a TPA-based detector can be used to suppress MAI in a four-channel OCDMA system. This system employed 31-chip, 40-Gchips/s quaternary phase-shifted codes with a chip duration of 25 ps with each channel operating at a data rate of 100 Mb/s. In the experimental setup shown in Figure 4.9, the output from one of the OCDMA decoders used in section 3.6 is simulated without actually performing the encoding/decoding process. This is achieved by assuming that the correctly decoded channel has a pulsewidth of 25 ps, i.e. the duration of a single chip in a given OCDMA code. In comparison, the incorrectly decoded channel remains spread over the entire bit period of 10 ns. This simulates the worst case scenario where the interfering channel will always interfere directly with the desired channel, resulting in both MAI and optical beat noise. To generate both of these simulated OCDMA channels, continuous-wave (CW) light with a central wavelength of 1556 nm was split equally through an optical coupler. In one arm an electro-absorption modulator (EAM) was used to pulse carve optical pulses at 10 GHz with a pulsewidth of 25 ps. This 10 GHz pulse train was then gated down to 100 MHz and modulated with a PRBS data signal. This arm simulated the correctly decoded OCDMA channel and is shown in Figure 4.10 (a). The second arm of the coupler was fed to a second MZM which carved out a 100 MHz PRBS signal from the CW light with a bit period of

10 ns. This arm simulated an improperly decoded OCDMA channel assuming the interference was spread out equally over the entire bit slot. The interfering channel is shown in Figure 4.10 (b). In this OCDMA system where the channels are at the same wavelength, optical beat noise can occur if the channels experience different optical path lengths or if they have partial coherence. As a result, when they are recombined at the second optical coupler, they can interfere randomly producing optical beat noise. The combined optical signal is shown in Figure 4.10 (c). This waveform clearly shows both MAI, present on the zero level, and beat noise, present on the one level, due to the presence of the interfering channel. Optical attenuators were used to control the average power in each arm before the two signals were recombined. This signal was amplified using an EDFA before passing through one of three different receiver structures shown in Figure 4.9.

Three different receiver structures were used in this experiment. The first receiver was a TPA-based receiver and consisted of a variable optical attenuator followed by an EDFA, a 2 nm bandpass filter, a second EDFA and a TPA-based detector. The photocurrent generated by the TPA-based detector was then analysed using a BER tester and an oscilloscope. The second receiver expanded on the TPA-based receiver and employed a saturable absorber. The saturable absorber was placed between the 2 nm bandpass filter and the second EDFA in the TPA-based receiver. This had the effect of improving the extinction ratio of the signal that was incident on the TPA-based detector by suppressing MAI while also filtering out ASE from the first EDFA. The third receiver incorporated an SOA directly after the saturable absorber and before the TPA-based detector in the second receiver structure. By operating the SOA in a gain saturated regime the beat noise on the one level of the optical signal could be suppressed. An additional variable optical attenuator was used before the SOA to optimize the performance achieved from the SOA.
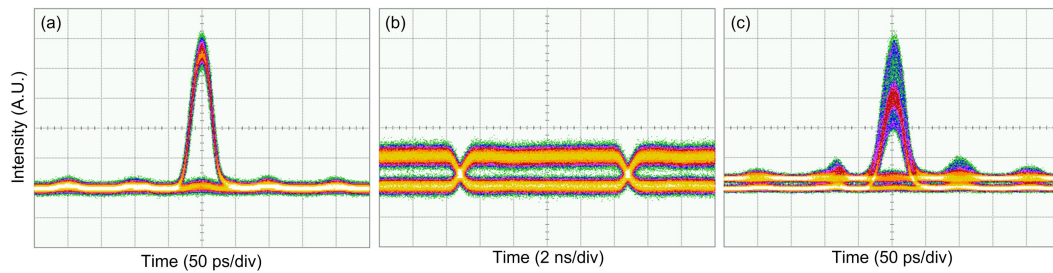
Figure 4.10: Experimentally measured eye diagrams for (a) the correctly 'decoded' OCDMA channel (b) the interfering OCDMA channel (c) the combined optical signal with both channels present. The eye diagrams were measured using a 50 GHz photodiode.

4.3.3 Experimental Results

The three nonlinear devices used in the receiver were characterised using the 100 MHz, 25 ps optical pulse train generated in the first arm of the experimental setup in Figure 4.9. The output photocurrent measured as a function of input average power for the TPA-based detector is shown in Figure 4.11 (a). At a average power of 250 μW, corresponding to a peak power of 100 mW for a 100 MHz repetition rate and a pulsewidth of 25 ps, the output begins to shift from linear absorption to TPA. At higher powers the output photocurrent tends towards an ideal square response. The optical loss as a function of input optical power for the saturable absorber is shown in Figure 4.11 (b). For low optical powers below –5 dBm, the optical loss experienced upon reflection from the device was measured as 15.3 dB. The optical loss of the saturable absorber is reduced by 3 dB at an input average power of 7 dBm. The optical gain of the SOA as a function of input power is shown in Figure 4.11 (c). It can be seen that as the input power increases above –5 dBm, the gain begins to saturate at an output power of 11 dBm. By ensuring that the one level of the incoming optical signal is close to the saturation point of the device, an SOA acts as a optical intensity limiter as higher intensity signals experience less gain than lower intensity signals. As a result, varying intensity levels are forced to a single level, hence the amount of beat noise present on an OCDMA signal can be reduced, improving overall system performance.
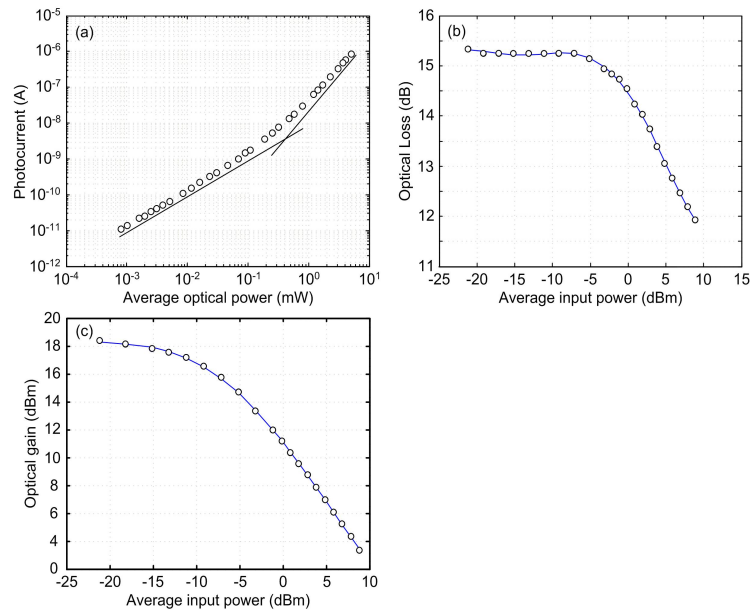
Figure 4.11: Plots of (a) TPA photocurrent as a function of average power (b) optical loss as a function of average input power for the saturable absorber and (c) optical gain as a function of input average power for the SOA.

4.3.3.1 TPA-Based Receiver

Figure 4.12 (a) shows the bit error-rate results measured using the TPA-based receiver. The BER results measured for only the desired channel transmitting are given by the triangles (△). It can be seen that error free performance for single channel operation can be achieved for a received power of –31 dBm. The BER results for two transmitting channels are given by the circles (○) in Figure 4.12 (a). The addition of the interfering channel results in a power penalty of ∼20 dB at an error rate of 1×10^{-9}. Figure 4.12 (b) shows the eye diagrams measured at the points shown in Figure 4.12 (a). When the interfering channel is added, it can be seen that eye diagram B closes in comparison to the single channel case due to MAI and beat noise. Eye diagram C was recorded when the average power in the interfering channel was increased by 3 dB i.e. the interfering channel has twice the average power of the desired channel. This eye diagram is almost completely closed due to the presence of the interference. As a result, no BER measurements could be obtained for this scenario.

Figure 4.12: (a) BER results as a function of received average power using a TPA-based receiver (b) measured eye diagrams for each BER trace.

4.3.3.2 SA-TPA Receiver

Figure 4.13 (a) shows the BER curves obtained when using the SA-TPA receiver. It can be seen that the addition of the saturable absorber results in error-free performance for both the single channel and two-channel cases. The power penalty associated with the addition of the second channel is 13 dB, a 7 dB reduction in comparison to the TPA-based receiver. The third BER result shown by the squares (□) in Figure 4.13 (a) is for both channels transmitting with the interfering channel having an average power that is 3 dB higher than the

desired channel. This extra 3 dB of average power is similar to the amount of interference generated by a third channel. With this increased level of interference , the receiver can still produce an error rate of 5×10^{-9} with a power penalty of 12 dB compared to the two-channel case. Figure 4.13 (b) shows the eye diagrams recorded for the three transmitting scenarios. For the single channel case, the eye opening in A is clearly defined allowing successful recovery of the transmitted data. For the two-channel case, the eye diagram B remains relatively open, however there is a large amount of noise present on the one level hence the associated power penalty in Figure 4.13 (a). The increased level of interference results in the eye opening in C degrading considerably with a further increase in the amount of noise on the one level of the signal. This degradation results in the introduction of an error floor in the BER curve at an error rate of 5×10^{-9}.

Figure 4.13: (a) BER results as a function of received average power using an SA-TPA-based receiver (b) measured eye diagrams for each BER trace.

4.3.3.3 SA-SOA-TPA Receiver

Figure 4.14 (a) shows the BER results obtained for the SA-SOA-TPA receiver. For this receiver, error free performance can be achieved for all three transmitting scenarios. For the single channel case, an error rate of 1×10^{-9} is possible for a received average power of −28 dBm. A power penalty of 5 dB is incurred with the addition of the interfering channel. However an error rate of 1×10^{-9} was still achieved despite the increased level of interference for a received average power of −23 dBm. A further power penalty of 7 dB was introduced when the average power in the interfering channel was increased by 3 dB. However, error free operation was still possible for this scenario using the SA-SOA-TPA receiver. It should be noted that there is an inherent 3 dB power penalty with the addition

of each channel to this system. Therefore the actual power penalties associated with the addition of each interfering channel is 3 dB less than those given by the experimental results. Figure 4.14 (b) shows the eye diagrams recorded at the points A, B and C in Figure 4.14 (a). For the single channel case, eye diagram A is free form interference allowing the data pattern to be recovered. In eye diagram B it can be seen that the presence of the interfering channel results in the eye opening closing slightly with the introduction of beat noise to the one level of the signal. However, it should be noted that the level of beat noise present has been reduced as a result of the SOA when compared to the same measurement for the SA-TPA receiver. This suppression of the beat noise is more evident when comparing eye diagram C to the same eye recorded using the SA-TPA receiver. Comparing these two eyes it is clear that the intensity variations present on the signal have been suppressed by the gain-saturated SOA. As a result, the eye opening is widened giving lower error rates and smaller power penalties when using the SA-SOA-TPA receiver. The power penalty associated with the transition from a single channel to a two-channel system was reduced by 15 dB for the SA-SOA-TPA receiver when compared to the same results for the TPA-based receiver. Therefore, the advantage of using the three nonlinear optical devices for the suppression of both MAI and optical beat noise are clearly evident in the results discussed above.
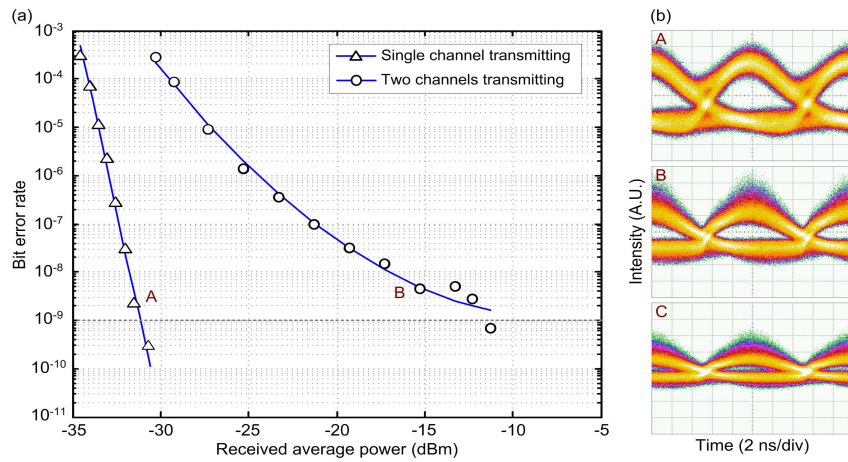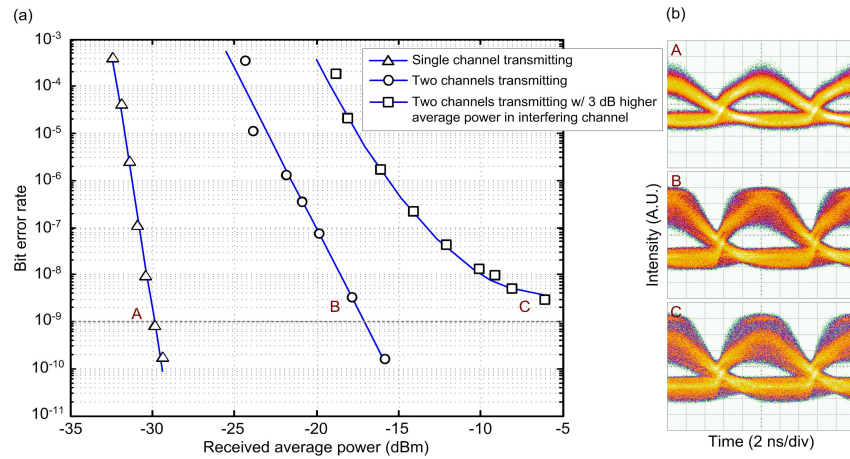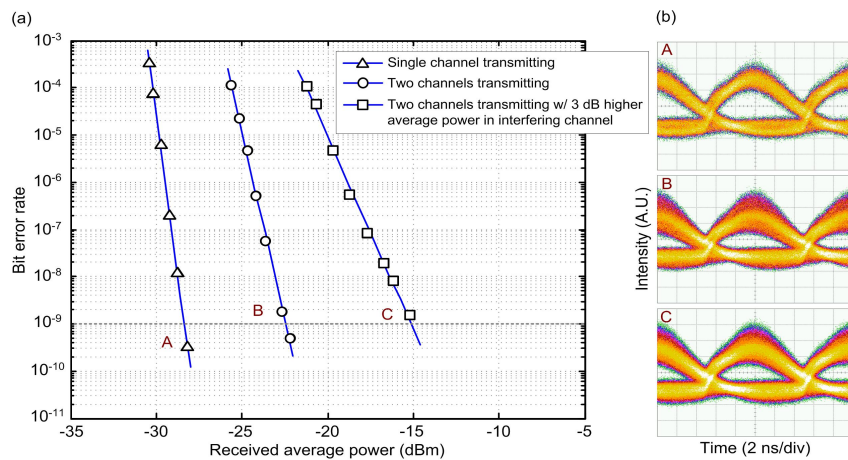

Figure 4.14: (a) BER results as a function of received average power using an SA-SOA-TPA-based receiver (b) measured eye diagrams for each BER trace.
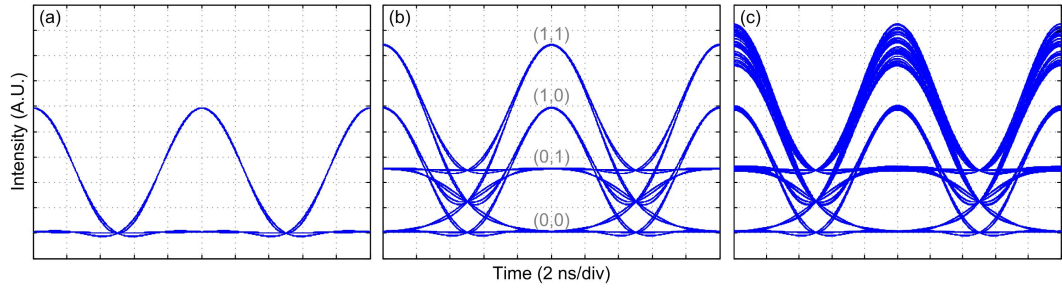
Figure 4.15: Simulated eye diagrams for (a) a single transmitting channel (b) two completely incoherent transmitting channels and (c) two coherent transmitting channels.

4.4 Simulation Model of an SA-SOA-TPA Receiver

In the previous section it was demonstrated that an SA-SOA-TPA-based receiver could be used to improve the performance of an OCDMA system through the successful suppression of both MAI and optical beat noise generated by the presence of interfering channels. In this section a simulation model of the SA-SOA-TPA-based receiver is presented. The two-channel optical system presented in section 4.3 is simulated to verify the performance improvement that is gained through the addition of each nonlinear optical device to the SA-SOA-TPA-based receiver.

In the simulation model, the first channel consisted of a train of optical pulses at a repetition rate of 100 MHz and a pulsewidth of 25 ps. This pulse train was data modulated with a data pattern of length $2^9 - 1$ using a model of a MZM. This resultant data signal represents the ideal output of an OCDMA decoder when the desired data signal has been correctly decoded. The second simulated channel models an incorrectly decoded OCDMA signal with a data rate of 100 MHz that is evenly spread out over the entire bit period of 10 ns.

Figure 4.15 shows three simulated eye diagrams from the model. These eye diagrams were generated by passing the optical signal to a model of a standard detector with a bandwidth of 100 MHz. Figure 4.15 (a) is the eye diagram obtained for the single 'desired' channel transmitting. Figure 4.15 (b) shows the eye diagram obtained for the two channel case when the two optical signals are completely incoherent i.e. no beating occurs between the two. From this eye diagram the multiple levels that result from the detector being band-limited to the data rate of the optical signal can be clearly seen. The eye levels (1,0) and (0,1) are slightly separated due to the roll-off of the filter function used to simulate the bandwidth of the optical detector. If this filter had an ideal frequency response, then these two eye

levels would merge in the centre of the eye diagram. As a result, the correct recovery of the data signal would be impossible. Figure 4.15 (c) shows the eye diagram obtained for the two channel case when the two channels are coherent with each other. As a result, the two signals beat together producing intensity variations on the top of the eye opening. The coherence between the two channels was simulated by adding phase noise to the electric field of the first channel. This phase noise is related to the linewidth of the optical source, which was assumed to be 10 MHz. This simulated optical signal complete with both MAI and beat noise was optically thresholded and detected using the models of the three receivers discussed in section 4.3; a TPA-based receiver, an SA-TPA-based receiver and an SA-SOA-TPA-based receiver.

4.4.1 TPA-Based Detector Model
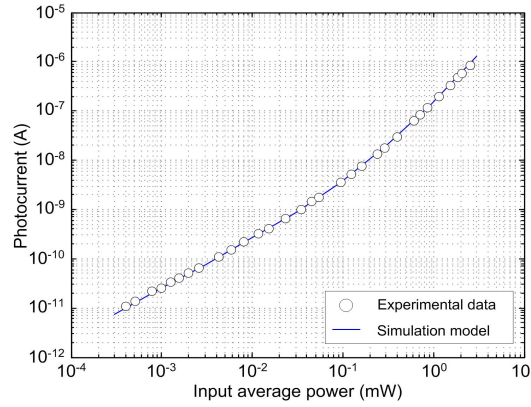
Figure 4.16: Plot of photocurrent versus input average power for the TPA-based detector model and the measured experimental data.

The total photocurrent generated in a TPA-based device can be given as,

$$I = \frac{q}{hf} \left(spa \, |E|^2 + tpa \, |E|^4 \right) \tag{4.1}$$

where I is the output photocurrent, spa is the linear contribution to the output photocurrent, tpa is the nonlinear contribution, E is the incident electric field, q is the charge of an electron, h is planck's constant and f is the frequency of the incoming light. Table 4.4.1 gives the values used for these parameters. It should be noted that both spa and tpa are not the SPA and TPA coefficients, α and β, that are discussed in section 3.2. These values for spa and tpa are the efficiencies for the linear and nonlinear contributions respectively. They include the contributions to the photocurrent from α and β, but also take into account

the size of the device and the spot size. Figure 4.16 shows the generated photocurrent as

Table 4.1: Simulation parameters for the TPA-based detector model.

Symbol	Physical constant	Value
q	Electron charge	1.6×10^{-19} C
h	Planck's constant	6.62×10^{-34} m^{2}kg/s
f	Frequency of the incoming light	193.5 THz
spa	Linear contribution to photocurrent	20×10^{-9} A/W
tpa	Nonlinear contribution to photocurrent	48×10^{-10} A/W^2

a function of incident average power for the TPA-based detector model. The experimental data measured for the TPA-based device in section 4.3 is also shown. The values for spa and tpa were found by fitting a curve to the experimental data using a fitting algorithm that incorporated equation 4.1. It can be seen that there is excellent agreement between the simulated output from the TPA-based device and the experimental data points.

4.4.2 Saturable Absorber Model
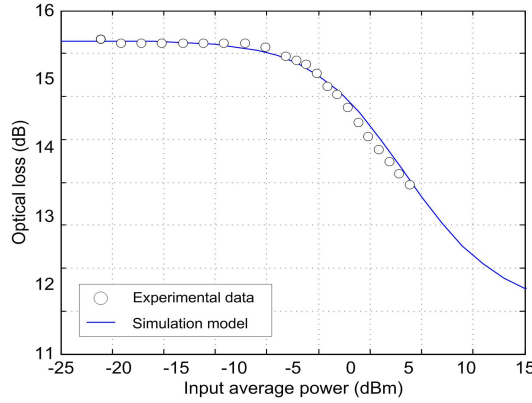
Figure 4.17: Plot of optical loss versus input average power for the saturable absorber model and the measured experimental data.

To create an accurate simulation model of the saturable absorber used in section 4.3, the characterisation results shown in Figure 4.11 (b) were used as the basis for a model. The change in absorption with respect to time for a saturable absorber can described by [12],

$$\frac{\delta a}{\delta t} = \frac{a_0 - a}{\tau_c} - \frac{a |E|^2}{I_{\text{sat}}}$$

(4.2)

where a_0 is the small signal absorption, τ_c is the relaxation time of the device, $|E|^2$ is

the intensity of the light and I_{sat} is the saturation intensity. In this case, the small signal absorption, $a_0 = SSL - NSL$, where SSL is the small-signal losses and NSL is the non-saturable losses. The small-signal losses are the losses experienced by low power signals reflected off the device while the non-saturable losses are losses experienced in the device that are not a result of the saturation process. The relaxation time of the saturable absorber, τ_c, is given as 5 ps. Since this value is less than the pulsewidth of 25 ps of the incoming data, it can be assumed that the device is operating in a steady-state condition. Therefore equation 4.2 is equal to zero, allowing the absorption of the device, a, to be given by,

$$a = \frac{a_0 I_{\text{sat}}}{I_{\text{sat}} + |E|^2 \tau_c}. \tag{4.3}$$

Table 4.2 shows the parameter values used for the simulation model. These parameters were derived from the experimental results given in section 4.3 for the saturable absorber. Figure 4.17 shows the optical loss versus the input average power for the saturable absorber model with the experimental data measured in section 4.3 also plotted for comparison. From this Figure it can be seen that there is good agreement between the experimental data measured for the saturable absorber and the response generated by the simulation model of the device.

Symbol	Physical constant	Value
a_0	Absorption of the saturable absorber	6.3 dB
τ_c	Relaxation time of the saturable absorber	5 ps
I_{sat}	Saturation intensity	30 pJ
SSL	Small-signal losses	15.3 dB
NSL	Non-saturable losses	9 dB

Table 4.2: Simulation parameters for the saturable absorber model.

4.4.3 SOA Model

A semiconductor optical amplifier can be described using the same equation as equation 4.3 with the device operating in a gain mode rather than an absorption mode. As was the case for the saturable absorber model, it is assumed that the SOA is in a steady-state condition. Therefore, the steady-state gain of an SOA can be described by,

$$g = \frac{g_0 E_{\text{sat}}}{E_{\text{sat}} + |E|^2 \tau_c}. \tag{4.4}$$

were g is the gain of the device, g_0 is the small-signal gain, E_{sat} is the saturation energy, τ_c is the carrier lifetime of the device and $|E|^2$ is the intensity of the incoming light. The values for these parameters used in the simulation model of the SOA are given in Table 4.3. The small-signal gain of the SOA was found from the experimental characterisation of the

Symbol	Physical constant	Value
g_0	Gain of the semiconductor optical amplifier	18.7 dB
τ_c	Carrier lifetime of the SOA	100 ps
E_{sat}	Saturation energy	150 pJ

Table 4.3: Simulation parameters for the SOA model.

device to be $\sim$ 18.7 dB. Assuming a carrier lifetime of 100 ps, and a saturation energy of 150 pJ, the simulated SOA output was found to match the experimental results with good accuracy. Figure 4.18 shows the optical gain as a function of input average power for the SOA model. The experimental results measured for the SOA are also shown. It can be seen from the Figure that there is good agreement between the simulation model using the parameters given in Table 4.3 and the measured experimental data.
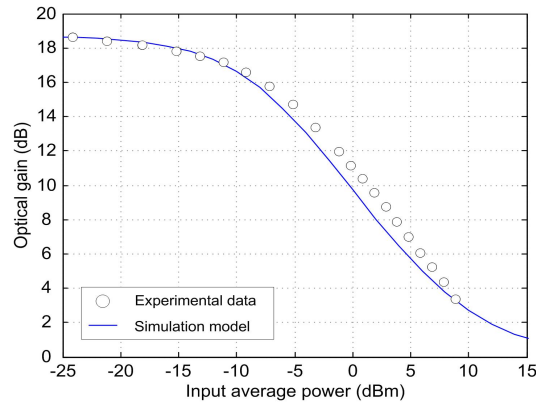
Figure 4.18: Plot of optical gain versus input average power for the SOA model and the measured experimental data.

4.4.4 BER Analysis

To measure the performance of the simulation model quantitatively, an algorithm for calculating the bit error rate of the detected signal in the presence of multiple eye levels was required. In an optical system where the received optical signal has two levels, the error

probability is given by [12],

$$\text{BER} = p(1)P(0/1) + p(0)P(1/0) \tag{4.5}$$

where $p(1)$ and $p(0)$ are the probabilities of receiving bits 1 and 0 respectively, $P(0/1)$ is the probability of deciding a 0 was received when a 1 was sent and $P(1/0)$ is the probability of deciding a 1 was received when a 0 was sent. Assuming 1 and 0 bits are equally likely to occur, $p(1) = p(0) = 1/2$. As a result, the BER becomes,

$$\text{BER} = \frac{1}{2}\left[P(0/1) + P(1/0)\right] \tag{4.6}$$

Assuming the mean values, I_1 and I_0, and the standard deviations, σ_1 and σ_0, for the 1 and 0 bits respectively are known, the conditional probabilities in equation 4.6 can be given as,

$$P(0/1) = \frac{1}{2}\text{erfc}\left(\frac{I_1 - I_D}{\sigma_1\sqrt{2}}\right) \tag{4.7}$$

$$P(1/0) = \frac{1}{2}\text{erfc}\left(\frac{I_D - I_0}{\sigma_0\sqrt{2}}\right) \tag{4.8}$$

where erfc is the complementary error function and I_D is the decision threshold. This decision threshold can be given as,

$$I_D = \frac{\sigma_0 I_1 + \sigma_1 I_0}{\sigma_0 + \sigma_1} \tag{4.9}$$

By substituting equations 4.7 and 4.8 into equation 4.6, the equation for the BER for a two level signal is given by,

$$\text{BER} = \frac{1}{4}\left[\text{erfc}\left(\frac{I_1 - I_D}{\sigma_1\sqrt{2}}\right) + \text{erfc}\left(\frac{I_D - I_0}{\sigma_0\sqrt{2}}\right)\right] \tag{4.10}$$

In the case of a multi-level eye diagram such as the one shown in Figure 4.15 (b) equation 4.10 must be extended to account for the additional power levels introduced by the interfering channels. Figure 4.19 illustrates the probability distributions for a four-level eye diagram. The ideal thresholding point for such a signal would be where the distributions for the (1,0) and (0,1) levels intersect. However, the contribution to the error-rate from the other levels must also be accounted for. Figure 4.19 shows the probability distribution of the (1,1) level. When the two signals are completely incoherent then the distribution can be assumed to be a standard Gaussian distribution. However, when the signals are coherent, this distribution becomes non-Gaussian as a result of the beating between the two signals with two peaks at either end of the distribution [13]. To overcome this, the calculation of the
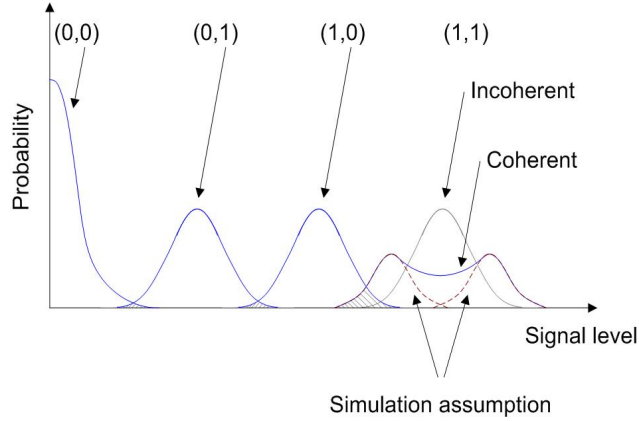
Figure 4.19: Illustration of the probability distributions for a four level eye diagram.

simulated BER assumes that the beating signal between the desired channel and the inter-ference channel can only have two levels; one completely constructive and one completely destructive, as shown in Figure 4.19. As a result, the 'two-pronged' non-Gaussian distribu-tion can be replaced with two individual Gaussian distributions. This assumption allows the BER analysis discussed above to be extended to incorporate five probability distributions. The total BER for the two-channel simulation model is given by,

$$\text{BER} = \frac{1}{4} \left[P(0/11) + P(0/10) + P(1/01) + P(1/00) \right] \tag{4.11}$$

where $P(0/11)$ is the probability of deciding a 0 when the desired channel and the inter-fering channel transmitted a 1, $P(0/10)$ is the probability of deciding a 0 when the desired channel was 1 and the interfering channel was 0, $P(1/01)$ is the probability of deciding a 1 when the desired channel was a 0 and the interferer was a 1 and $P(1/00)$ is the probability of deciding a 1 when both channels were 0. The probability of error due to $P(0/11)$ is given by,

$$P(0/11) = \frac{1}{4} \left[\text{erfc} \left(\frac{I_{11D} - I_D}{\sigma_{11D} \sqrt{2}} \right) + \text{erfc} \left(\frac{I_{11C} - I_D}{\sigma_{11C} \sqrt{2}} \right) \right] \tag{4.12}$$

where I_{11D} and I_{11C} are the mean values for the destructive and constructive beating sig-nals respectively, and σ_{11D} and σ_{11C} are the standard deviations for the destructive and constructive beating signals respectively. Equation 4.12 is essentially the same as equa-tion 4.7 except in this case the probability of error is a combination of two possible states. The remaining conditional probabilities are given as,

$$P(0/10) = \frac{1}{2} \text{erfc} \left(\frac{I_{10} - I_D}{\sigma_{10} \sqrt{2}} \right) \tag{4.13}$$

107

$$P(1/01) = \frac{1}{2}\text{erfc}\left(\frac{I_D - I_{01}}{\sigma_{01}\sqrt{2}}\right) \tag{4.14}$$

$$P(1/00) = \frac{1}{2}\text{erfc}\left(\frac{I_D - I_{00}}{\sigma_{00}\sqrt{2}}\right) \tag{4.15}$$

In the two-channel simulation, the decision threshold, I_D, occurs between the levels $(0, 1)$ and $(1, 0)$ which is the only part of the eye opening where the desired data signal can be correctly recovered. Therefore, I_D is given as,

$$I_D = \frac{\sigma_{01}I_{10} + \sigma_{10}I_{01}}{\sigma_{01} + \sigma_{10}} \tag{4.16}$$

These equations for the calculation of the BER for an optical signal containing multiple levels, in combination with the simulation models developed for the saturable absorber, SOA and TPA-based device, allow the two-channel system discussed in section 4.3 to be simulated and analysed in terms of the performance improvement gained through the use of the nonlinear devices in the receiver.

4.4.5 Simulated TPA-Based Receiver

Figure 4.20: (a) BER curves as a function of received average power for the TPA-based receiver simulation model (b) Eye diagrams measured for each transmitting scenario.

Figure 4.20 shows the simulation results obtained for the two-channel system using the TPA-based receiver model. The measured bit error rate curves as a function of received average power for the different scenarios are shown in Figure 4.20 (a). The three transmitting scenarios are the same at those discussed in section 4.3 where the the first case consists of only the desired channel transmitting, the second case introduces the interfering channel

and the final case consists of the desired channel and the interfering channel with the average power of the interferer increased by 3 dB in comparison to the desired channel. The extra 3 dB of optical power in the interfering channel simulates the level of interference introduced by a second interfering channel. From Figure 4.20 (a) it can be seen that there is a power penalty of ~ 10 dB at a BER of 1×10^{-9} with the introduction of the interfering channel in comparison to the single channel case. Increasing the power in the interfering channel by 3 dB results in an additional power penalty of 21 dB, giving an overall power penalty of 31 dB when moving from a single channel system to a system with the interference levels of three channels.

Figure 4.20 (b) shows the simulated eye diagrams for the three transmitting scenarios. The three eye diagrams were measured at the points A, B and C shown in Figure 4.20 (a). It can be seen in the eye diagram for the two-channel case that the presence of the interfering channel reduces the opening of the eye diagram in comparison to the single channel case. This is similar to the experimental results in section 4.3 in that the presence of the interfering channel reduces the amount of TPA photocurrent that is generated by the TPA-based device, resulting in the closure of the electrical eye diagram. When the average power of the interfering channel is increased by 3 dB it can be seen that eye diagram is closed further, limiting the opening allowing the correct detection of the data signal, resulting in a higher bit error rate.

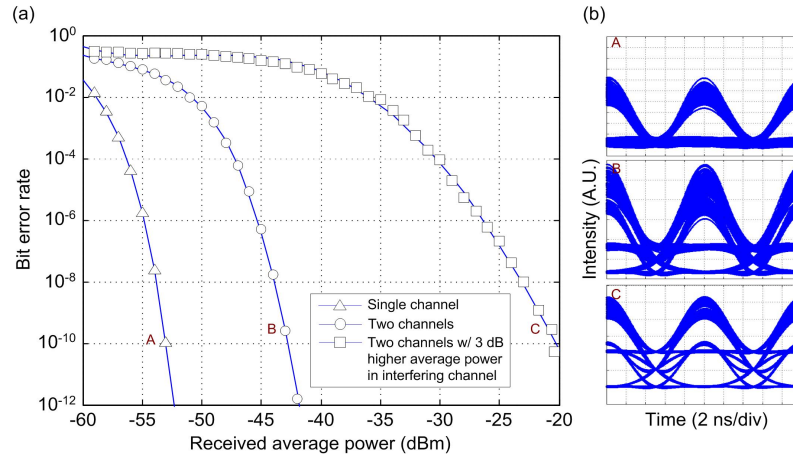### 4.4.6 Simulated SA-TPA-Based Receiver
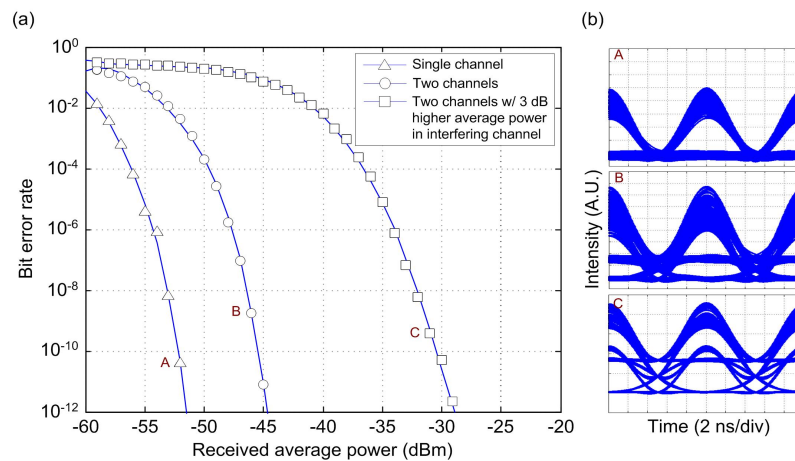
Figure 4.21: (a) BER curves as a function of received average power for the SA-TPA-based receiver simulation model (b) Eye diagrams measured for each transmitting scenario.

Figure 4.21 shows the simulation results obtained for the SA-TPA-based receiver model. The simulated BER curves for the two-channel system are shown in Figure 4.21 (a). The power penalty associated with the addition of the interfering channel at a bit error rate 1×10^{-9} was found to be 7 dB when using the SA-TPA-based receiver. This represents a 3 dB improvement over the TPA-based receiver for the same scenario. Doubling the power of the interfering channel results in an additional power penalty of 15 dB. Again, this is a reduction of 6 dB in comparison to the same power penalty incurred when using the TPA-based receiver. As a result, the overall power penalty incurred is 22 dB which is a 9 dB improvement compared to the TPA-based receiver.

The measured eye diagrams using the SA-TPA receiver are shown in Figure 4.21 (b). Comparing these eye diagrams to those shown for the TPA-based receiver in Figure 4.20 (b), it can be seen that the shape of the eyes are very similar. However, in the case of the SA-TPA receiver, the received power required to generate these eye diagrams is lower than for the TPA-based receiver, hence a reduction in the power penalties.

4.4.7 Simulated SA-SOA-TPA-Based Receiver
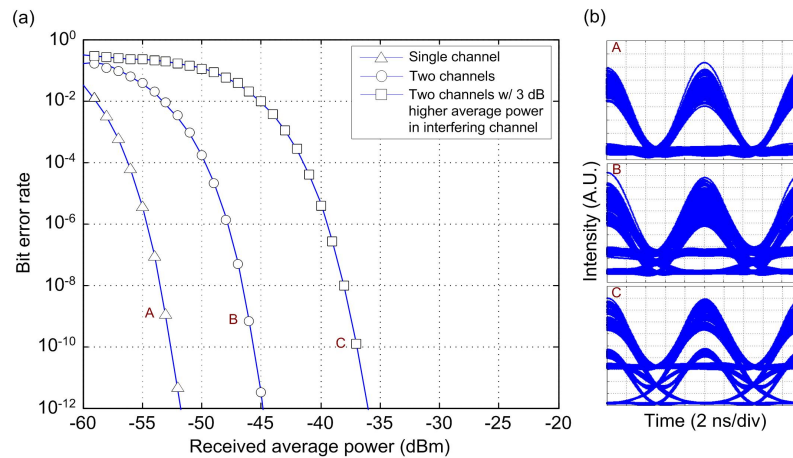
Figure 4.22: (a) BER curves as a function of received average power for the SA-SOA-TPA-based receiver simulation model (b) Eye diagrams measured for each transmitting scenario.

Figure 4.22 shows the simulated results for the SA-SOA-TPA-based receiver. Again, the simulated BER curves as a function of received average power are shown in Figure 4.22 (a) with the simulated eye diagrams recorded at bit error rates of 1×10^{-9} shown in Figure 4.22 (b). From Figure 4.22 (a) it can be seen that the power penalty associated with the addition of the interfering channel to the system is 7 dB. This value is the same as

that for the SA-TPA receiver, resulting in no improvement between the SA-TPA and SA-SOA-TPA receivers when adding a single interferer. However, the addition of 3 dB to the interfering channels power results in a power penalty of 9 dB. In comparison to the same result for the SA-TPA receiver, there is an improvement of 6 dB in this power penalty. As a result, the overall power penalty of this system using the SA-SOA-TPA-based receiver is 16 dB. This is an overall reduction of 15 dB when compared to the TPA-based receiver.

The simulation results presented above reinforce the experimental data discussed in section 4.3 that shows that the addition of each nonlinear optical device can significantly improve the performance of an OCDMA system in the presence of both MAI and optical beat noise. These results also demonstrate that a nonlinear receiver consisting of a saturable absorber, an SOA and a TPA-based detector can successfully recover a data pattern in the presence of both MAI and beat noise while operating at the data rate of the incoming signal rather than requiring a higher-speed photodetector in the receiver.

4.5 Summary

Multiple access interference and optical beat noise generated by the presence of interfering channels in an OCDMA system place strict limits on the performance that can be achieved for such a system. Optical beat noise becomes a significant problem when there is some level of coherence between the optical signals used in each channel resulting in a large amount of noise at the receiver. In this chapter it was shown that a saturable absorber can be used directly before a TPA-based detector in order to suppress MAI and improve the extinction ratio of the incoming signal. However, the nonlinear responses of both the saturable absorber and the TPA-based detector, while successful in the suppression of MAI, can increase the level of optical beating present on the optical signal. Therefore some form of beat noise suppression is also required. In this chapter it was shown that a gain-saturated SOA can be used in conjunction with a saturable absorber and a TPA-based detector to successful reject both MAI and optical beat noise while operating at the data rate of the incoming optical signal, resulting in improved system performance. Such a receiver structure has the advantage of the possible integration of each device into a single, higher-speed, small area device that could be used in future OCDMA applications due to the semiconductor nature of the nonlinear devices.

References

[1] O. Leclerc, B. Lavigne, D. Chiaroni, and E. Desurvire, "All-optical regeneration: Principles and WDM implementation," in *Optical Fibre Telecommunications IV A: Components*, I. Kaminow and T. Li, Eds.   New York: Academic Press, 2002.

[2] F. X. Kärtner, I. D. Jung, and U. Keller, "Soliton mode-locking with saturable absorbers," *IEEE Journal of Selected Topics in Quantum Electronics*, vol. 2, no. 3, pp. 540–556, 1996.

[3] H. A. Haus and Y. Silberberg, "Theory of mode-locking of a laser diode with a multiple-quantum-well structure," *Journal of the Optical Society of America B*, vol. 2, no. 7, pp. 1237–1243, 1985.

[4] D. Rouvillain, P. Brindel, E. Seguineau, L. Pierre, O. Leclerc, H. Choumane, G. Aubin, and J. L. Oudar, "Optical 2R regenerator based on passive saturable absorber for 40 Gbit/s WDM long-haul transmissions," *Electronics Letters*, vol. 38, no. 19, pp. 1113–1114, 2002.

[5] M. Gay, L. Bramerie, D. Massoubre, A. O' Hare, A. Shen, J. L. Oubar, and J. C. Simon, "Cascadability assessment of a 2R regenerator based on a saturable absorber and a semiconductor optical amplifier in a path switchable recirculating loop," *IEEE Photonics Technology Letters*, vol. 18, no. 11, pp. 1273–1275, 2006.

[6] D. Reid, P. J. Maguire, L. P. Barry, Q.-T. Le, S. Lobo, M. Gay, L. Bramerie, M. Joindot, J.-C. Simon, D. Massoubre, J.-L. Oudar, and G. Aubin, "All-optical sampling and spectrographic pulse measurement using cross-absorption modulation in multiple-quantum-well devices," *Journal of the Optical Society of America B*, vol. 25, no. 6, pp. 133–139, 2008.

[7] E. Le Cren, S. Lobo, S. Fève, and J.-C. Simon, "Observation of thermal effects due to an optical incident signal and high fluence on InGaAs/InP multiple-quantum-well saturable absorber nonlinear mirrors: Evolution of characteristics and time constants," *Applied Optics*, vol. 45, no. 26, pp. 6831–6838, 2006.

[8] J. M. Senior, *Optical fiber communications: Principles and practice*, 3rd ed. Prentice Hall, 2009.

[9] M. J. Connelly, *Semiconductor optical amplifiers*. Kluwer Academic Publishers, 2002.

[10] A. D. McCoy, P. Horak, B. C. Thomsen, M. Ibsen, and D. J. Richardson, "Noise suppression of incoherent light using a gain-saturated SOA: Implications for spectrum-sliced WDM systems," *IEEE Journal of Lightwave Technology*, vol. 23, no. 8, pp. 2399–2409, 2005.

[11] Y.-Y. Won, H.-C. Kwon, S.-K.Han, E.-S. Jung, and B.-W. Kim, "OBI noise reduction using gain saturated SOA in reflective SOA based WDM/SCM-PON optical links," *Electronics Letters*, vol. 42, no. 17, pp. 992–993, 2006.

[12] G. P. Agrawal, *Fiber-optic communication systems*, 3rd ed. John Wiley & Sons Inc., 2002.

[13] X. Wang and K. Kitayama, "Analysis of beat noise in coherent and incoherent time-spreading OCDMA," *IEEE Journal of Lightwave Technology*, vol. 22, no. 10, pp. 2226–2235, 2004.

Chapter 5

Comparison of an SA-SOA Receiver to the Mamyshev Filtering Technique

5.1 Introduction

The use of a saturable absorber (SA), a semiconductor optical amplifier (SOA) and a TPA-based detector for the suppression of multiple access interference and optical beat noise in an optical system has been clearly demonstrated in chapter three and four of this thesis. It has been shown that an SA-SOA-TPA-based receiver can be employed to successfully reject both multiple access interference (MAI) and optical beat noise. As previously discussed in chapter two, a number of alternative techniques have been demonstrated in the literature for the purpose of noise suppression in OCDMA systems. Two commonly demonstrated techniques for noise suppression are optical thresholding using a nonlinear optical loop mirror (NOLM) and optical time gating using a terahertz optical asymmetric demultiplexer (TOAD). A third technique that has been experimentally demonstrated for noise suppression in an OCDMA system is the Mamyshev filtering technique. This technique takes advantage of the nonlinear effects experienced by high power optical pulses in optical fibre to reject noise present on the incoming optical signal. The relative simplicity of implementing the Mamyshev filter in comparison to the TOAD and the NOLM makes it an attractive nonlinear thresholding method and an ideal candidate for comparison with the nonlinear thresholding devices presented in this thesis.

In this chapter an optical system that simulates both MAI and optical beat noise is used to compare the performance of an SA-SOA receiver with the performance of a Mamyshev filter. These experimental results will allow the performance of the nonlinear optical elements that are discussed in this chapter to be compared directly to the performance of

an established optical thresholding technique. A simulation model is used to verify the experimental results while also highlighting the effect various parameters of the optical thresholders have on the overall performance improvement that can be achieved.

5.2   Mamyshev Filtering Technique

The Mamyshev filtering technique was first demonstrated in [1]. This filtering technique was proposed as a 2R optical regenerator for an optical system. The main purpose of such a regenerator was the regeneration and reshaping (hence the 2R) of an optical signal after the signal had propagated through a large optical link resulting in the degradation of the optical signal and the accumulation of noise. The regeneration process is based on the phenomenon of self-phase modulation (SPM), a nonlinear effect present in an optical fibre, followed by an optical bandpass filter. A diagram showing the operation of a Mamyshev filter as an optical thresholder is shown in Figure 5.1. A typical filter consists of an erbium-doped fibre
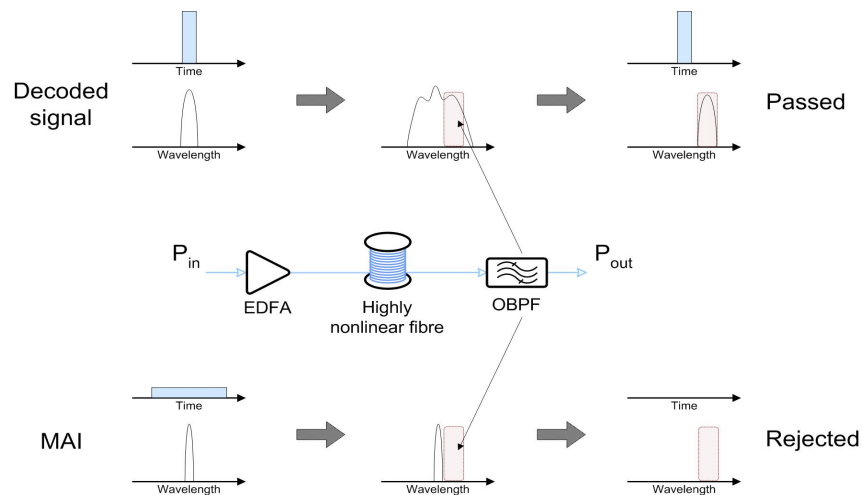
Figure 5.1: Operating principle of a Mamyshev filter for optical thresholding.

amplifier (EDFA) followed by a length of optical fibre typically with a large nonlinear coefficient and an optical bandpass filter. The output from the Mamyshev filter is dependent on the input optical signal. If the input signal has a large peak power and a narrow pulsewidth, then this signal can generate SPM as it propagates through the optical fibre. This SPM effect results in a broadening of the spectrum of the optical signal. The centre wavelength of the optical bandpass filter is offset from the central wavelength of the original signal, allowing only the broadened portion of the spectrum to be passed through. This process in essence wavelength shifts the original high peak power optical signal, allowing it to pass through to the output of the Mamyshev filter.

115

For the case where the input signal is MAI, the signal is temporally spread over a larger time span with a low peak power. As a result the MAI signal does not have sufficient power to generate SPM in the nonlinear fibre. This results in the optical spectrum of the signal after propagating through the fibre occupying the same spectral range as it did before entering. The optical filter then filters out this signal as it is outside its passband, hence rejecting the MAI. Therefore, a Mamyshev filter can be used to recover a correctly decoded OCDMA signal without MAI noise. This form of optical thresholding has been successfully demonstrated for temporal phase OCDMA [2, 3] and spectral phase OCDMA [4] systems.

5.3 Comparison of an SA-SOA Receiver and a Mamyshev Filter

In this section, the performance of an SA-SOA receiver similar to that presented in chapter four is experimentally compared to the performance of a Mamyshev optical thresholder in an optical system in the presence of both MAI and optical beat noise. The Mamyshev filter used in this experiment consisted of an EDFA followed by 100 m of highly nonlinear fibre (HNLF) and a 2 nm optical bandpass filter. Table 5.1 shows the parameters of the HNLF used. These parameters play an important role in the performance of the Mamyshev filter as they determine the amount of suppression that can be achieved by the filter. The attenuation parameter is important as a high level of attenuation reduces the power of the optical signal as it propagates through the fibre, reducing the nonlinear effect experienced, hence reducing the level of suppression. Similarly, the dispersion of the fibre is also required to be as low as possible. Since the input pulses of the desired data channel have narrow pulsewidths, they consequently have broad spectral widths. Therefore a low dispersion value is required to prevent the optical pulse from dispersing as it travels through the fibre. Finally, a high nonlinear coefficient is desirable as the amount of SPM generated in the fibre is dependent on this value.

Table 5.1: Parameters of highly nonlinear fibre used in the Mamyshev filter.

Parameter	Value
Attenuation @ 1550 nm	0.47 dB/km
Dispersion @ 1550 nm	-0.774 ps/nm/km
Dispersion slope @ 1550 nm	0.0035 ps/nm^2/km
Nonlinear coefficient γ @ 1550 nm	7.5 /W/km

To characterise the Mamyshev filter, a train of optical pulses at various bit rates and with

pulsewidths of 2 ps, were passed to the optical thresholder. Figure 5.2 (a) shows the normalised optical spectrum obtained for the optical pulse train at a repetition rate of 1 GHz. The central wavelength of the optical pulses was 1555.9 nm. After propagating through the EDFA and the HNLF, the spectrum of the optical pulses was measured again. It can be seen from Figure 5.2 (a) that the normalised optical spectrum is significantly broadened due to SPM after propagating through the HNLF. The final trace shown in Figure 5.2 (a) shows the filtered optical spectrum after the bandpass filter in the Mamyshev filter. The central wavelength of the 2 nm bandpass filter was set to 1557 nm. From this trace it can be seen that the majority of the original spectrum centered around 1555.9 nm is filtered out while the additional frequencies generated by SPM are passed through.

Figure 5.2 (b) shows the transmission through the Mamyshev filter as a function of input average power for repetition rates of 100 MHz, 500 MHz and 1 GHz. It can be seen that at low input powers the transmission for all three bit rates remains at –22 dB. As the input power is increased and hence the peak power is increased, SPM begins to occur in the HNLF. At an input average power of $\sim$ 5 dBm, the transmission value begins to increase nonlinearly as the amount of SPM increases, resulting in a larger optical spectrum and a larger amount of optical signal passing through the optical bandpass filter. It can be seen
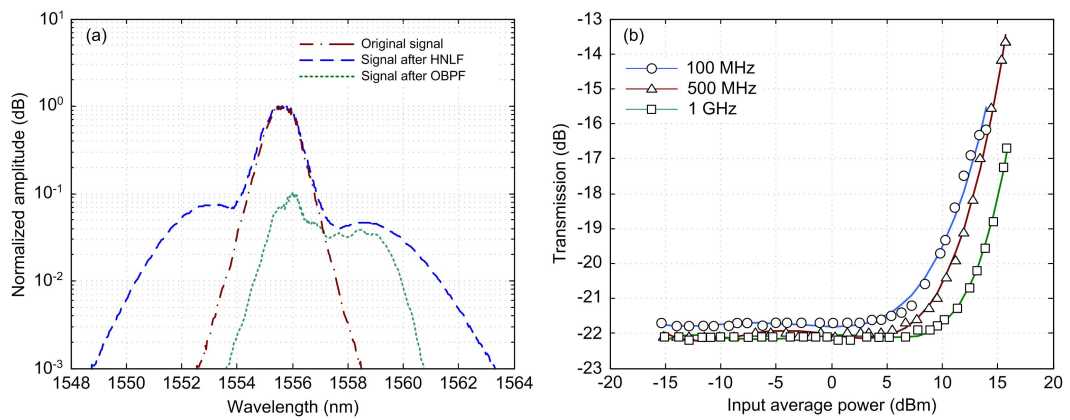
Figure 5.2: Characterisation of the Mamyshev filter (a) Measured optical spectra and (b) the transmission of the filter as a function of input average power for various data rates.

from Figure 5.2 (b) that the operating power of the Mamyshev filter is dependent on the data rate of the input signal. This is due to the relationship between the peak power of a signal and the data rate of the signal. As a result, a signal operating at a repetition rate of 100 MHz contains more peak power than a signal at 1 GHz for the same average power. Therefore the operating power of the filter will be lower for a lower data rate optical signal.

These results show that the constructed Mamyshev filter is capable of providing a nonlinear response that can be used for optical thresholding and compared experimentally to an SA-SOA optical thresholder. Additionally, the Mamyshev filter does not have a strict limitation of the data rate provided the pulses are sufficiently narrow to generate the required peak power. In comparison, the data rate of the SA-SOA receiver is limited by the recovery time of the slowest element, in this case the gain recovery time of the SOA which is 100 ps, limiting the data rate to 10 Gb/s.

5.3.1 Experimental Setup
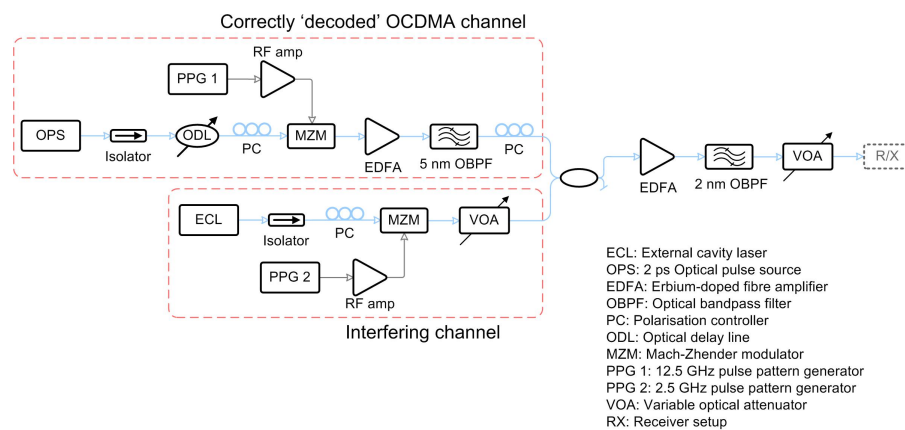
Figure 5.3: Experimental setup used to simulate the output of an OCDMA decoder to compare the performance of an SA-SOA receiver and a Mamyshev filter for optical thresholding.

Figure 5.3 shows the experimental setup used to compare the performance of an SA-SOA optical thresholder and a Mamyshev filter in an optical system designed to simulate MAI and optical beat noise that would be present in an OCDMA system. To simulate a correctly decoded signal from an OCDMA decoder, a tuneable mode-locked laser source was used to generate a train of optical pulses at 10 GHz with pulsewidths of 2 ps. The central wavelength of the optical pulses was set as 1555.9 nm. This optical pulse train was then gated down to 1 GHz and patterned with a pseudo-random bit sequence (PRBS) of length $2^7 - 1$ using a Mach-Zhender modulator (MZM). The MZM was driven by a 12.5 GHz pulse pattern generator (PPG). The resultant data signal was amplified using an EDFA and filtered using a 5 nm bandpass filter. The interfering channel was generated using an external cavity laser (ECL) operating in a continuous wave (CW) mode. The central wavelength of the ECL was set to 1555.9 nm to match the wavelength of the desired channel. The CW light from the ECL was passed to a second MZM that carved out 1 GHz pulses with a pulsewidth

118

Figure 5.4: Four receiver structures used to compare the performance of various nonlinear receivers with the performance of a standard linear receiver in a simulated OCDMA system.

of 1 ns. A variable optical attenuator (VOA) was used to ensure that the power in the interfering channel was kept the same as the desired channel. The two optical channels were combined using an optical coupler with the combined signal amplified by a second EDFA and filtered using a 2 nm bandpass filter. The resultant signal passed through a VOA that has used to varying the average power that was incident on the receiver.
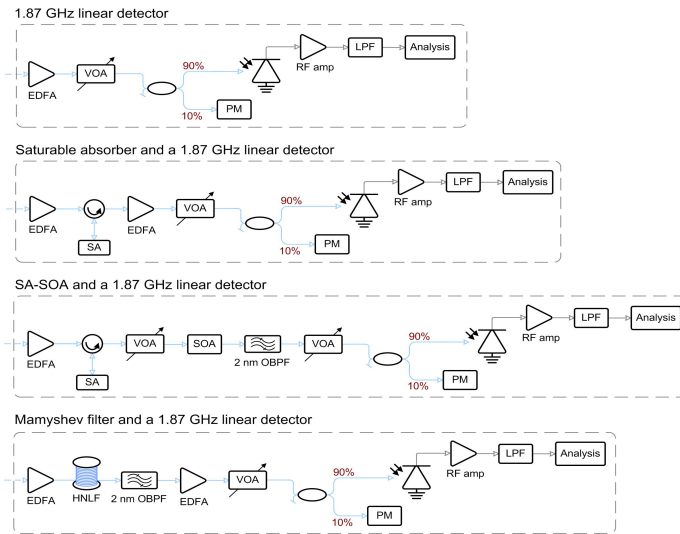
Four different receiver structures were used and are shown in Figure 5.4. The first receiver was a standard linear receiver structure. This consisted of an EDFA followed by a VOA. This VOA was used to ensure that the average power incident on the linear detector was kept constant. A 90 : 10 optical coupler was used to measure the optical power falling on the detector at a given time. The optical signal was detected using a 10 GHz linear detector with the electrical signal amplified using an electrical amplifier. A low-pass filter with a bandwidth of 1.87 GHz was used to simulate the bandwidth response of a 1 GHz detector. Finally, the bit error rate (BER) and electrical eye diagrams were recorded. The second receiver structure used the same setup as described above for the linear detector with the addition of a second EDFA at the front end along with an optical circulator and a saturable absorber. This receiver allows the performance of a saturable absorber followed by a standard linear detector to be measured. The third receiver expands upon the SA receiver by including a VOA after the saturable absorber followed by an SOA. The VOA was used to ensure that the optimum optical power was input to the SOA. The final receiver structure shown in Figure 5.4 incorporates a Mamyshev filter before the 1.87 GHz linear detector.

The Mamyshev filter consisted of an EDFA followed by 100 m of HNLF and a 2 nm optical bandpass filter. A second EDFA was used after the bandpass filter to ensure that sufficient optical power was incident on the linear detector. Each receiver structure was used in the experimental setup shown in Figure 5.3. The performance for each of these receivers was measured in the presence of the simulated MAI and optical beat noise.

5.3.2   Experimental Results

The bit error rates and electrical eye diagrams for the four receiver structures discussed in the previous section were measured to determine the performance of a two-channel optical system in the presence of MAI and optical beat noise. In all four cases the performance for a single transmitting channel and two transmitting channels was measured. The optical sources for both channels had a central wavelength of 1555.9 nm to ensure the maximum amount of optical beating between the two channels. A polarisation controller was also used in the desired channel to ensure that the polarisation was aligned between the two channels, again ensuring that the worst-case scenario was achieved in terms of optical beating.

5.3.2.1   Linear Receiver Results

Figure 5.5: Measured (a) BER curves as a function of received average power and (b) electrical eye diagrams for the linear receiver.

Figure 5.5 (a) shows the BER curves as a function of received average power for the linear receiver. From this graph it can be seen that error rate operation at a error rate of 1×10^{-9} can be achieved for a single transmitting channel for a received average power of –33 dBm. The addition of the interfering channel results in an error floor at 1×10^{-6} due to MAI and optical beat noise. The power penalty associated with the interfering channel is 15 dB at 1×10^{-6}. Figure 5.5 (b) shows the electrical eye diagrams measured for the linear receiver

at the points A and B shown in Figure 5.5 (a). For the single channel case given by eye diagram A, it can be seen that there is a relatively clear eye opening in which to successfully recover the electrical data. In contrast, the eye opening for the two-channel case as given by eye diagram B is closed significantly due to the MAI and optical beat noise introduced by the interferer. The eye diagram also shows the four intensity levels that are introduced by the presence of the interfering channel. In this case the linear detector can distinguish between the desired channel and the interfering channel due to the lowpass filter having a bandwidth of 1.87 GHz which is slightly greater than the data rate of 1 GHz.
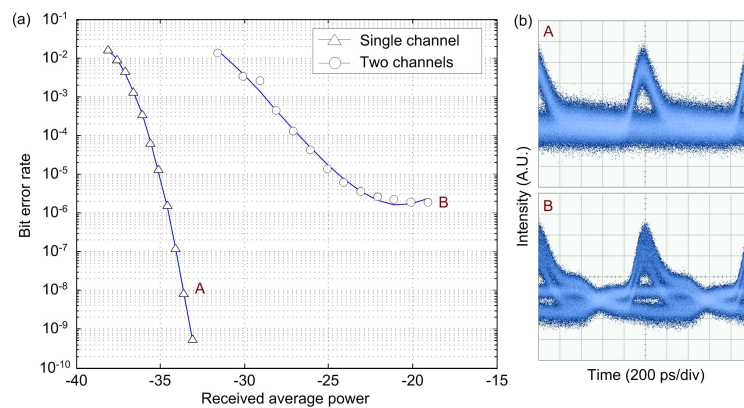
5.3.2.2 Mamyshev Receiver Results

Figure 5.6: Measured (a) BER curves as a function of received average power and (b) electrical eye diagrams for the Mamyshev receiver.

Figure 5.6 (a) shows the BER curves measured as a function of received average power for the Mamyshev receiver. It can be seen that error free operation can be achieved for a received average power of –31 dBm with a single channel transmitting. The addition of the second channel results in the forming of an error floor at an error rate of 1×10^{-8} at a received power of –19 dBm. The associated power penalty at this error rate is shown to be 13 dB. This is an improvement of 3 dB when compared to the results for the linear receiver with a two orders of magnitude improvement in the achievable bit error rate. Figure 5.6 (b) shows the electrical eye diagrams measured for the Mamyshev receiver. Eye diagram A was measured for the single channel case and shows a clear eye opening allowing the recovery of the transmitted data signal. Eye diagram B was measured for the two channel case. It can be seen that the eye opening is closed slightly due to MAI and beating between the two channels. However, the amount of closing of the eye is not as extreme as was shown for the linear receiver in Figure 5.5 (b), hence the improvement in the power penalty and low

bit error rate. The presence of the MAI in this eye diagram is most likely due to leaking of the interfering channel into the passband of the optical filter in the Mamyshev filter. This is shown in Figure 5.1 (a). From this graph it can be seen that a portion of the amplified input signal passes through the optical filter along with the SPM induced frequencies. As a result, the ability of the Mamyshev filter to completely suppress the MAI noise is diminished. This situation could be improved by using a bandpass filter that has a steeper rolloff at the edges of the passband frequencies or by using a narrower passband filter or a combination of both.
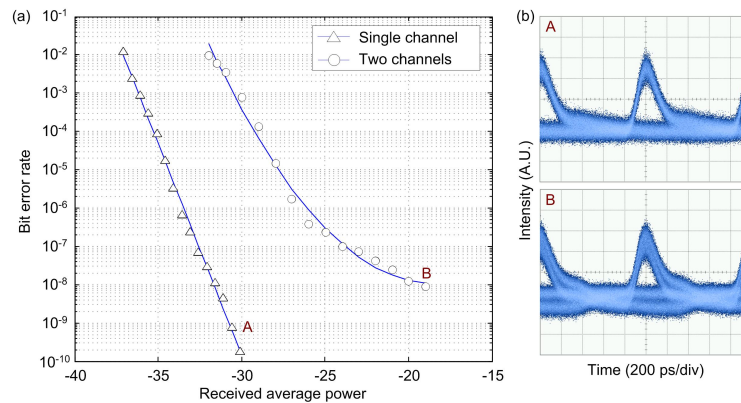
5.3.2.3   SA Receiver Results

Figure 5.7: Measured (a) BER curves as a function of received average power and (b) electrical eye diagrams for the SA receiver.

Figure 5.7 (a) shows the BER curves measured as a function of received average power for the SA receiver. From this graph it can be seen that error free transmission can be achieved for a single channel at a received average power of –29 dBm. With the addition of the interfering channel error free operation can still be achieved for a received power of –22 dBm, giving a power penalty of 7 dB. This result is a 9 dB improvement over the same results using the linear receiver and a 6 dB improvement compared to the Mamyshev receiver. Figure 5.7 (b) shows the eye diagrams obtained for the SA receiver. For both the single and two-channel cases, there is a clear eye opening from which the transmitted data that be recovered. In eye diagram B there is a significant amount of beat noise present on the top of the electrical eye. Again the nonlinear response of the saturable absorber will increase the level of beat noise present on the input signal. As a result, an SOA is required to provide a measure of suppression of this beat noise of the optical signal.
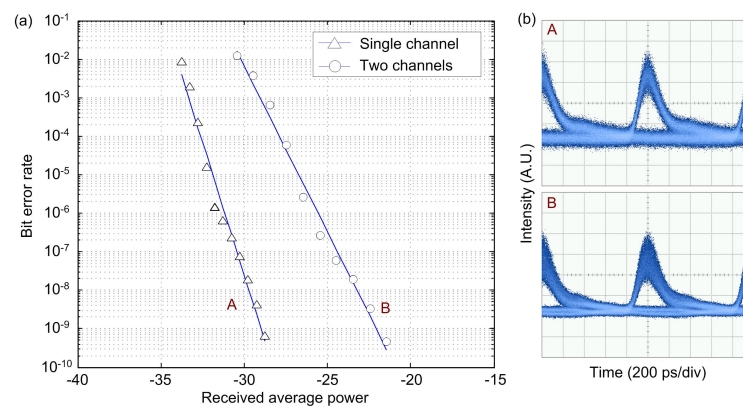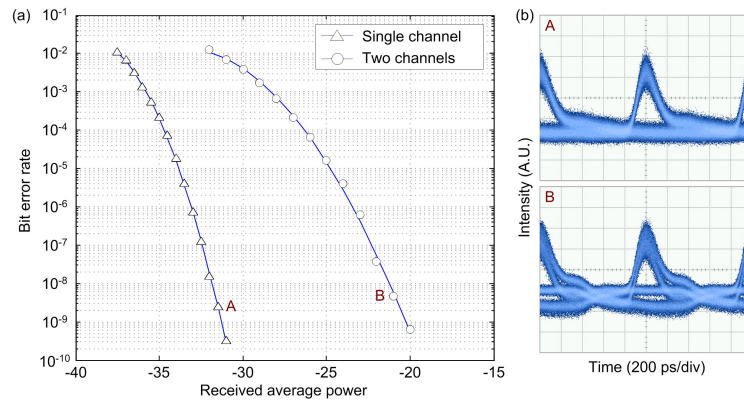
Figure 5.8: Measured (a) BER curves as a function of received average power and (b) electrical eye diagrams for the SA-SOA receiver.

5.3.2.4 SA-SOA Receiver Results

The measured BER curves for the SA-SOA receiver are shown in Figure 5.8 (a). From this plot it can be seen that for the single transmitting channel, a BER of 1×10^{-9} can be achieved for a received average power of –31 dBm. When the interfering channel is added to the system, the received power required for error free operation becomes –20 dBm, a power penalty of 11 dB. Comparing this value to the results shown for the SA receiver, the power penalty has increased by 4 dB. This can be understood by examining the eye diagrams shown in Figure 5.8 (b). For the single channel case, eye diagram A shows a clear eye opening. However, eye diagram B measured for the two-channel case shows that MAI is present on the detected signal. This is due to the gain-saturated SOA. While the saturable absorber can suppress this MAI, as demonstrated in the results shown above, the gain-saturated SOA re-amplifies the remaining MAI present in the optical signal. Since the gain-saturated SOA is being used to limit the one level of the signal, the power of the interference is increased disproportionately compared to the desired signal. Therefore, while the SOA succeeds in removing some of the optical beat noise, the extinction ratio is decreased due to the amplification of the MAI, resulting in a larger power penalty.

5.3.3   Simulation Model Results

To verify the experimental results presented above, the simulation model developed in section 4.4 in chapter four was used. For this set of simulation results, the data rate was changed to 1 Gb/s with the pulsewidth of the desired channel reduced to 2 ps to match the tuneable mode-locked laser source used in the experimental setup. Similarly, the pulsewidth of the interfering channel was reduced to 1 ns. The method for the calculation of the bit error rates

was also the same as that discussed in section 4.4.

In order to create a model of the Mamyshev filter, a simple model for the process of SPM was required. When this phenomenon occurs in an optical fibre, the nonlinear coefficient of the fibre, γ, produces a nonlinear phase shift given by [5],

$$\phi_{NL} = \gamma P_{in} L \tag{5.1}$$

where P_{in} is the input power of the optical signal and L is the length of the fibre. The nonlinear coefficient, γ, used is given in Table 5.1 while the length L was 100 m. This nonlinear phase shift was then multiplied by the electric field of the signal in the simulation model, creating the SPM effect. The resultant signal from the fibre is filtered using a bandpass optical filter that is offset from the central wavelength of 1555 nm by 300 GHz or 2.4 nm.

5.3.3.1 Linear Receiver Results

Figure 5.9: Measured BER curves as a function of received average power for (a) the linear receiver and (b) the Mamyshev receiver.

Figure 5.9 (a) shows the BER curves as a function of received average power for the simulated linear receiver. These results show that a BER of 1×10^{-9} can be achieved for a single transmitting channel at a received average power of –44 dBm. The addition of the second channel results in a power penalty of 12 dB at 1×10^{-9}. This value is in good agreement with the experimental results that show that the power penalty associated with the presence of the interfering channel was 15 dB.

5.3.3.2 Mamyshev Results

Figure 5.9 (b) shows the BER curves as a function of received average power for the Mamyshev receiver. For single channel operation, error free operation can be achieved for a received average power of –43 dBm. With the addition of the interfering channel, a bit error rate of 1×10^{-9} can be achieved for a received power of –34 dBm; a power penalty of 9 dB. This represents of improvement of 3 dB compared to the linear receiver results. This improvement is in excellent agreement with the experimental results shown in section 5.3.2.

5.3.3.3 SA Receiver Results

Figure 5.10 (a) shows the BER curves measured as a function of received average power for the SA receiver. For a received power of –43 dBm a bit error rate of 1×10^{-9} was possible for the single channel case using the SA receiver. The addition of the interfering channel introduces a power penalty of 7 dB, resulting in error rate operation for the two channel case at a power of –36 dBm. This is a 5 dB improvement in comparison to the linear receiver and a 2 dB improvement when compared to the Mamyshev receiver. Again, these results are in good agreement with the experimental results presented in section 5.3.2.
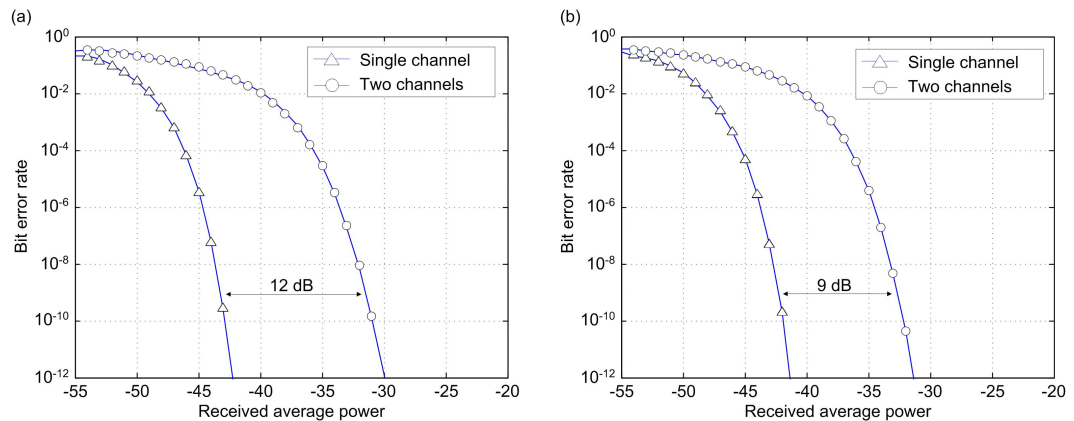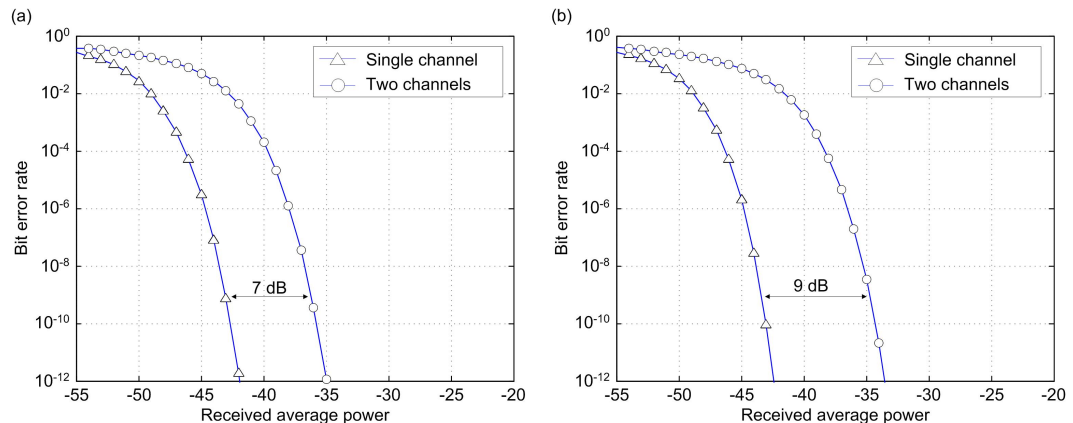

Figure 5.10: Measured BER curves as a function of received average power for (a) the SA receiver and (b) the SA-SOA receiver.

5.3.3.4 SA-SOA Receiver Results

Figure 5.10 (b) shows the BER curves as a function of received average power for the SA-SOA receiver. These results show that for single channel operation a BER of 1×10^{-9} can be achieved for a received power of –43 dBm. Moving to a two channel scenario introduces a power penalty of 9 dB, showing good agreement with the experimental results. This also

confirms the experimental results demonstrated for the SA-SOA receiver where the SOA limits the one level of the optical signal while amplifying the MAI noise, hence the increase in the power penalty associated with the addition of the interfering channel. Therefore, in this case the SA receiver would be preferred over the SA-SOA receiver. However, despite the increase in the power penalty, the performance of the SA-SOA receiver is the same as that for the Mamyshev receiver demonstrating that the SA-SOA receiver is comparable in performance to an established optical thresholding technique. A third nonlinear optical device, such as a TPA-based detector, could be added to the receiver to remove the amplified MAI from the SOA, providing an additional improvement to the extinction ratio of the signal and hence the performance of the system.

5.4 Summary

The Mamyshev filter is a device that has been successfully demonstrated as an optical regenerator in long-haul optical systems. More recently, this technique has been adapted for the purpose of optical thresholding in OCDMA systems. In this chapter, it was shown that the Mamyshev filter used as an optical thresholder provides a increase in system performance when compared to the results measured for a linear receiver. However, the performance of a Mamyshev filter is highly dependent on a number of factors. These include the attenuation experienced in the fibre, the amount of dispersion experienced and the nonlinear coefficient of the fibre. The parameters of the optical bandpass filter used in the Mamyshev filter are also an important consideration. This is because both the width of the passband and the roll-off of the passband play an important role in the performance that can be achieved through the use of a Mamyshev filter for optical thresholding.

In comparison to a Mamyshev filter, an SA-SOA receiver offers a similar level of performance improvement in optical systems where MAI and optical beat noise is present. This receiver can be more easily implemented than a Mamyshev filter with the main requirement for an SA-SOA receiver being the input optical power levels to each device. This receiver also has the added advantage that both devices are semiconductor in nature, allowing the possibility of integration into a small footprint, low-cost device. This device can include a standard linear photodetector, as used in the experimental results demonstrated in this chapter, or a high-speed TPA-based detector, providing further improvement in the suppression of noise present on the received signal.

References

[1] P. V. Mamyshev, "All-optical data regeneration based on self-phase modulation effect," in *Proceedings of European Conference on Optical Communications (ECOC)*, Madrid, Spain, 1998, pages 475-476.

[2] J. H. Lee, P. C. Teh, Z. Yusoff, M. Ibsen, W. Belardi, T. M. Monro, and D. J. Richardson, "A holey fiber-based nonlinear thresholding device for optical CDMA receiver performance enhancement," *IEEE Photonics Technology Letters*, vol. 14, no. 6, pp. 876–878, 2002.

[3] X. Wang, T. Hamanaka, N. Wada, and K. Kitayama, "Dispersion-flattened-fiber based optical thresholder for multiple-access-interference suppression in OCDMA system," *Optics Express*, vol. 13, no. 14, pp. 5499–5505, 2005.

[4] R. P. Scott, K. Li, V. J. Hernandez, B. H. Kolner, J. P. Heritage, and S. J. Ben Yoo, "Demonstration of an error-free 4×10 Gb/s multiuser SPECTS O-CDMA network testbed," *IEEE Photonics Technology Letters*, vol. 16, no. 9, pp. 2186–2188, 2004.

[5] G. P. Agrawal, *Fiber-optic communication systems*, 3rd ed.   John Wiley & Sons Inc., 2002.

Chapter 6

Discussion and Conclusions

Discussion

As the demand for broadband services continues to grow unabated worldwide, it becomes necessary for service providers to increase the capacity of their optical networks through some form of optical multiplexing. While this is certainly the case for the backbone networks, current electrical access networks are limited in terms of speed and transmission distance that can be achieved. Therefore, optical networks are required to move closer and closer to the end consumer through deployments such as fibre-to-the-home (FTTH) to meet this growing demand. However, these optical networks also need to be cost-effective while maintaining a high degree of flexibility and scalability in order to compete with current access technologies. Therefore, the choice of network employed and the associated multiplexing technology becomes vital to meet these requirements.

The success of code division multiple access (CDMA) in cellular networks has resulted in a large amount of interest and subsequent experimental research in translating this multiplexing technique from radio frequency networks to optical networks. This is because CDMA networks have a number of inherent advantages such as asynchronous transmission, the potential for increased security, quality of service control etc., that allow the network to meet demands of flexibility, scalability, efficiency and hence, cost-efficiency. However, these inherent properties of a CDMA-based network also result in the two major sources of noise that can are present in such a network; multiple access interference and optical beat noise. These noise sources are a result of each channel present on the network sharing the same time and bandwidth resources, and can severely limit the capacity of an optical CDMA network if some method of noise removal is not used. In this thesis, three semiconductor-based devices are used as nonlinear optical elements in a receiver structure that can be used to suppress noise present on an OCDMA signal.

In Chapter 3, a commercially available 1.3 μm Fabry-Pérot laser operating as a nonlinear optical thresholder was investigated. This device used the nonlinear optical-to-electrical conversion process of two-photon absorption (TPA) as a means to discriminate between the desired optical pulses and the interference signals based on their respective peak powers. One advantage of using the TPA process in a semiconductor device is that the optical signal is simultaneously optically thresholded and detected by a single device, removing the requirement for an additional photodetector after the thresholder. The feasibility of using such a TPA-based detector was experimentally demonstrated in a back-to-back setup to ensure that an electrical data pattern could be successfully recovered using such a device. It was shown that such a device can improve the extinction ratio between the desired optical pulse and the interference by 5 dB compared to a standard linear detector. The use of a TPA-based detector in a four-channel OCDMA system was also demonstrated in this chapter. The experimental results showed that three channels could be supported at an error rate of 1×10^{-3} using a linear detector. In comparison, a TPA-based detector could support 4 channels with an achieveable error rate of $\sim 1 \times 10^{-6}$. It is believed that this figure could be further improved, resulting in lower error rates and possibly an increased number of channels, by improving the optical signal-to-noise ratio (OSNR) of the transmitted signal. By increasing the level of the desired signal in relation to the noise, a larger amount of nonlinear photocurrent can be generated by the TPA-based detector, hence improving the suppression of the noise signal.

While the advantages of using a TPA-based device have been clearly demonstrated, such a device is limited by a number of factors. Firstly, due to the inefficiency of the TPA process, a high input optical power is required to generate a sufficient nonlinear response. These high powers can be achieved by either increasing the launch power of the signal or by using amplification before the TPA device. However, the nonlinear effects in an optical fibre and the additional cost associated with the addition of optical amplifiers must be accounted for. The inefficiency of the TPA process also limits the maximum achievable data rate due to the relationship between the peak power of the signal and the duty cycle. Therefore, in order to generate meaningful photocurrent from the device that can be electrically amplified, the repetition rate and the optical pulsewidth are required by be sufficiently small. In relation to the device presented in this thesis, the limitation on the bandwidth of the device was due to the transimpedance amplifier that directly followed the TPA-based detector. However, with a high bandwidth electrical amplifier, the average power would need to be increased to account for the reduction of the peak power, due to the increase in the duty cycle, hence ensuring that a nonlinear response is generated from the device.

Chapter 4 focused on the combination of a saturable absorber and a TPA-based detector to suppress interference that is present in OCDMA systems. The OSNR of an optical signal being detected by a TPA-based detector can be improved through the use of a saturable absorber (SA) before the TPA-based detector. The SA operates in a similar fashion to the TPA-based detector by exhibiting an intensity-dependent transmission characteristic with high peak power signals reflected from the device while lower power signals are absorbed. The response of the SA is also wavelength dependent allowing unwanted wavelengths to be attenuated before being incident on the TPA-based detector. It was shown that the inclusion of a SA before a TPA-based detector improved the power penalty associated with the addition of an interfering channel by 2 dB. However, although an SA-TPA-based detector can suppress multiple access interference (MAI) generated in an OCDMA system, the nonlinear responses of both devices can increase the level of optical beat noise present on an optical signal. This beat noise is a result of mixing between two or more optical signals and can severely limit the capacity of an OCDMA system. The experimental demonstration discussed above applied temporal offsets between the optical signals to prevent optical beating and hence examine the effects of MAI only and the subsequent suppression of this noise using an SA and a TPA-based detector. However, for the worst-case scenario in an OCDMA system, all optical signals can overlap at any given point in time, resulting in the generation of optical beat noise. Therefore, the second part of chapter 4 investigated the use of a gain-saturated semiconductor optical amplifier (SOA) as an optical limiter.

The relationship between the input power and the output power of a gain-saturated SOA is such that high input powers receive very little gain while lower power signals receive a larger gain. This property of an SOA can allow an optical signal to be clamped to a single level. Since the one level of an optical signal in an OCDMA system can fluctuate due to optical beat noise, an SOA can effectively be used to suppress this form of noise. This premise was investigated in chapter 4 with the construction of an SA-SOA-TPA-based receiver. The performance of this receiver was examined using a two-channel optical system that simulated the worst-case scenario in terms of MAI and optical beat noise that can be present in an OCDMA system. Using only the TPA-based detector, there was a power penalty of 20 dB due to MAI and optical beat noise when the interfering channel was added to the system. This penalty was reduced by 7 dB when the SA was placed before the TPA-based detector and was reduced by a further 8 dB, to give an overall power penalty of 5 dB, with the inclusion of the SOA between the SA and the TPA-based detector. These results show clearly the advantage of using such a receiver structure for nonlinear optical thresholding in an OCDMA system. The latter half of this chapter also presented a simulation model of this

optical system and the SA-SOA-TPA-based receiver. The models of the nonlinear devices were based on their experimental characterisation results to ensure that the model behaved as close as possible to the real-world devices. The simulated results for the system were in good agreement with the experimental results showing the same level of performance improvement with the addition of each nonlinear element to the receiver.

Table 6.1 compares the SA-SOA-TPA receiver with a number of different optical thresholding techniques. It can be seen that the bandwidth of the SA-SOA-TPA device is the main disadvantage of this nonlinear receiver compared to the other most commonly used techniques. However, it should be noted from this table that the pulsewidth used in the SA-SOA-TPA experiments is 10 times greater than the next largest pulsewidth of 2.5 ps. Therefore, the data rate of the signal could be increased to 1 Gb/s while maintaining the optical peak power by reducing the pulsewidth by a factor of 10. From Table 6.1 it can be seen that the periodically poled lithium-niobate (PPLN) waveguide is currently the best performing nonlinear thresholder in terms of operational data rate and energy required to achieve error free performance. However, the three alternative methods; the Mamyshev filter, the nonlinear optical loop mirror (NOLM) and the PPLN, require varying lengths of fibre with high nonlinear coefficients and low dispersion parameters to ensure a nonlinear response from the device. In comparison, the SA-SOA-TPA receiver consists of three commercially available semiconductor devices that allow for the possibility of future integration into a single, low-cost device.

| Technique | Data Rate | Pulsewidth | Optical Power | | | Fibre |
			Average	Peak	Energy	
SA-SOA-TPA	100 Mb/s	25 ps	10 mW	4 W	100 pJ/bit	N/A
Mamyshev [1]	10 Gb/s	400 fs	25 mW	6.3 W	2.5 pJ/bit	500 m
NOLM [2]	2.5 Gb/s	2.5 ps	9.4 mW	1.5 W	3.8 pJ/bit	6.6 km
PPLN [3]	10 Gb/s	400 fs	0.3 mW	70 mW	28 fJ/bit	67 mm

Table 6.1: Performance comparison of different optical thresholding techniques.

Table 6.1 shows that the most commonly used techniques for the suppression of noise in OCDMA systems are fibre-based solutions. The Mamyshev filtering technique is one of those methods and makes use of self-phase modulation in a highly nonlinear fibre and an optical bandpass filter to distinguish and hence separate the desired optical signal from the noise signals that are present. In comparison to other fibre-based techniques, the Mamyshev filter is relatively simple to implement experimentally. Therefore chapter 5 examines the performance of an SA-SOA-based receiver and a receiver using a Mamyshev filter in

the presence of MAI and optical beat noise. The experimental results show that the performance improvement gained through the use of the SA-SOA receiver is similar to that for the Mamyshev filter in terms of the power penalty associated with the addition of the interfering channel. The simulation model results again show good agreement with the experimental data. These results also highlight some other important considerations for these two methods of optical thresholding. The performance of the Mamyshev filter, and other fibre-based thresholders, is highly dependent on the type of fibre used and the nonlinear coefficient of that fibre. Some important parameters of the fibre include the attenuation, nonlinearity and dispersion which can affect the level of performance that is possible from a given thresholder. The optical bandpass filter used after the fibre is also an important consideration. Ideally this filter would be as narrow as possible to ensure that only the desired signal is passed while the noise is rejected. However, if the bandwidth is too narrow, then signal power can be lost again reducing the performance of the Mamyshev filter. In relation to the SA-SOA receiver, the experimental results show that while the SOA can suppress optical beat noise, it can reduce the contrast ratio between the signal and the noise. This is a result of the one level being clamped to a single power due to gain-saturation in the SOA but the noise signal experiences no clamping and is amplified, reducing the contrast ratio. Therefore an additional nonlinear element, such as a TPA-based detector, would be required after the SOA to remove the noise signal that has been reintroduced.

Future Work

In this thesis three nonlinear optical devices used in an SA-SOA-TPA receiver for nonlinear optical thresholding in OCDMA systems were examined both experimentally and analytically. While the results presented showed that such receiver can successfully reject and suppress noise sources in an OCDMA system, there are a number of avenues that could be explored for future work on the topic. Firstly, as mentioned in the discussion section previous, the SA-SOA-TPA receiver lacks the bandwidth capabilities of the most commonly employed optical thresholding techniques that typically operate in the GHz range. As a result, one aspect of future work would be improve the bandwidth of the receiver. In the case of the SA-SOA-TPA receiver presented here, the bandwidth limitation was due to the TPA detector and the transimpedance electrical amplifier at the back end being two discrete components. In a standard detector both the photodiode and the subsequent electrical amplifier are integrated onto the same substrate and are placed as close as possible to each other to maximise the bandwidth. Therefore, the possible integration of a TPA-based detector and an electrical amplifier onto a single chip would be highly desirable as it would allow the

TPA detector approach operating bandwidths similar to those of competing thresholding techniques.

The TPA-based detector itself is also an area that can be further investigated in future work. In the experimental demonstrations a 1.3 μm InGaASP FP laser was used as a TPA-based device. However, other devices either made of similar or different materials, such as Si, with narrow operating wavelength band could be used. These devices can be characterised to determine their nonlinear response allowing comparison to the device used in this thesis. In relation to the TPA-based device, further characterisation could be performed to determine the feasibility of using the device in a 2-D wavelength-time OCDMA system. While TPA has been shown to be suitable for use in OCDMA systems employing 1-D time spreading optical codes, the wavelength selective nature of the TPA device would result in varying performance for different wavelengths. This variation could be characterised to determine the maximum number of wavelengths that could be used in a 2-D OCDMA system employing TPA thresholding and the maximum separation allowable between the coding wavelengths.

Finally, the semiconductor nature of the three nonlinear devices discussed in this thesis allow for the possible integration of these devices into a single component. This possibility of integration provides an advantage over other fibre-based thresholding solutions as an SA-SOA-TPA device can be cost effective with a small physical footprint. However, a number of issues would need to be addressed to determine the feasibility of making such a device. These include ensuring adequate power levels can be maintained throughout the device allowing optimal performance from the device, minimising the insertion losses of each device and high-speed packaging of the device. Therefore, if an SA-SOA-TPA receiver is to be a realistic device for nonlinear optical thresholding in OCDMA systems, then optimisation of the integration and packaging process to ensure maximum performance from the nonlinear devices in the receiver would be paramount aspect of the future work on this topic.

Summary

An SA-SOA-TPA-based receiver has been shown to provide a clear performance improvement in the presence of MAI and optical beat noise in an OCDMA system. It has also been shown that an SA-SOA receiver can provide the same level of improvement as a fibre-based thresholder commonly used in experimental OCDMA demonstrations. Therefore, an integrated SA-SOA-TPA-based receiver could be a viable alternative to current fibre-based thresholders in future OCDMA applications. This receiver can deal effectively with both major sources of noise present in OCDMA systems and has the advantage of being semi-

conductor based. This allows for the possibility of integrating the three nonlinear optical elements into a single, high-speed, small footprint, low-cost device. In comparison, current thresholding and time gating techniques for the removal of MAI and optical beat noise require relatively long lengths of optical fibre and additional components. If OCDMA were to become the dominant multiplexing technique in future optical access networks then these criteria of size, cost and performance would become important considerations for service providers, with an integrated SA-SOA-TPA-based receiver providing a realistic alternative to current thresholding methods.

References

[1] R. P. Scott, K. Li, V. J. Hernandez, B. H. Kolner, J. P. Heritage, and S. J. Ben Yoo, "Demonstration of an error-free 4 × 10 Gb/s multiuser SPECTS O-CDMA network testbed," *IEEE Photonics Technology Letters*, vol. 16, no. 9, pp. 2186–2188, 2004.

[2] J. H. Lee, P. C. Teh, P. Petropoulos, M. Ibsen, and D. J. Richardson, "A grating-based ocdma codingdecoding system incorporating a nonlinear optical loop mirror for improved code recognition and noise reduction," *IEEE Journal of Lightwave Technology*, vol. 20, no. 1, pp. 36–46, 2002.

[3] Z. Jiang, D. Seo, S. Yang, D. E. Leaird, R. V. Roussev, C. Langrock, M. M. Fejer, and A. M. Weiner, "Four-user, 10-Gb/s, spectrally phase-coded O-CDMA system operating at ∼30 fJ/bit," *IEEE Photonics Technology Letters*, vol. 17, no. 3, pp. 705–707, 2005.

Appendix I – List of Publications Arising From This Work

Referred Journals

Reduction of MAI and beat noise in OCDMA systems using an SA-SOA-TPA-based receiver
K. J. Dexter, D. A. Reid and L. P. Barry
IEEE Photonics Technology Letters, vol. 21, no. 22, pp. 1662–1664, Nov. 2009.

Multiple access interference rejection in OCDMA using a two-photon absorption based semiconductor device
K. J. Dexter, D. A. Reid, P. J. Maguire, L. P. Barry, C. Tian, M. Ibsen, P. Petropoulos and D. J. Richardson
Optics Communications, vol. 282, no. 7, pp. 1281–1286, Apr. 2009.

Two-photon absorption-based OSNR monitor for NRZ-PSK transmission systems
D. A. Reid, K. Bondarczuk, K. J. Dexter, K. Shi, P. M. Anandarajah, L. P. Barry, W. H. Guo, J. O'Dowd, M. Lynch, A. L. Bradley and J. F. Donegan
IEEE Photonics Technology Letters, vol. 22, no. 5, pp. 275–277, Mar. 2010.

Conference Papers

Nonlinear optical thresholding in a 4-channel OCDMA system via two-photon absorption
K. J. Dexter, D. A. Reid, L. P. Barry, P. Petropoulos and D. J. Richardson
Conference on Optical Fiber Communication (OFC), San Diego, CA., paper OTuF5, 2009.

Nonlinear optical thresholding using a saturable absorber and two-photon absorption based device

K. J. Dexter, D. A. Reid and L. P. Barry

Conference on Lasers and Electro-Optics Europe (CLEO), Munich, Germany, 2009.

Reduction of multiple access interference in OCDMA systems using a semiconductor based TPA device

K. J. Dexter, P. J. Maguire and L. P. Barry

International Conference on Transparent Optical Networks (ICTON), Rome, Italy, paper TuA1.5, 2007.

Performance improvement in an OCDMA system via two-photon absorption

K. J. Dexter, P. J. Maguire and L. P. Barry

China-Ireland International Conference on Information and Communications Technologies (CIICT), Dublin, Ireland, pp. 645–649, 2007.

All-optical chromatic dispersion monitoring and multiple access interference reduction via two-photon absorption

K. Bondarczuk, K. J. Dexter, P. J. Maguire, D. A. Reid, L. P. Barry, J. O'Dowd, W. H. Guo, M. Lynch, A. L. Bradley and J. F. Donegan

China-Ireland International Conference on Information and Communications Technologies (CIICT), Beijing, China, pp. 657–660, 2008.

All-optical pulse processing for advanced photonic communication systems

L. P. Barry, K. Bondarczuk, K. J. Dexter, P. J. Maguire, D. A. Reid, J, O'Dowd, W. H. Guo, M. Lynch, A. L. Bradley and J. F. Donegan

International Conference on Transparent Optical Networks (ICTON), Athens, Greece, paper TuC2.3, 2008.

Appendix II – Data Sheets

The following pages contain the datasheets for the devices listed below:

- ○ TPA-based detector

- ○ Saturable absorber

- ○ Semiconductor optical amplifier

ML1030 series

1310 nm FP coaxial laser diode module for digital applications

Overview

The ML1030 series is comprised of 1310 nm FP coaxial laser diode modules for digital applications. The lasers have a low threshold current and a narrow spectral linewidth. The ML1030 series is available with optical isolators, various connectors and different flange options. Please check the section on ordering information for details on the different options.

Applications

Communications

High speed optical fiber communication
Short and intermediate reach
SONET OC-48 systems
SDH STM-16 systems

Electro-optical Characteristics

Parameter	Symbol	Min	Typical value	Max	Unit	Test condition
Threshold Current	I_{TH}	-	11	18	mA	25°C
Operating Current	I_{OP}	-	35	45	mA	25°C, P_f=3mW
		-	50	70	MA	85°C, P_f=3mW
Optical Output	P_f	-	2	3	mW	25°C, $I_{OP}= I_{TH} + 26$mA
Operating Voltage	V_{OP}	-	1.2	1.5	V	25°C, $I_{OP}= I_{TH} + 26$mA
Slope Efficiency	η	0.08	0.12	-	W/A	25°C
Peak Wavelength	λ	1270	1310	1340	nm	0°C-85°C, Pf=3mW
Spectral Width	Δλ	-	0.85	2	nm	25°C, Pf=3mW
Temperature Shift of Wavelength	dλ/dt	-	0.46	-	nm/K	0°C-85°C, Pf=3mW
Monitor Current	I_m	0.4	0.8	-	MA	25°C, Pf=3mW
Monitor Dark Current	I_{md}	-	-	100	nA	V_{RPD}=10V

Absolute Maximum Ratings

Parameter	Symbol	Min	Max	Unit
Light Output	P_f	-	4	mW
LD Reverse voltage	V_{RLD}	-	2	V
PD Reverse voltage	V_{RPD}	-	10	V
Operating Temperature	T_{OP}	-20	85	°C
Storage Temperature	T_S	-40	85	°C
Soldering Temperature	T_{SOL}	-	260	°C

version: 1.4   ·   release date: 04-Dec-09   ·   page 1

BATOP
o p t o e l e c t r o n i c s

FC-SANOS-15XX-TEC

Preliminary data sheet of fiber-coupled SANOS @ λ = 1530 … 1560 nm with TEC

SANOS – Saturable noise suppressor

SANOS applications

- Suppression of noise (ASE – amplified spontaneous emission) after an optical amplifier (passive optical signal regeneration)
- All-optical wavelength conversion of pulsed optical signals

Main SANOS data

Resonance wavelength	λ = 1530 nm, 1535 nm, … ,1555 nm, 1560 nm in steps of $\Delta\lambda$ = 5 nm
	temperature dependent resonance wavelength shift of $\Delta\lambda$ = 6 nm
Full width at half maximum	FWHM = 16 nm
Low intensity transmittance	3 %
High intensity transmittance	45 %
Noise suppression factor	6 … 18 (dependent on the input signal/noise ratio)
Insertion loss	3 dB
Saturation	P_{sat} = 500 mW pulse peak power
Relaxation time constant	τ ~ 5 ps
Maximum input power	P_{max} = 1 W
Directivity	$\geq$ 50 dB
Fiber connector type	FC/PC, other on request
Thermoelectric cooler/heater	$-$ 2 ℃ … + 80 ℃

SANOS description

A SANOS is a resonant saturable absorber mirror (RSAM), mounted on a circulator. The RSAM has a strong non-linear reflectance. For a low input signal level the transmittance of the FC-SANOS is only 3% (97% loss), whereas high intensity pulses are transmitted with a lower loss of 50%. The needed peak pulse power for saturation is about 500 mW. Because the RSAM is a resonant device, the noise is only suppressed at the resonance wavelength. The input isolation is better than 50 dB. The RSAM is temperature regulated using a thermoelectric cooler/heater (TEC) for fine tuning of the resonance wavelength with a maximum shift of 6 nm.
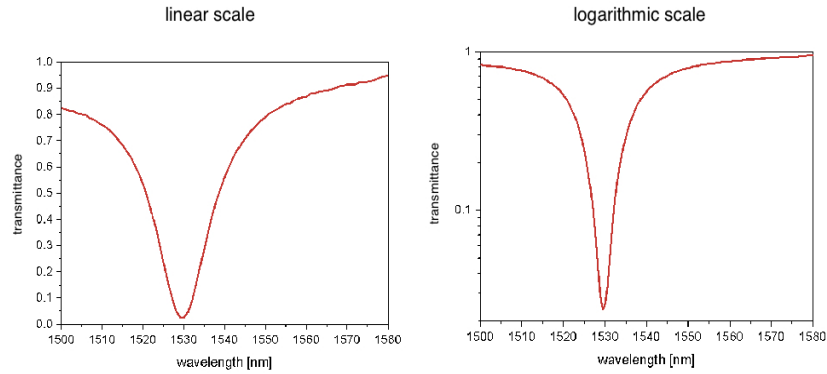
Order information

FC-SANOS-15XX-TEC: Fiber coupled SANOS with resonance wavelength of 15XX nm and thermoelectric cooler
SANOS with resonance wavelengths between 1530 nm and 1560 nm are available
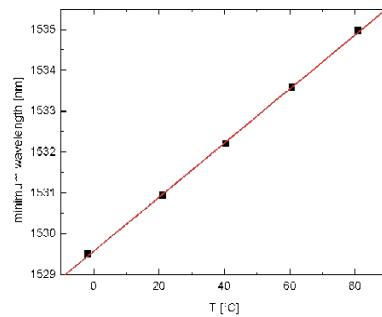
Spectral transmittance I_{out}/I_{in}

Low intensity (unsaturated) transmittance of a FC-SANOS-1530

linear scale

logarithmic scale

1530 nm FC-SANOS-1550-TEC
Temperature dependency of the resonance

Shift of the resonance wavelength using TEC
Low intensity (unsaturated) transmittance
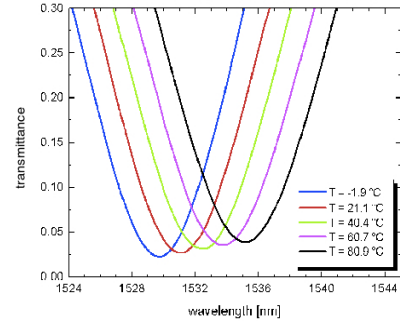
141

kamelian

OPTICAL PRE-AMPLFIER

Description

This high gain semiconductor optical amplifier is primarily intended for use as an optical pre-amplifier in high bit rate applications (10 Gbit/s and 40 Gbit/s). Its high gain and low noise figure provide a high performance, compact and price competitive alternative to single channel EDFAs in receiver subsystems. The optical preamplifier includes a thermistor and thermo-electric cooler in a 14-pin butterfly package with single mode fiber pigtails.

Applications

This product is appropriate for both metro and long haul applications where the use of an optical pre-amplifier increases the sensitivity of the receiver system, particularly where high data rates are used. With appropriate electronic circuitry, the device can be configured to provide a constant output power level over a wide dynamic range of input powers.

FEATURES

- 1550nm WINDOW
- HIGH GAIN
- LOW POLARISATION DEPENDENCE
- LOW NOISE FIGURE
- COMPACT PACKAGE
- MSA COMPLIANT

Specifications
(C Band 1529-1563nm)

PARAMETER	MIN SPECIFICATION	TYPICAL SPECIFICATION	MAX SPECIFICATION
Fiber-to-fiber gain - (Min)	20dB		
Noise figure		6dB	7dB
Saturation output power	10dBm	11dBm	
Polarisation dependence		0.5dB	1.0dB
Gain ripple		0.3dB	0.5dB
Bias current		200mA	250mA
Operating temp	-5°C		70°C
TEC Drive Max		0.7A/1.5V	

Pin Allocation & Package Dimensions

PIN	DEFINITION	PIN	DEFINITION
1	TEC +	8	NC
2	THERMISTOR	9	NC
3	NC	10	SOA ANODE (+)
4	NC	11	SOA CATHODE (–)
5	THERMISTOR	12	NC
6	NC	13	CASE GND
7	NC	14	TEC –
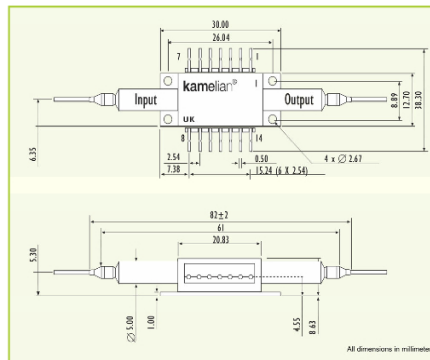
FIBER CONNECTOR	
CODE	**CONNECTOR TYPE**
FP	FC/PC
FA	FC/APC
FU	FC/UPC
LP	LC/PC
LA	LC/APC
LU	LC/UPC
SP	SC/PC
SA	SC/APC
SU	SC/UPC
ØØ	None

Ordering Information

O P A – YY – N – W – ZZ

Gain (18 for >18dB and 20 for >20dB are standard)

N = Non isolated is standard

Wavelength (C for C Band is standard)

Connector Type (See Table Above)

ATTENTION
OBSERVE
PRECAUTIONS FOR
HANDLING
ELECTROSTATIC
DISCHARGE
SENSITIVE DEVICES

**INVISIBLE LASER RADIATION
DO NOT VIEW DIRECTLY
WITH OPTICAL INSTRUMENTS
CLASS 1M LASER PRODUCT**

Amphotonix reserves the right to make changes in design, specifications and other information at any time, and without prior notice. The information contained within this Data Sheet is believed to be accurate. However, no responsibility is assumed for possible inaccuracy or omission. Any information contained herein shall legally bind Amphotonix only if it is specifically incorporated into the terms and conditions of a sales agreement.